

MODIS

Algorithm Technical Background Document

**ATMOSPHERIC CORRECTION ALGORITHM: SPECTRAL
REFLECTANCES (MOD09)**

Version 4.0, April 1999

NASA contract NAS5-96062

**E. F. Vermote and A. Vermeulen
University of Maryland, Dept of Geography**

ABSTRACT

The following document is a description of the atmospheric correction algorithm from which the surface reflectances will be calculated for MODIS channels 1 to 7: 0.648 μm , 0.858 μm , 0.470 μm , 0.555 μm , 1.240 μm , 1.640 μm , and 2.13 μm . The algorithm corrects for the effects of gaseous and aerosol scattering and absorption as well as adjacency effects caused by variation of land cover, Bidirectional Reflectance Distribution Function (BRDF) and atmosphere coupling effects, and contamination by thin cirrus. At launch, the correction of aerosol scattering will be based on aerosol climatology. Climatology will be superseded by MODIS-derived measurements of aerosol optical thickness soon after launch when the MODIS aerosol product has been successfully evaluated. The correction is achieved by means of a look-up table which provides the transmittances and path radiances for a variety of sun-sensor geometry's and aerosol loadings. This document presents the algorithm theoretical background and an outline of the pre-launch research agenda. This is a working document that will evolve as the research and the product are developed.

TABLE OF CONTENTS

1. INTRODUCTION	5
2.0 OVERVIEW AND BACKGROUND INFORMATION	11
2.1 EXPERIMENTAL OBJECTIVE.....	11
2.2 HISTORICAL PERSPECTIVE	11
2.3 INSTRUMENT CHARACTERISTICS.....	14
3. ALGORITHM DESCRIPTION	19
3.1 THEORETICAL BACKGROUND.....	19
3.1.1 <i>Physics of the Problem</i>	21
3.1.2 <i>Implementation of the Algorithm</i>	24
LUT approach.....	24
Rayleigh Scattering	25
Tropospheric Aerosol.....	25
Stratospheric Aerosol.....	28
Gaseous Absorption	29
Cirrus Correction.....	31
Surface Adjacency Effect.....	32
Spatial Grid.....	35
Correction for Non-Lambertianity	36
Algorithm Summary.....	37
3.1.3 <i>Uncertainty Estimates</i>	38
Radiative Transfer.....	39
Absolute Calibration.....	41
Input Parameter: τ_a	42
Aerosol Modell.....	44
Lambertian Approximation Error.....	46
Gaseous Absorption, Polarization, Vertical Distribution.....	48
Adjacency Effect.....	48
Cirrus Effect.....	48
Look-Up Table Interpolation.....	49
3.2 PRACTICAL CONSIDERATIONS	49
3.2.1 <i>Numerical Computation Considerations</i>	49
3.2.2 <i>Programming/Procedural Considerations</i>	49

3.2.3 Data dependencies.....	50
3.2.4 Output product.....	50
3.2.3 Validation.....	51
3.2.4 Quality Control and Diagnostics.....	57
3.2.5 Exception Handling.....	58
4. CONSTRAINTS, LIMITATIONS AND ASSUMPTIONS.....	59
5.0 RESEARCH AGENDA.....	60
REFERENCES.....	61
APPENDIX A: RAYLEIGH SCATTERING.....	68
APPENDIX B: ERROR SENSITIVITY STUDY.....	70
APPENDIX B1) TOP OF THE ATMOSPHERE SIGNAL (AT 3 OPTICAL DEPTHS AT 550NM: 0.1,0.3,0.5) AND SENSITIVITY TO ERROR ON OPTICAL DEPTHS (ERROR BARS) FOR EACH COVER TYPE.....	70
APPENDIX B2) ERRORS DUE TO CALIBRATION UNCERTAINTIES ($\pm 2\%$) AT OPTICAL DEPTH AT 550NM OF 0.3.....	90
APPENDIX B3) ERRORS DUE TO AEROSOL MODEL CHOICE (AT OPTICAL DEPTH OF 0.3 AT 550NM).....	94
APPENDIX B4) ERROR DUE TO BRDF ATMOSPHERE COUPLING (AT OPTICAL OF 0.3 AT 550NM).....	101
APPENDIX C ANSWERS TO THE SWAMP 96 LAND PRODUCT REVIEW.....	105

1. Introduction

The use of Moderate Resolution Imaging Spectroradiometer (MODIS) data for land products algorithms such as BRDF/albedo, vegetation indices or LAI/FPAR (Leaf Area Index/Fraction of Photosynthetically Active Radiation) requires that the top of the atmosphere signal be converted to surface reflectance. The process necessary for that conversion is called atmospheric correction. By applying the proposed algorithms and associated processing code, MODIS level 1B radiances are corrected for atmospheric effects to generate the surface reflectance product. Atmospheric correction requires inputs that describe the variable constituents that influence the signal at the top of the atmosphere (see Figure 1) and a correct modeling of the atmospheric scattering and absorption (ie. band absorption model and multiple scattering vector code). In addition an accurate correction requires a correction for atmospheric point spread function (PSF) (for high spatial resolution bands) and the radiation coupling of the surface BRDF and atmosphere (see Tables 1a and 1b for relative effects on existing environmental sensors).

Table 1a: Order of magnitude of atmospheric effects for Advanced Very High Resolution Radiometer (AVHRR) channel 1 and 2 and $NDVI = \frac{Channel2 - Channel1}{Channel2 + Channel1}$.

The proportional effect (transmission) is given as percentage (%) of increase (↗) or decrease (↘) of the signal. All the other effects as well as effect on NDVI test cases are given in absolute units.

	Ozone 0.247-0.480 [cm/atm]	Water Vapor 0.5-4.1 [g/cm2]	Rayleigh 1013mb	Aerosol V: 60km-10km Continental
ρ1 620 ± 120nm	↘ 4.2% to 12%	↘ 0.7% to 4.4%	↗ 0.02 to 0.06	↗ 0.005 to 0.12
ρ2 885 ± 195nm	–	↘ 7.7% to 25%	↗ 0.006 to 0.02	↗ 0.003 to 0.083
NDVI (bare soil) ρ1=0.19, ρ2=0.22	↗ 0.02 to 0.06	↘ 0.011 to 0.12	↘ 0.036 to 0.094	↘ 0.006 to 0.085
NDVI (deciduous forest) ρ1=0.03 ρ2=0.36	↗ 0.006 to 0.017	↘ 0.036 to 0.038	↘ 0.086 to 0.23	↘ 0.022 to 0.35

Table 1b: Order of magnitude of atmospheric effects for Landsat Thematic Mapper (TM) channel 1 to 5 and 7 and NDVI= $\frac{Channel4 - Channel3}{Channel4 + Channel3}$. The proportional effect (transmission) is given as percentage (%) of increase or decrease of the signal. All the other effects as well as effect on NDVI test cases are given in absolute units.

	Ozone 0.247-0.480 [cm/atm]	Water Vapor 0.5-4.1 [g/cm ²]	Rayleigh 1013mb	Aerosol V: 60km-10km Continental
ρ1 490 ± 60nm	↘ 1.5% to 2.9%	-	↗ 0.064 to 0.08	↗ 0.007 to 0.048
ρ2 575 ± 75nm	↘ 5.2% to 13.4%	↘ 0.5% to 3%	↗ 0.032 to 0.04	↗ 0.006 to 0.04
ρ3 670 ± 70nm	↘ 3.1% to 7.9%	↘ 0.5% to 3%	↗ 0.018 to 0.02	↗ 0.005 to 0.034
ρ4 837 ± 107nm	-	↘ 3.5% to 14%	↗ 0.007 to 0.009	↗ 0.003 to 0.023
ρ5 1692±178nm	-	↘ 5% to 16%	↗ 0.000 to 0.001	↗ 0.001 to 0.007
ρ7 2190±215nm	-	↘ 2.5% to 13%	-	↗ 0.001 to 0.004
NDVI (bare soil) ρ ₃ =0.19, ρ ₄ =0.22	↗ 0.015 to 0.041	↘ 0.015 to 0.06	↘ 0.03	↘ 0.006 to 0.032
NDVI (deciduous forest) ρ ₃ =0.03 ρ ₄ =0.36	↗ 0.004 to 0.011	↘ 0.005 to 0.018	↘ 0.08 to 0.085	↘ 0.022 to 0.13

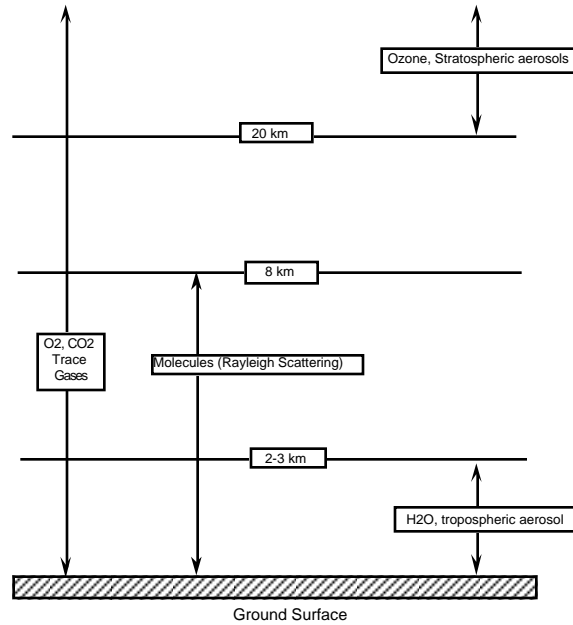


Figure 1: Description of the components affecting the remote sensing signal in the 0.4-2.5 μm range.

i) inputs: Our plan is to use MODIS atmospheric products (MOD04 : aerosols, MOD05 : water vapor, MOD07 : ozone, MOD35 : cloud mask) and ancillary data sets (Digital Elevation Model, Atmospheric Pressure) as an input to the atmospheric correction. Collaboration in the area of aerosol retrieval has been active for several years with the MODIS aerosol group (Holben et al. 1992, Holben et al. 1998, Kaufman et al, 1997). Specifics of the proposed improvements to the current MODIS algorithm are provided in section 3.

ii) modeling: Over the past few years, we have been actively involved in the modeling of atmospheric effects at the Laboratoire d’Optique Atmosphérique of Lille. The 6S radiative code was released in 1997 (Vermote et al., 1997), and is well suited for various remote sensing applications. The code is fully documented and a new version adapted for ocean remote sensing in a vector form is on test. It includes simulation of the effects of the atmospheric point spread function and surface directionality. We intend to use the 6S code as the reference to enable inter-comparison of algorithms and to verify the correct implementation of the MODIS atmospheric correction algorithm.

iii) PSF: As part of a NASA funded collaboration with the NSF Long Term Ecological Research (LTER) site network on atmospheric correction validation, a

technique for correction of the atmospheric Point Spread Function was developed ((Ouaidrari and Vermote,1999). This technique was applied to the Landsat Thematic Mapper (TM) at 30 meters resolution up to a distance of 20 pixels around the viewed pixel in a reasonable processing time. For MODIS the surface adjacency effect correction will be made up to a distance of 10 pixels using the same technique developed for the TM.

iv) coupling: The earth surface scatters anisotropically. This, combined with the anisotropic diffuse irradiance incident upon earth, means a simple Lambertian representation of earth scattering would result in significant errors in radiance calculations. A correction for atmosphere/BRDF coupling can be achieved if we have a-priori estimate of the surface BRDF. In this case, we can use the ratio between the BRDF coupled with the atmosphere and the surface BRDF to correct the measured values (corrected with the Lambertian assumption). By doing so, only the shape of the BRDF influences the correction process and not the actual “magnitude” of the estimated BRDF. This approach gives more weight to the actual observation than to the estimated BRDF. Both the BRDF and atmosphere coupled BRDF can be pre-computed and stored in tables. We are investigating two alternative approaches for obtaining BRDF inputs. One approach relies on the BRDF associated with land cover categories used in the MODIS FPAR/LAI product look-up tables and uses a multispectral approach to determine the element to be chosen. The other approach is to use the linear kernel weights derived from previous 16 days period, generated as part of the MODLAND BRDF product. In this latter case the look-up table contains coupled atmospheric kernels. The advantage of using the first approach is that the coupling correction can be investigated in real time, in the second case the advantage is that the BRDF shape is more variable.

One of the most important aspects of this document is the product validation. There are two tasks that need to be addressed when generating/validating a global “product”. The first task is to validate how the algorithm is performing prior to launch. In general, it is difficult to validate any remote sensing product with ground truth data due to difference in scale. Still, we propose to prototype and validate the atmospheric correction algorithm for selected test sites. This will continue and expand upon the LTER atmospheric correction project. The LTER project was particularly relevant as the TM data used in this study includes several of the land bands planned for MODIS. The LTER sites also provided a prototype for the

MODLAND validation sites proposed by Running et al. (1994). Sun photometer data were collected at these sites contemporaneously with the satellite data. Using these data, we can test the atmospheric correction over the sites as well as the aerosol product which will be used as input to the atmospheric correction (MODIS Land Aerosol ATBD). A further approach to pre-launch validation was to use high altitude airborne data from the MODIS Airborne Simulator (MAS) collected during specific validation campaigns such as the Sulfate Cloud Aerosol Reflectance-Atlantic (SCAR -A) regional experiment (Roger et al, 1994).

The second task concerns validating the global applicability and robustness of the algorithm. We can test the flow of data into the algorithm processing thread by using MODIS synthetic data, but the science cannot be thoroughly tested using these data because we are comparing one model output with another. The global processing issue has to be addressed with real "data". We have prototyped the global applicability of the MODIS algorithm using the Advanced Very High Resolution Radiometer (AVHRR) time series data. Collaboration has been developed with the NASA EOS AVHRR Pathfinder 2 project (Co-I: E. Vermote), whose goal was to design and test global processing of AVHRR 1km and 4km land data as a pathfinder for MODIS. This MODIS prototyping using AVHRR included operational correction for Rayleigh, ozone, water vapor and stratospheric aerosol and investigated the possibility of correcting for tropospheric aerosols. These corrections were conducted at the global scale over a range of actual atmospheric and surface conditions. The previous AVHRR Land Pathfinder project did not address either tropospheric aerosols or water vapor.

The atmospheric correction also requires accurate absolute calibration of each spectral band. This ATBD proposes to assist in the validation of MODIS calibration. We propose to augment the MODIS team calibration activities with a vicarious calibration method developed for AVHRR that enables a check on the absolute calibration values (Vermote and Kaufman, 1995). The method validates the on-board calibration, our understanding of the aerosol and molecular signal and therefore gives us confidence in our correction procedure. This is presented in the validation section.

2. Overview and Background Information

2.1 Experimental Objective

The purpose of this algorithm is to provide atmospherically corrected land surface reflectances to the global change community. The surface reflectances which are the product of applying atmospheric correction algorithms to the radiances measured by MODIS, are the seminal input parameter for all of the land products which rely on the reflectance portion of the spectrum. These products include surface albedo, snow cover, land cover, land cover change, vegetation indices and biophysical variables. The quality of these products depends directly on the quality of the atmospheric correction algorithm and the accuracy of the surface reflectance (Running et al., 1994). Our purpose is to provide an automated, global data set applicable to studies at scales exceeding 250 m. It is not intended to replace the need for localized atmospheric correction for individualized field studies.

2.2 Historical Perspective

Large field of view sensors aboard sun synchronous satellite platforms allow for a global survey of the planet earth. There has been much interest in such a data set for the study of the geosphere/biosphere system as demonstrated by Tucker (1986), Justice et al. (1985), Rasool (1987), and Townshend (1992) among many others. Inherent in any study of the earth's surface or vegetation from space is the need to extract the surface contribution from the combined surface/atmosphere reflectance received at the satellite (Deschamps et al., 1983; Gordon et al., 1988; Justice et al., 1991; Tanré et al., 1992). Failure to do so correctly creates the largest source of error in the use of time series data for surface parameterization with satellites.

Decoupling the atmosphere and the surface is a challenging problem and historically the research community attempted to bypass atmospheric correction by developing vegetation indices such as the Normalized Difference Vegetation Index (NDVI) (Tucker, 1979) which significantly reduced the atmospheric effect due to the normalization involved in its definition (Kaufman and Tanré, 1992). Further

reductions of atmospheric effects including the effect of subpixel clouds are achieved by means of compositing techniques in which several consecutive images are examined and the value corresponding to the maximum vegetation index for each pixel is chosen to represent the “correct” value for the time period (Holben, 1986; Tanré et al, 1992; Kaufman, 1987; Kaufman and Tanré, 1992).

Besides trying to minimize atmospheric effects with the above bypass procedures, there have also been attempts to perform explicit atmospheric correction by using radiative transfer codes (Moran et al., 1992). If these codes are used in conjunction with field measurements of atmospheric optical depth the results are quite accurate (Holm et al., 1989; Moran et al., 1990). However, the requirement of aerosol optical depth data at every location, found with ground-based sunphotometers, is a global impossibility. Simplified methods rely on assumptions of atmospheric conditions, but have varying degrees of accuracy (Otterman and Fraser, 1976; Singh, 1988; Dozier and Frew, 1981). Optimally, the information about the atmospheric optical properties needed by the radiative transfer code to perform atmospheric correction should be acquired from the satellite scene itself. Such methods are described by Ahern et al. (1977), Kaufman and Sendra (1988), Holben et al. (1992) and Kaufman and Tanré (1996). An operational atmospheric correction procedure applicable to a global data set, but limited to Rayleigh and ozone effects is described by James et al. (1993). A new processing system was also developed, Pathfinder II (El Saleous et al., 1999) and will serve as a prototype for the MODIS surface reflectance products. The correction so far corrects for Rayleigh, ozone, stratospheric aerosols, water vapor effects and uses Data Assimilation Office (DAO) ancillary data set, tropospheric aerosol correction is under development. An example of the surface reflectances obtained globally using that processing is shown figure 2a,b.

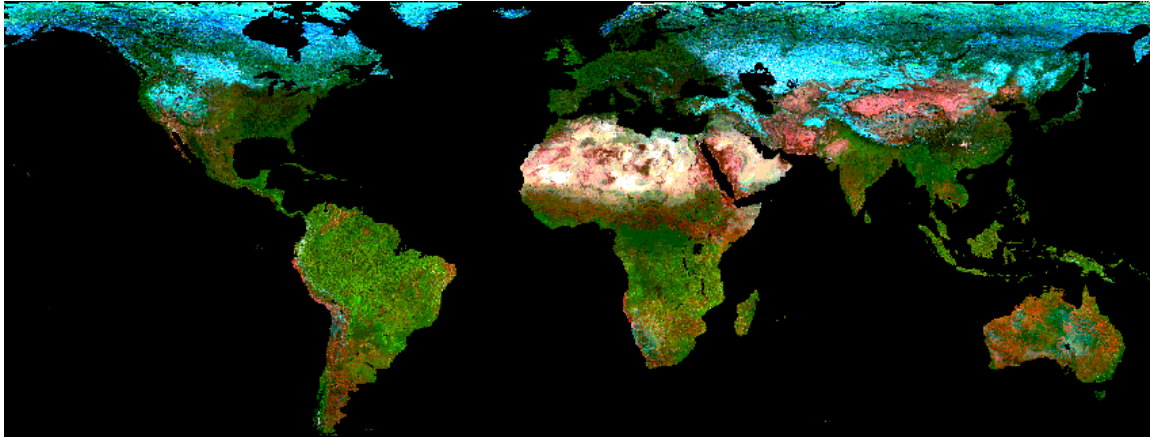


Figure 2a: RGB composite (Red=3.75 μm , Green=0.87 μm , Blue=0.67 μm) January 89

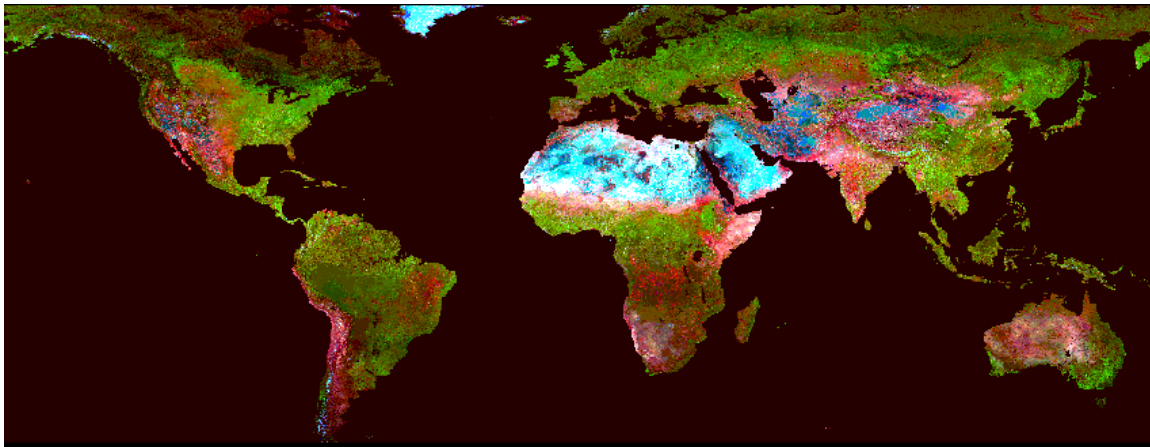


Figure 2b: RGB composite (Red=3.75 μm , Green=0.87 μm , Blue=0.67 μm) July 89

Figure 2a,b: These images were generated from AVHRR reflectances in channels 1 (0.67 μm), 2 (0.87 μm) and 3 (3.75 μm); channels 1 and 2 were corrected for atmospheric effects from rayleigh scattering, ozone (using TOMS gridded ozone product) and water vapor (using DAO total precipitable water). They reflect the state of land cover for January and July 89 : the green color produced by low values in AVHRR channels 1 and 3 and high values in channel 2 represents vegetated areas. Blue color in the January composite is produced for snow and residual clouds. The blue color over the desert in the July composite is due to the saturation of AVHRR channel 3 which leads to erroneous values of reflectance at 3.75 μm

The experience gained with AVHRR and TM has suggested a way to solve the

MODIS atmospheric contamination problem. Based on this experience, we present here the algorithm intended to be applied to the MODerate Imaging Spectroradiometer to be launched on EOS platforms.

2.3 Instrument Characteristics

The MODIS instrument contains several features which will help make the atmospheric correction algorithm more accurate than in the past. Most important is the availability of seven channels in the spectral interval 0.41-2.1 μm that enable the derivation of aerosol loading or aerosol optical thickness. (See Kaufman and Tanré, 1996). Therefore, we can attempt an accurate atmospheric correction for aerosol scattering and absorption at every geographic location. This is an improvement to what was possible in the past and a direct result from increasing the number of reflectance channels from two in the AVHRR to seven in MODIS (Salomonson et al., 1989).

Another important innovation is the smaller bandwidths in the reflectance channels which avoid overlap with the water vapor absorption bands in all but the 0.659 μm and 2.1 μm channels. Therefore, the error introduced by water vapor absorption is substantially reduced and the need to correct for it is minimized. Figure 3 shows the spectral absorption by water vapor, ozone, oxygen, carbon dioxide and the position of the reflectance channels of MODIS and their respective bandwidths. Figure 4 shows for MODIS band 2,

Likewise, reducing pixel size from 1 km in the AVHRR to 250 m in MODIS (Salomonson et al., 1989) increases our ability to detect cloudy pixels and reduces the contamination by subpixel clouds.

Besides the seven reflectance channels, two other MODIS channels are important to the atmospheric correction algorithm. The 3.75 μm channel will aid in the algorithms for determining aerosol optical thickness. Details are described in Kaufman and Tanré (1996) . The 1.38 μm channel is vital to detecting thin cirrus and stratospheric aerosols thereby making it possible to correct for these phenomena for the first time.

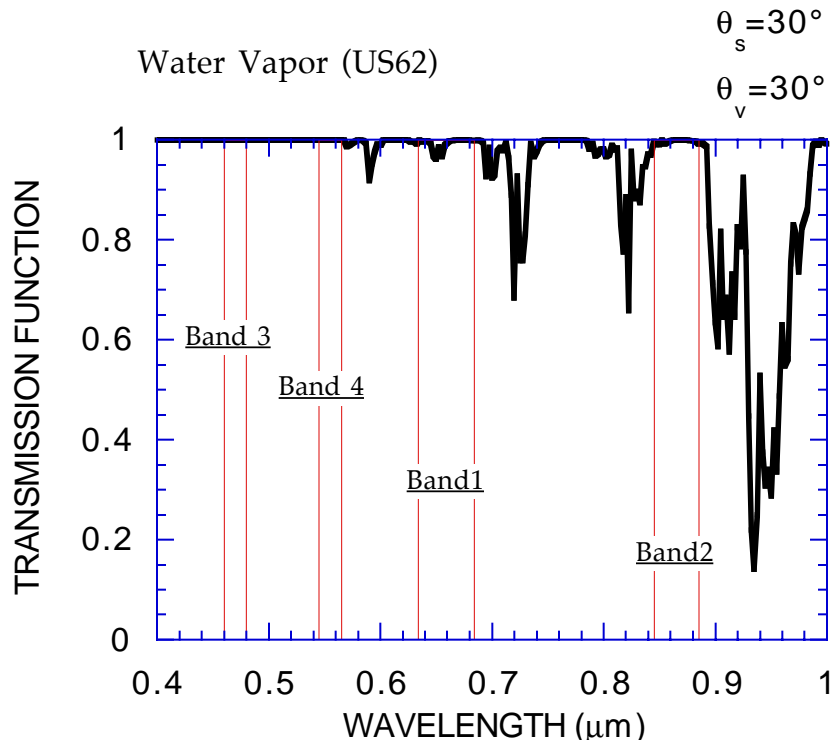


Figure 3a : Gaseous absorption in the MODIS channels. Water vapor absorption for channels 0.4 to 1 μm .

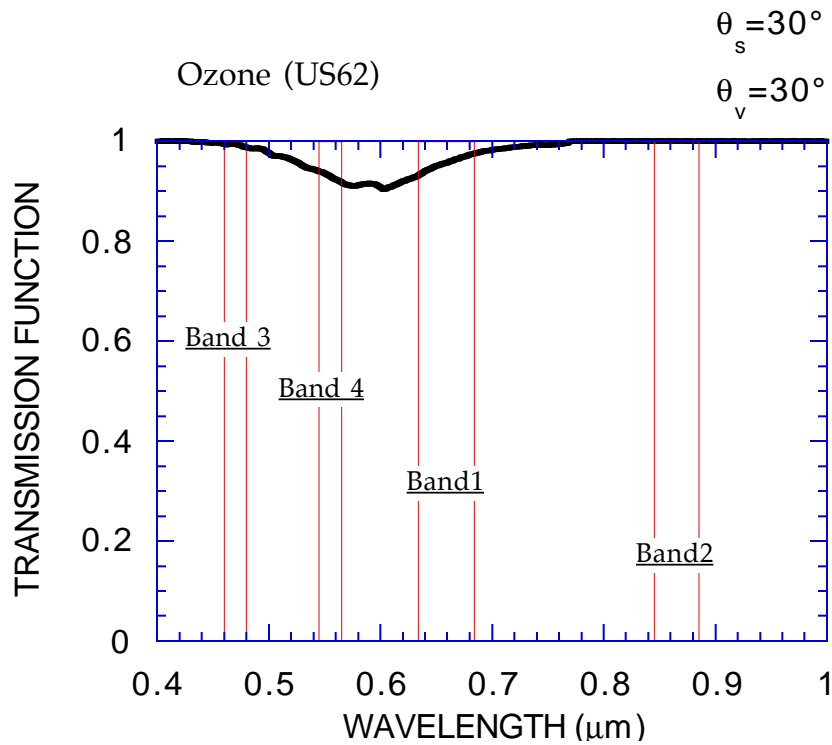


Figure 3b : Gaseous absorption in the MODIS channels. Ozone absorption for channels 0.4 to 1 μm .

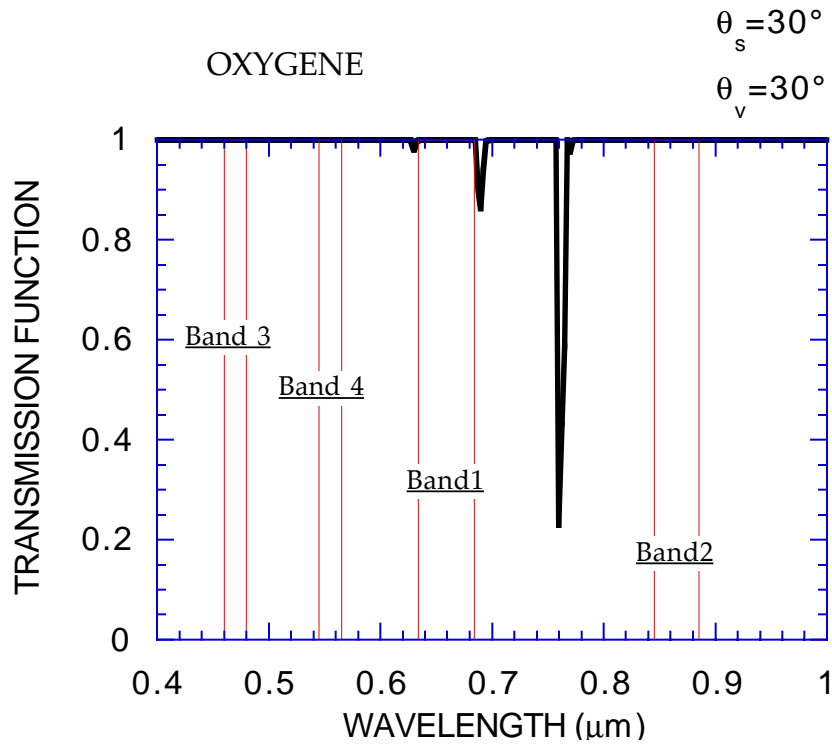


Figure 3c: Gaseous absorption in the MODIS channels. Oxygen absorption for channels 0.4 to 1 μm .

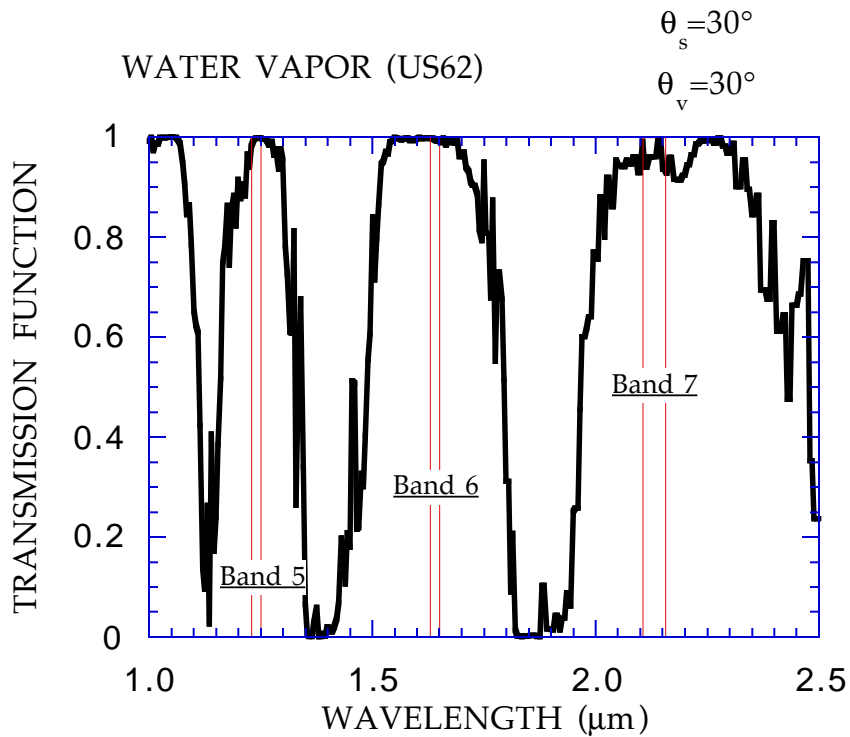


Figure 3d: Gaseous absorption in the MODIS channels. Water vapor absorption for channels 1.0 to 2.5 μm .

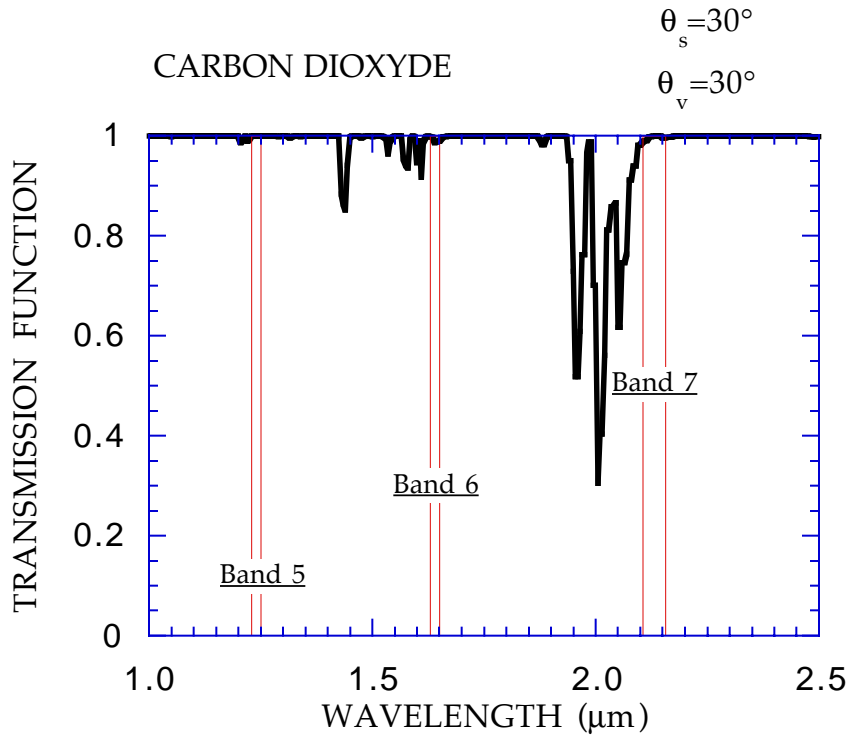


Figure 3e : Gaseous absorption in the MODIS channels. Carbon dioxide absorption for channels 1.0 to 2.5 μm .

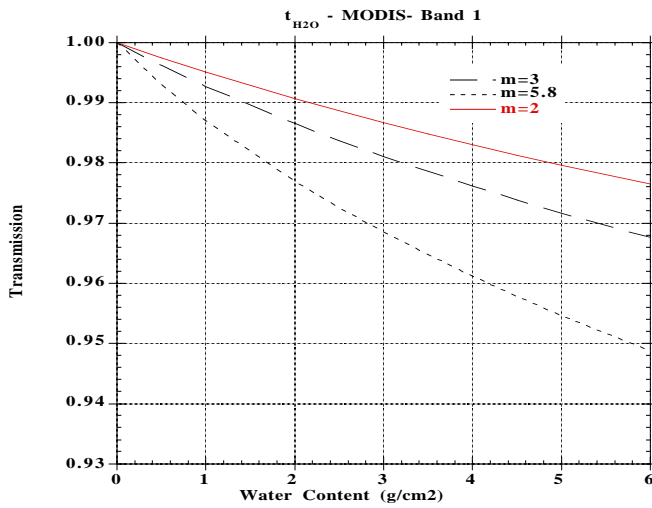


Figure 4a : Transmission of water vapor in MODIS band 1 vs water vapor content for a set of air mass

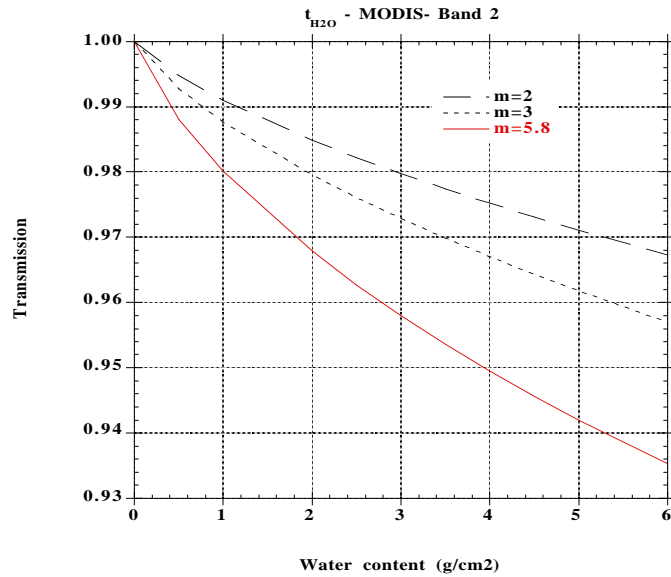


Figure 4b : Transmission of water vapor in MODIS band 2 vs water vapor content for a set of air mass

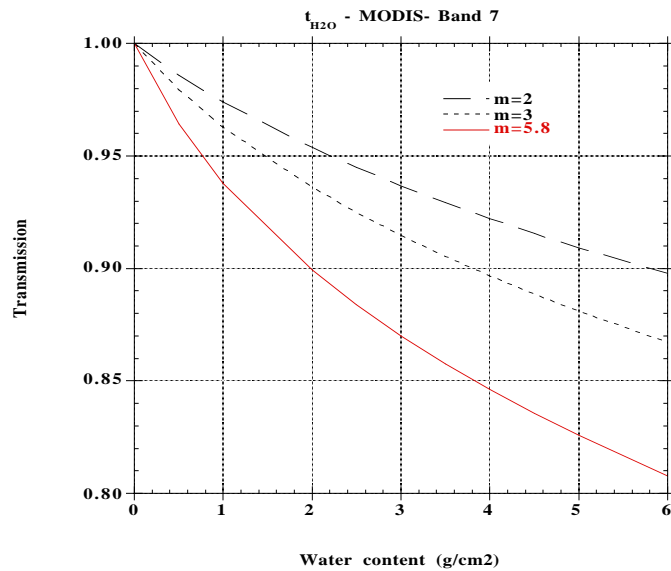


Figure 4c: Transmission of water vapor in MODIS band 7 versus water vapor content for a set of air mass

3. Algorithm Description

3.1 Theoretical background

In this section we describe the algorithms which will make the atmospheric

corrections for gaseous scattering and absorption, aerosol scattering and absorption, cirrus contamination, BRDF coupling and the adjacency effect. Figure 5 gives an overview of the processing chain. Because the atmosphere's gaseous composition will be relatively known, we propose that the correction for gaseous scattering and absorption be implemented at launch. However, the correction for aerosol effects depends on other MODIS products as input which should be evaluated before employment in the atmospheric correction scheme. Thus we would, at launch, implement an aerosol correction based on the regionally dependent climatological aerosol loading "clear" days. Further details are given in Section 3.1.2 under tropospheric aerosol. A simple, first-order cirrus correction scheme will be implemented at launch, with more sophisticated techniques replacing it post-launch. Both correction for BRDF coupling and correction for surface adjacency effects, which are part of the at-launch algorithm, will only be activated when the other part of the algorithms and the interface with the aerosol product are fully tested and quality controlled.

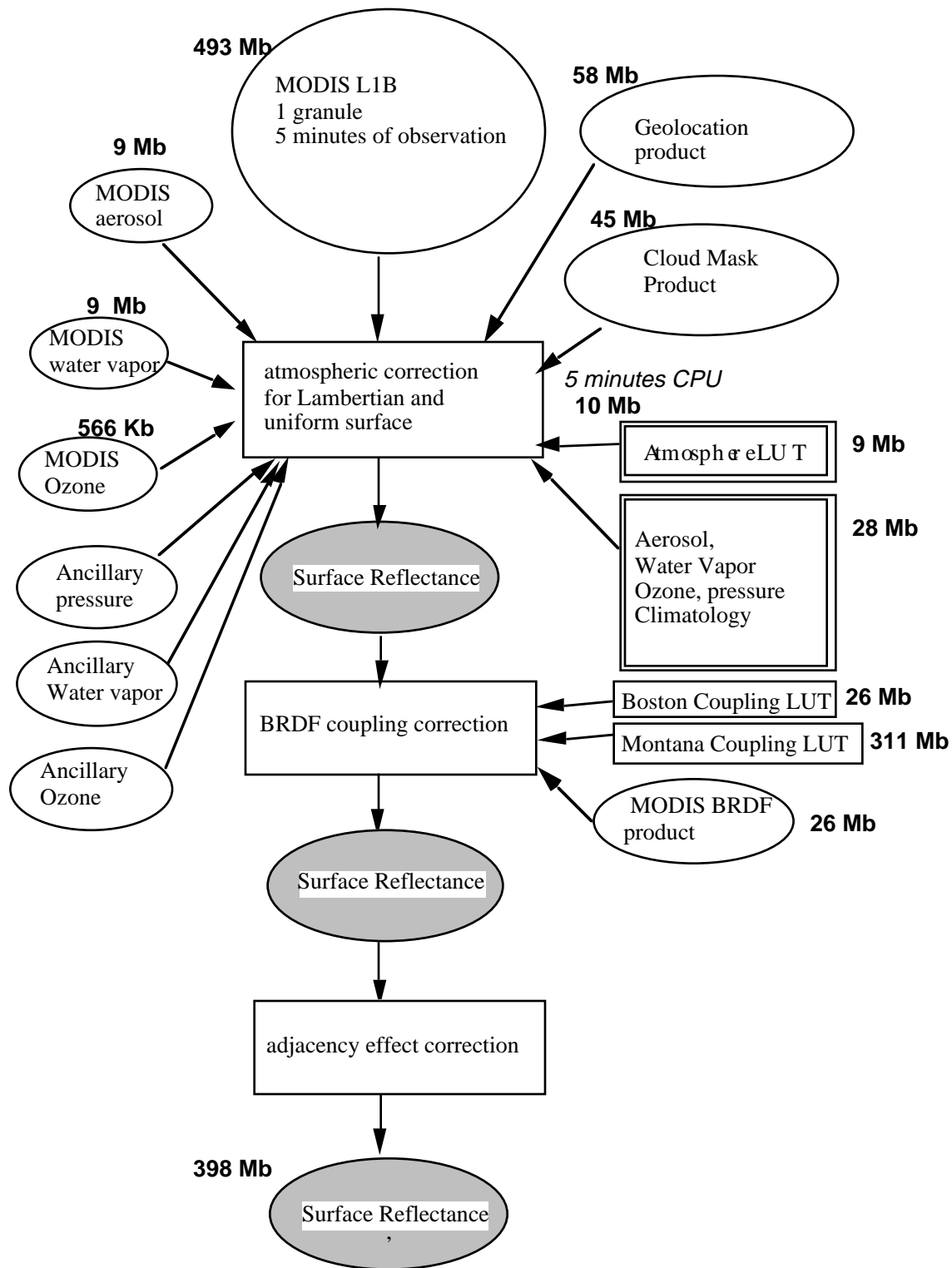


Figure 5 : Version 1 atmospheric correction processing thread flow chart. Times are given for running on a 195 Mflops processors.

3.1.1 Physics of the Problem

The radiance in the solar spectrum which reaches the MODIS instrument at the top of the atmosphere valid for lambertian surface reflectance, can be described as

$$L_{\text{TOA}}(\mu_s, \mu_v, \phi) = L_0(\mu_s, \mu_v, \phi) + \frac{T(\mu_s)T(\mu_v)F_0\mu_s\rho_s(\mu_s, \mu_v, \phi)}{\pi[1 - \rho_s(\mu_s, \mu_v, \phi)S]} \quad (1)$$

where L_{TOA} is the radiance received by the satellite at the top of the atmosphere, L_0 is the path radiance, $T(\mu_s)$ is the total transmittance from the top of the atmosphere to the ground along the path of the incoming solar beam, $T(\mu_v)$ is the total transmittance from the ground to the top of the atmosphere in the view direction of the satellite, F_0 is the solar radiance at the top of the atmosphere, $\rho_s(\mu_s, \mu_v, \phi)$ is the surface reflectance with no atmosphere above it, S is the reflectance of the atmosphere for isotropic light entering the base of the atmosphere, μ_s is the cosine of the solar zenith angle, μ_v is the cosine of the view angle and ϕ is the azimuthal difference between the two zenith angles. The radiances in Eq. (1) can be normalized by the incident solar radiance, $F_0\mu_s/\pi$, which results in the following equation:

$$\rho_{\text{TOA}}(\mu_s, \mu_v, \phi) = \rho_0(\mu_s, \mu_v, \phi) + \frac{T(\mu_s)T(\mu_v)\rho_s(\mu_s, \mu_v, \phi)}{[1 - \rho_s(\mu_s, \mu_v, \phi)S]} \quad (2)$$

where ρ_{TOA} is the reflectance at the top of the atmosphere and ρ_0 is path radiance in reflectance units. When T is divided into a direct and diffusive part such that

$$T(\mu) = e^{-\tau/\mu} + t_d(\mu) \quad (3)$$

and likewise for $T(\mu_s)$, where τ is the total optical thickness and t_d the diffuse transmittance. If the surface is non-Lambertian, the result of the correction using (1) is inexact, due to the coupling between the surface BRDF and atmosphere BRDF not being taken into account (Lee and Kaufman, 1986). An approach to model this effect that stems from the work of Tanre et al (1983) has been implemented in the 6S code as:

$$\begin{aligned} \rho_{\text{TOA}}(\theta_s, \theta_v, \phi_s - \phi_v) &= \rho_{\text{R+A}} + e^{-\tau/\mu_v} e^{-\tau/\mu_s} \rho_s(\theta_s, \theta_v, \phi_s - \phi_v) \\ &+ e^{-\tau/\mu_v} t_d(\mu_s) \bar{\rho} + e^{-\tau/\mu_s} t_d(\mu_v) \bar{\rho}' + t_d(\mu_s) t_d(\mu_v) \bar{\rho} + \frac{T_{\text{R+A}}^\downarrow(\mu_s) T_{\text{R+A}}^\uparrow(\mu_v) S(\bar{\rho})^2}{1 - S\bar{\rho}} \end{aligned} \quad (4)$$

with:

$$\bar{\rho}(\mu_s, \mu_v, \phi) = \frac{\int_0^{2\pi} \int_0^1 \mu L_{\text{R+A}}^\downarrow(\tau_A, \tau_R, \mu_s, \mu, \phi') \rho_s(\mu, \mu_v, \phi' - \phi) d\mu d\phi}{\int_0^{2\pi} \int_0^1 \mu L_{\text{R+A}}^\downarrow(\tau_A, \tau_R, \mu_s, \mu, \phi') d\mu d\phi} \quad (5a)$$

$$\bar{\rho}'(\mu_s, \mu_v, \phi) = \bar{\rho}(\mu_v, \mu_s, \phi) \quad (5b)$$

$$\bar{\rho} = \overline{\bar{\rho}'(\mu_s, \mu_v, \phi)} \quad (5c)$$

$$\bar{\rho} \cong \frac{\int_0^{12\pi} \int_0^1 \int_0^1 \rho_s(\mu, \mu', \phi) \mu \mu' d\mu' d\mu d\phi}{\int_0^{12\pi} \int_0^1 \int_0^1 \mu \mu' d\mu' d\mu d\phi} \quad (5d)$$

An important aspect is the validation of the parametrization of the signal which is presented in Figure 6 where the parametrization of equation (4) is compared versus the complete computation of the successive order of scattering that include a non-lambertian boundary conditions (Deuze et al, 1989).

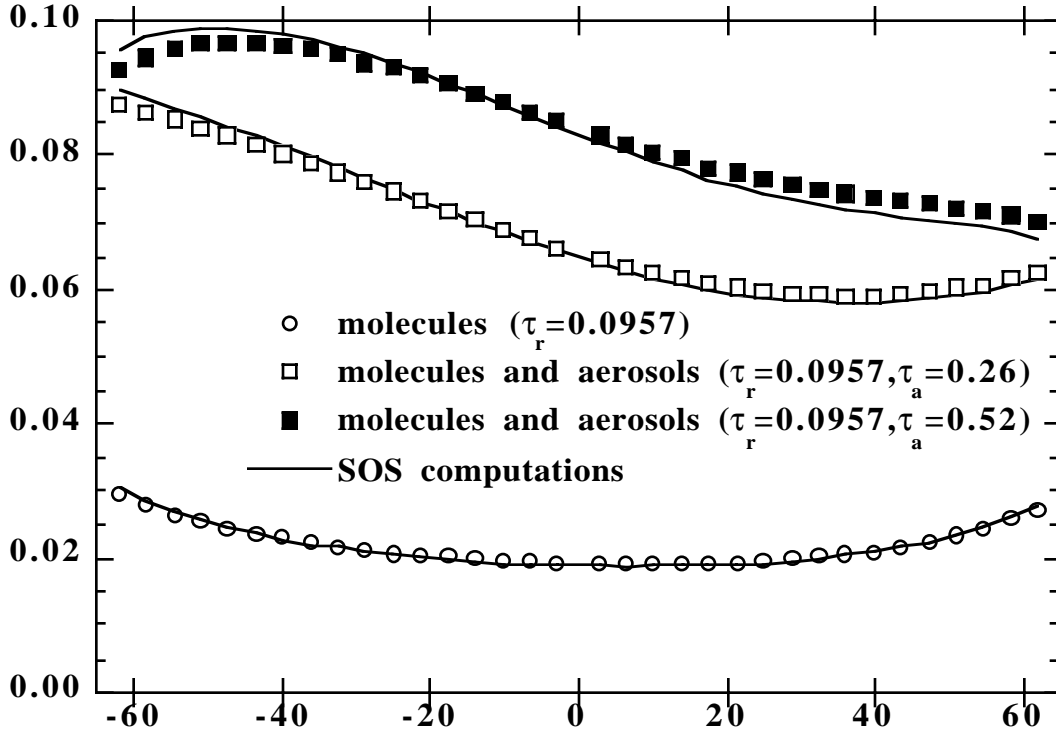


Figure 6: Comparison of the sum of the atmosphere-BRDF coupling terms computed using 6S and the same quantity computed by the Successive Order of Scattering code for different atmospheric conditions (clear, average, turbid). The ground BRDF is from Kimes measurements over a plowed field fitted with Hapke BRDF model. The x axis is the view zenith angle in the principal plane, the values are negative for back-scattering and positive for forward scattering.

To account for BRDF function provided, quantities in (5a-d) can be computed and the surface reflectance by solving a second degree equation, the details are given in the implementation section.

In case of heterogeneous landscape, at the resolution of the finest MODIS band (250m) we have to consider adjacency effects. Adjacency effects occur when a different but adjacent land cover influences the satellite measured radiance of a given land cover due to atmospheric scattering. The case of inhomogeneous ground boundary conditions has been addressed by several researchers (Tanré et al, 1979; Kaufman, 1982; Mekler and Kaufman, 1980; Vermote, 1990). The approach is to assume that the signal received by the satellite is a combination of the reflectance of the target pixel and reflectances from surrounding pixels, each weighted by their distance from the target

The correction procedure stems from the modeling work by Tanré et al (1981) and is simplified in this code for operational application. When taking into account the adjacency effect, the signal at the top at the atmosphere can be rewritten by decoupling the photons coming directly from the target ($e^{-\tau/\mu_v}$) from those coming from areas adjacent to the target and then scattered to the sensor ($t_d(\mu_v)$) :

$$\rho_{TOA} = \rho_{R+A} + \frac{\rho_s T_{R+A}(\mu_s) e^{-\tau/\mu_v} + \langle \rho_s \rangle T_{R+A}(\mu_s) t_d(\mu_v)}{1 - \langle \rho_s \rangle S_{R+A}} \quad (6)$$

where ρ_s is the pixel reflectance and $\langle \rho_s \rangle$ is the contribution of the pixel background to the top of the atmosphere signal that is computed as:

$$\langle \rho_s \rangle = \int_{-\infty}^{+\infty} \int_{-\infty}^{+\infty} f(r(x,y)) \rho(x,y) dx dy \quad (7)$$

where x,y denote the coordinate to a local reference centered on the target, and $f(r)$ is the atmospheric point spread function.

3.1.2 Implementation of the Algorithm

LUT approach

The quantities $\rho_O(\mu_s, \mu_v, \phi)$, $t_d(\mu)$ and S are functions of the optical thickness (τ), single scattering albedo (ω), and phase function ($P(\theta)$) of the scatterers and absorbers in the atmosphere. The calculation of $\rho_O(\mu_s, \mu_v, \phi)$, $t_d(\mu)$ and S is achieved with the aid of an atmospheric radiative transfer program such as the Dave and Gazdag (1970) model. However, it is computationally prohibitive to run a radiative transfer model for every pixel in a daily global data set. Thus, we create a look-up table with the 6S code (Vermote et al., 1997) which will supply the needed $\rho_O(\mu_s, \mu_v, \phi)$, $t_d(\mu)$, S for a variety of sun-view geometries and aerosol loadings. $\rho_O(\mu_s, \mu_v, \phi)$ are precomputed 73 relative azimuth angles, 22 solar zenith angles, 22 view zenith angles and 10 aerosol optical depth. $t_d(\mu)$ is precomputed for 16 zenith angles and 10 aerosol optical thickness. S is precomputed for 10 aerosol optical thickness.

The radiative transfer computations are dependent on the model inputs. These are discussed below.

Rayleigh Scattering

Scattering by the gaseous constituents of the air is a well-defined problem depending only on the wavelength of the radiation, air pressure and temperature profiles. In the radiative transfer code pressure and temperature profiles are given by McClatchey (1971) where different profiles are described for various climatic regions and seasons. Surface altitude information for each pixel will be available through a digital elevation model at the resolution of 5 minutes (ETOPO5). This is roughly 8 km by 8 km. The mathematical procedure for Rayleigh scattering is given in Appendix A. The algorithm will assume a surface elevation of 0 km for use by the radiative transfer code and adjust the Rayleigh outputs in the look-up table for variations in elevation and Global Assimilation Model output if available (Fraser et al, 1989; Fraser et al., 1992).

Tropospheric Aerosol

Quality of the surface reflectance estimates is strongly driven by the knowledge of the aerosol optical thickness. The algorithm will use the MODIS aerosol product (Kaufman and Tanré, 1998). At launch, we will use an aerosol optical thickness data set that we are developing. The data set will consist of monthly values interpolated to a 5° by 5° grid. It will be based on tabulations of d'Almeida (1991) modified with additional data from ground-based sunphotometer measurements, in particular the Aerosol Robotic Network (Holben et al., 1998) and from the literature. Figure 7 shows the AERONET sites (about 130) where data were collected between 1993 and 1998.

The aerosol optical thickness will also be derived from remote sensing measurements: the Advanced Very High Resolution Radiometer (AVHRR) and Sea-viewing Wide Field-of-view Sensor (SeaWiFS) data. Such a database is particularly useful to determine geographic and temporal aerosol patterns. It will be profitable also for the quality assurance (QA) analyses (see section 3.2.4).

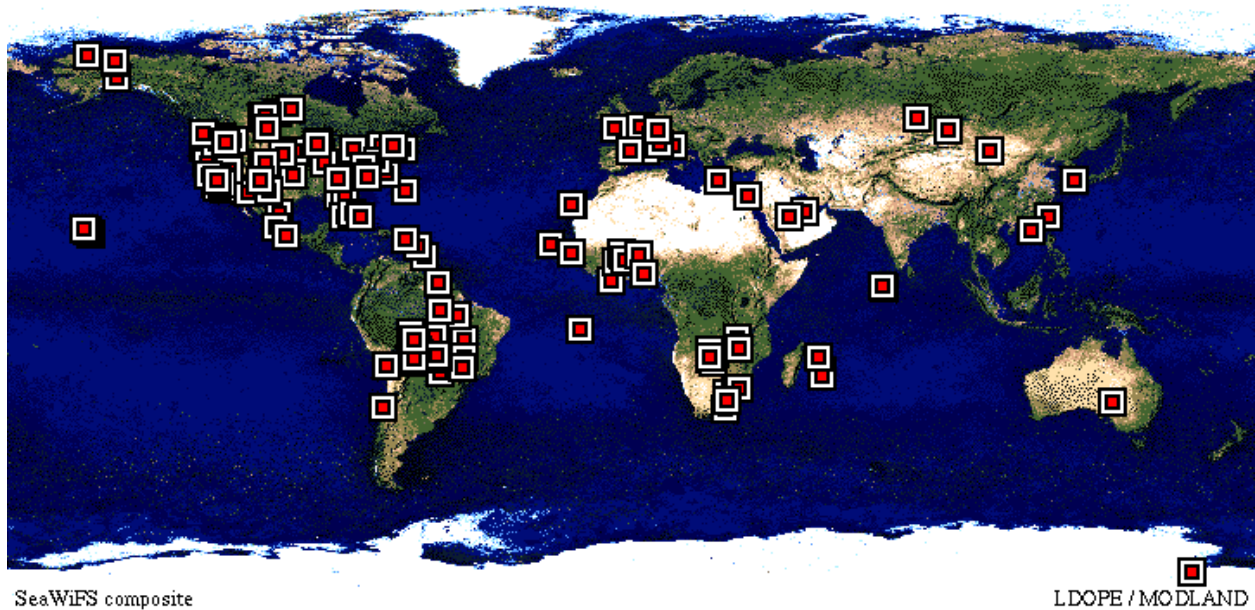


Figure 7 : AERONET sunphotometer sites with data over the 1993-1997 period

A monthly average optical thickness is currently considered. MODIS surface reflectance data will be composited using a minimum-blue criterion, that selects the clearest conditions over the period (Descloitres and Vermote, 1999). Moreover, in multi-day composite of NDVI, it is the clearest days and not the average days that selected to represent the period (Kaufman et al., 1992). An atmospheric correction based on the monthly or annual mean aerosol loading rather than the clearest value during a specific time period will “over correct” the surface reflectance in a composite. So, a monthly “average clear day” optical thickness will be considered too, i.e. the mean of the clearest third of all of the days on record. Such values would be $\tau_a^\lambda=0.05$ for Canada (Ahern et al., 1991), $\tau_a^\lambda=0.10$ for the eastern United States in winter and $\tau_a^\lambda=0.20$ for the eastern United States in summer (Kaufman and Fraser, 1983; Peterson et al., 1981). The average climatological data will be used to assess the uncertainties in daily corrected values.

Immediately post-launch, validation will begin on the aerosol optical

thickness derived from other MODIS algorithms (Kaufman and Tanré, 1996). As soon as it is determined where and when accurate aerosol optical thicknesses are produced, these new data will be used as input into the atmospheric correction algorithm. The MODIS-derived data will enable us to correct for the aerosol loading directly for the specific day and location, and will be a significant improvement to using the aerosol loading of climatological data. The correction will be applied to regions and periods of time where and when τ_a is available which is expected to be areas near dark, dense vegetation. This improvement will be implemented post-launch after the aerosol algorithms are evaluated. Climatological data will continue to be used where there are spatial and temporal gaps in the τ_a .

The remaining aerosol characteristics needed for the radiative transfer program are the single scattering albedo, $\omega_{\text{oa}}^\lambda$ and the phase function, $P_a^\lambda(\theta, z)$. These will come from aerosol models appropriate for season and location (Shettle and Fenn, 1979).

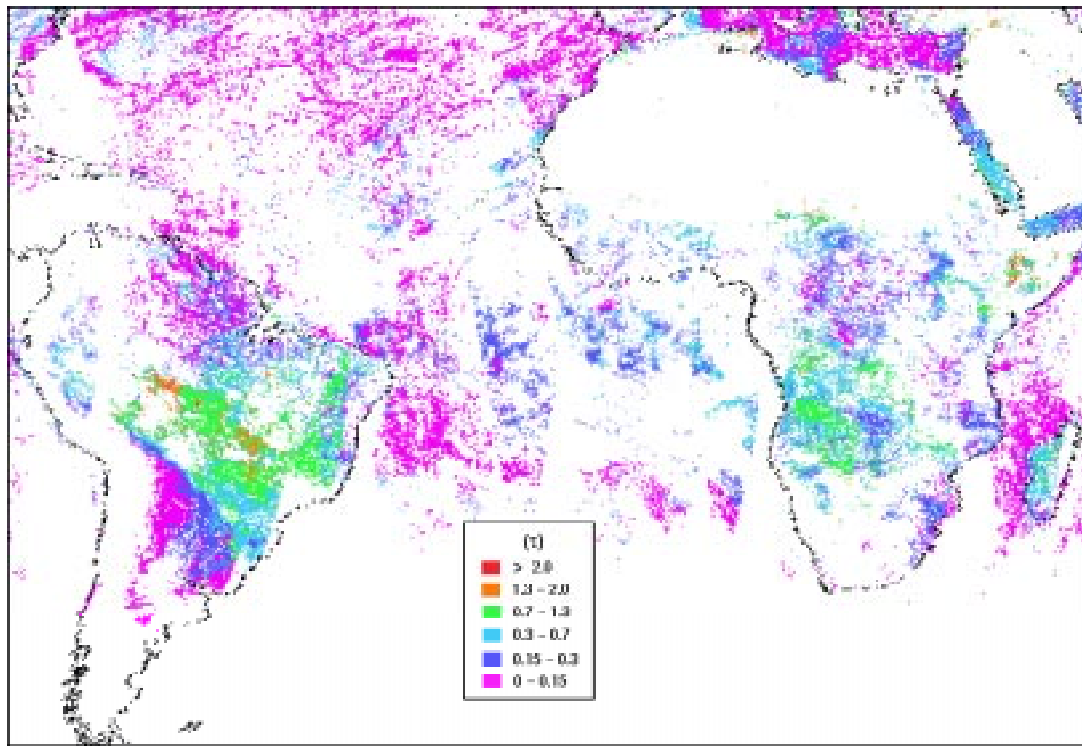


Figure 8: composite aerosol optical thickness at 550nm during the week 09/03/93-09/09/93, derived from NOAA AVHRR Global Area Coverage (GAC) data.

Stratospheric Aerosol

The stratosphere may at times have a significant optical thickness due to volcanic eruptions. These aerosol layers may cover a large portion of the globe and persist on the time scales of months to years. This phenomena can seriously compromise vegetation monitoring. An example is the Pinatubo eruption of 1991 (Vermote et al, 1994). The stratospheric aerosol optical thickness may be determined from MODIS algorithms using the 1.38 μm channel (Kaufman and Tanré, 1996) or it may be provided from other sources e.g. Stratospheric Aerosol and Gas Experiment (SAGE) instrument (McCormick and Vega, 1992). The stratospheric phase function will be obtained from King et al. (1984) who used El Chichon data to determine the properties of volcanic aerosol in the stratosphere. The single scattering albedo, ω_{oS}^{λ} , for the stratospheric aerosol will be computed from the refractive indices tabulated by Lenoble (1993).

Not only must τ_a be determined for the column, but it must be decoupled into stratospheric and tropospheric components. During an important volcanic eruption (e.g. Mt Pinatubo, figure 14) interpreting the aerosol as being located entirely in the troposphere will result in errors on the order of up to several hundredths in reflectance units.

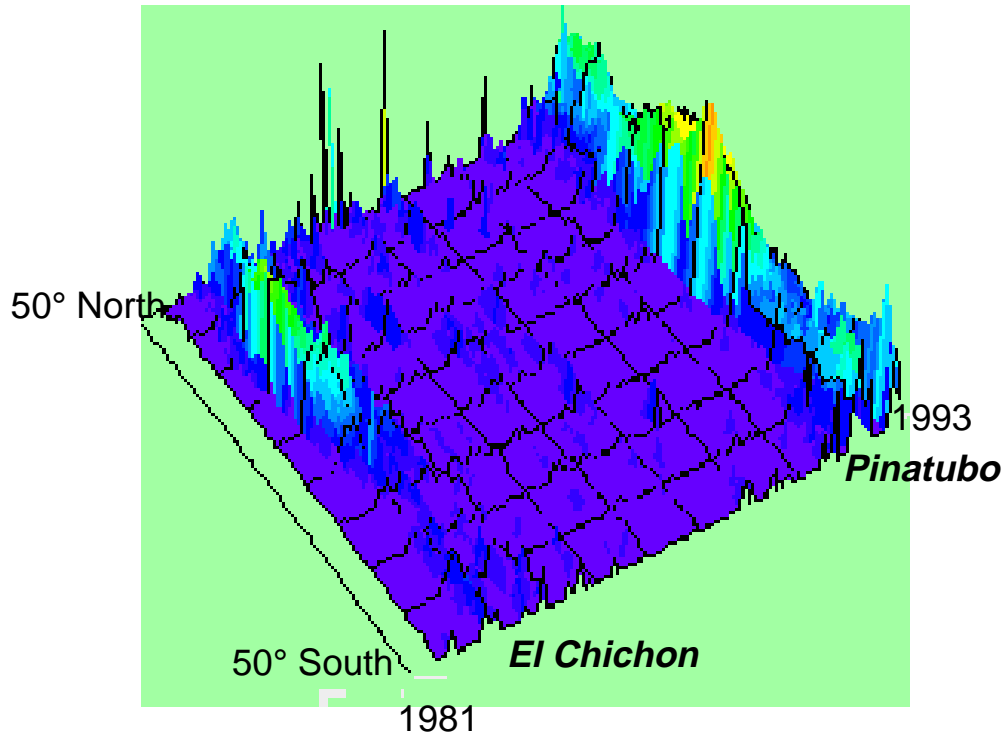


Figure 9: Monthly average of the stratospheric aerosol optical depth deduced from AVHRR data showing major eruptions of El Chichon and Pinatubo.

Gaseous Absorption

To account for gaseous absorption, the reflectance at the top of the atmosphere, $\rho_{TOA}(\mu_s, \mu_v, \phi)$ is modified as:

$$\rho_{TOA}(\theta_s, \theta_v, \phi_s - \phi_v) = Tg(O_3, O_2, CO_2, m) \left[\begin{array}{l} \rho_R + (\rho_0 - \rho_R) Tg^{H_2O} \left(M, \frac{U_{H_2O}}{2} \right) \\ + T^\downarrow(\theta_s) T^\uparrow(\theta_v) \frac{\rho_s}{1 - S\rho_s} Tg^{H_2O}(M, U_{H_2O}) \end{array} \right] \quad (8)$$

with ρ_R the molecular intrinsic reflectance, M is the air mass, given by :

$$M = \frac{1}{\mu_s} + \frac{1}{\mu_v}$$

$T_g(O_3, O_2, CO_2, M)$ is the gaseous transmission of O_3 , O_2 and CO_2 , $T_g^{H_2O}$ is the water vapor transmission.

The 6S radiative transfer model is used to calculate the gaseous transmission for each gas in each land bands for a range of total amount of gas and a range of view angles.

$$T_g(O_3, M) = \exp(-aMU_{O_3}) \quad (9a)$$

where U_{O_3} is the total amount ozone in units of cm/atm.

a is a coefficient which depend on the response of the given spectral band. Details can be found in Tanré et al. (1990).

The formula adopted for oxygen and carbon dioxide is :

$$T_g\left(M, \frac{p}{p_0}\right) = 1 + aM^b \left[\frac{1}{1 + c \frac{p}{p_0} + d \left(\frac{p}{p_0}\right)^2} - 1 \right]$$

p is the pressure at the altitude z and p_0 is the pressure at sea level. Oxygen and carbon dioxide are taken to be constant and are given in units of parts per billion, their amount is directly provided by the altitude. The parameters a, b, c, d are adjusted for the MODIS spectral responses.

The total precipitable water U_{H_2O} [g/cm²] is a MODIS product (Gao and Kaufman, 1993). It is assumed that the path radiance, ρ_0 , is generated above the middle of the boundary layer. Thus the additional attenuation is made by half the precipitable water. The formula adopted for the water vapor transmission is:

$$T_g(H_2O, M) = \exp\left[-\exp\left(a + b \ln(MU_{H_2O}) + c \left[\ln^2(MU_{H_2O})\right]\right)\right] \quad (9b)$$

with a, b, c adjusted for the MODIS spectral responses.

Fig. 3 shows that correction for gaseous absorption is only important to bands 1 and 4 for ozone and bands 1, 2 and 7 for water vapor. MODIS-derived values of total column O_3 and H_2O will be used as inputs.

Cirrus Correction

Correcting for cirrus effects may take several layers of implementation. All levels of cirrus correction rely on the MODIS 1.38 μm channel to detect cirrus clouds. This channel is nearly completely absorbed by water vapor in the lowest 6 km of the atmosphere. Thus, reflectances measured by this channel are almost exclusively high level clouds (Gao et al., 1993). The zero-order cirrus correction is simply a cloud mask in which all pixels identified as contaminated by cirrus using the 1.38 μm channel will be flagged as such. Such procedures are part of the cloud mask products and beyond the scope of this document. However, because thin cirrus transmits most of the radiance to and from the surface, it acts in a similar manner to other atmospheric constituents such as aerosols and should be addressed by atmospheric correction algorithms.

Rather than throwing out all cirrus-contaminated pixels, we intend to eliminate only those pixels where the reflectance in 1.38 μm exceeds a predetermined threshold. Contaminated pixels below that threshold would undergo a correction and be used to determine surface reflectance. The simplest correction would be to assume that the cirrus reflectance has no spectral dependence and is spatially homogeneous in a range of 20 km. Therefore, we could correct all channels with a simple subtraction:

$$\rho_{\lambda}(\mu_s, \mu_v, \phi) = \rho_{\lambda}(\mu_s, \mu_v, \phi) - \rho_{1.38}(\mu_s, \mu_v, \phi) / T_{1.38} \quad (10)$$

where $\rho_{\lambda}(\mu_s, \mu_v, \phi)$ is the reflectance at wavelength λ and $\rho_{1.38}(\mu_s, \mu_v, \phi)$ is the reflectance measured at 1.38 μm and $T_{1.38}$ the transmission of water vapor on the height of the cirrus cloud 0.6 ± 0.2 . The subtraction has the added advantage of transforming a systematic bias to random error.

An even more sophisticated technique would be to correct for cirrus adjacency effect and inhomogeneity. Ice clouds have strong forward scattering thereby affect path radiance of adjoining pixels which are otherwise cloud-free. Cirrus inhomogeneity is even more important. Pixels viewed by the satellite as cloud free may be illuminated by radiance which transversed cirrus. Thus the surface reflectance would be in the cirrus "shadow" although the "shadow" of thin

cirrus may escape cloud shadow masking techniques. This would produce erroneous values for the surface reflectance. The correction of cirrus adjacency and inhomogeneity effects presents an interesting problem that will be left to future research and development.

Surface Adjacency Effect

In the previous processing step, we obtained a corrected reflectance assuming uniform target that is, ρ_s^{ae} , which is computed from:

$$\rho_{TOA} = \rho_{R+A} + \frac{\rho_s^{ae} T_{R+A}(\mu_s) T_{R+A}(\mu_v)}{1 - \rho_s^{ae} S_{R+A}} \quad (11)$$

We can see that if we consider that: $\frac{1}{1 - \langle \rho_s \rangle S_{R+A}} \cong \frac{1}{1 - \rho_s S_{R+A}}$, then ρ_s and ρ_s^{ae} are related through the following equation:

$$\rho_s^{ae} = \rho_s \frac{e^{-\tau/\mu_v}}{T(\mu_v)} + \langle \rho_s \rangle \frac{t_d(\mu_v)}{T(\mu_v)} \quad (12)$$

therefore, we can correct the reflectance obtained in the previous step, ρ_s^{ae} for the adjacency effect using:

$$\rho_s = \frac{\rho_s^{ae} T(\mu_v) - \langle \rho_s \rangle t_d(\mu_v)}{e^{-\tau/\mu_v}} \quad (13)$$

with $t_d(\mu_v) = T_{R+A}(\mu_v) - e^{-\tau/\mu_v}$, with $\tau = \tau_A + \tau_R$

In practice, $\langle \rho_s \rangle$ is computed from a sub-zone of 21x21 pixels of the original image centered on the pixel to be corrected usingⁱ:

ⁱwe here used $\rho_s^{ae}(i, j)$ instead of $\rho_s(i, j)$ since the latter is not available, the error introduced can be reduced by using

$$\langle \rho_s \rangle = \sum_{j=-10}^{10} \sum_{i=-10}^{10} f(r(i,j)) \rho_s^{ae}(i,j) \quad (14)$$

with $r(i,j)$ representing the distance between the pixels (i,j) and the center of the zone.

In practice, the computation as denoted in equation (14), may involve up to 441 floating point multiplications, even if tabulated values of $f(r(i,j))$ are used. This will increase the amount of megaflops needed for atmospheric correction by a factor of 400. We have therefore developed and tested a practical approach to the problem applied to TM images for a moving window of 41x41 pixels. Two optimizations were necessary to arrive at an acceptable processing time (about twice the amount of time of a simple correction). First, we generated over the range of expected values a table of the product $f(r(i,j)) \rho_s^{ae}(i,j)$. By using that table we don't perform any multiplication to compute (14) and reduce the processing time significantly. Secondly the computation for pixel $\langle \rho_s(k,l) \rangle$ was computed from $\langle \rho_s(k,l-1) \rangle$, the advantage being that the atmospheric point spread function is rather smooth and that the difference matrix between two adjacent pixels contains many zeroes. By performing a sort of the difference matrix and eliminating the zero elements, we were further able to reduce the number of operations to be performed by roughly a factor of 10.

Figure 10 illustrates the results of the adjacency effect correction for TM band 1. The scene was acquired over Eastern United States. On the left side is the corrected image, on the right side is the original digital count image. The top part represents the full subset (1000x1000 pixels), the bottom part an enlargement of a part of the scene. The corrected scene appears more contrasted than the uncorrected scene due to the correction of atmospheric reflectance and transmission terms. The enlarged detail shows the impact and correction of the adjacency, the small dark area in the original scene was previously less visible because it was surrounded by brighter pixels.

The atmospheric point spread function varies with the view angle as illustrated by

successive iterations but is small (Putsay, 1992)

figure 11. We will take account for this effect in the MODIS algorithm, by using pre-computed tables as a function of view angle.

Figure 11: Isolines of the pixel background contribution to the signal at the top of the atmosphere for a pure molecular case. The energy source is 10^4 Watts and each pixel is considered to have a lambertian reflectance of 1. The contribution of the background is presented as the number of Watts coming from each cell (201 cells x 201 cells). The plain lines are for nadir viewing, the broken lines are for a view angle of 70° (from Vermote et al, 1996)

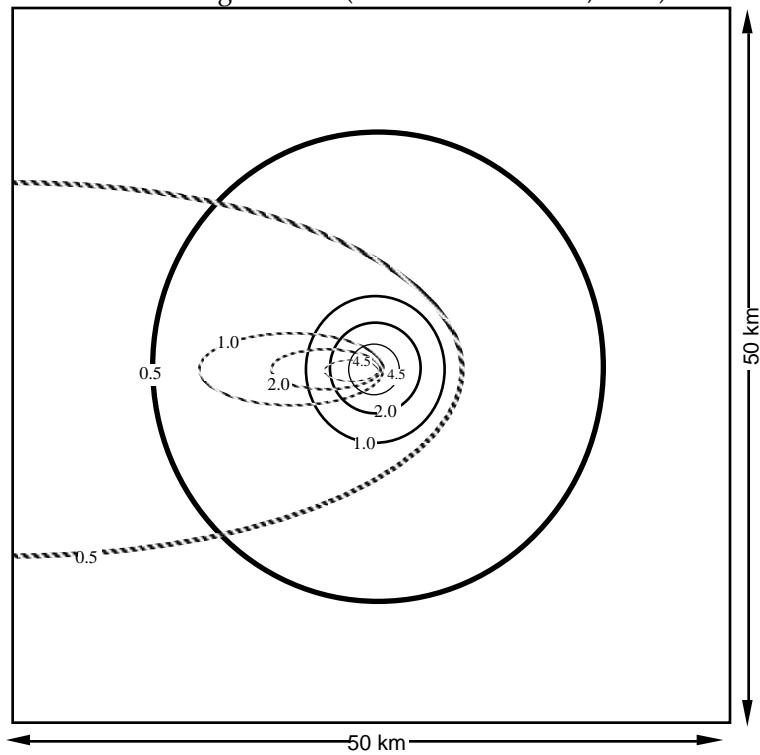


Figure 10: Comparison of TM band 1 data corrected for atmosphere (left side) to uncorrected counts (right side). The correction includes adjacency effect correction.



Spatial Grid

The aerosol loading will be calculated from MODIS products on a 10 km by 10 km grid over land. The digital elevation model has a resolution of 5 minutes which is roughly 8 km by 8 km. It is unnecessary to calculate the correction parameters: $\rho_0(\mu_s, \mu_v, \phi)$, $t_d(\mu)$, $L^\downarrow(\mu, \mu', \phi')$ and τ , on a higher resolution than the given input parameters. Thus the correction will be calculated for a spatial grid of 8 km by 8 km

in complex terrain and perhaps as coarse a grid as 10 km by 10 km in flat terrain.

Correction for Non-Lambertianity

We use the ratio between the estimated BRDF (ρ_s^m) and the actual surface BRDF (ρ_s) to correct the measured values. We rewrite equation (7) as:

$$\begin{aligned} \rho_{\text{TOA}}(\mu_s, \mu_v, \phi) = & \rho_0 + e^{-\tau M} \rho_s(\mu_s, \mu_v, \phi) \\ & + \rho_s(\mu_s, \mu_v, \phi) \left[\begin{aligned} & e^{-\tau/\mu_v} t_d(\mu_s) \bar{\rho}^* + e^{-\tau/\mu_s} t_d(\mu_v) \bar{\rho}'^* + t_d(\mu_s) t_d(\mu_v) \bar{\rho}^{\bar{\bar{*}}} + \\ & \rho_s(\mu_s, \mu_v, \phi) \frac{T_{R+A}^\downarrow(\mu_s) T_{R+A}^\uparrow(\mu_v) S(\bar{\rho}^*)^2}{1 - S\bar{\rho}} \end{aligned} \right] \end{aligned} \quad (15)$$

with:

$$\bar{\rho}^*(\mu_s, \mu_v, \phi) = \frac{\bar{\rho}(\mu_s, \mu_v, \phi)}{\rho_s^m(\mu_s, \mu_v, \phi)} \quad (16a)$$

$$\bar{\rho}'^*(\mu_s, \mu_v, \phi) = \bar{\rho}^*(\mu_v, \mu_s, \phi) \quad (16b)$$

$$\bar{\rho}^{\bar{\bar{*}}}(\mu_s, \mu_v, \phi) = \frac{\bar{\bar{\rho}}(\mu_s, \mu_v, \phi)}{\rho_s^m(\mu_s, \mu_v, \phi)} \quad (16c)$$

When using (15) to retrieve, ρ_s we have to solve a second degree equation which only has one positive solution

To compute the different terms (16a-c), we have to use a BRDF model. We have two approaches for obtaining modeled BRDF inputs implemented on the version 1 code.

The first solution is to use the bidirectional reflection function that will be provided on a 1 km by 1 km grid, for the previous 16-day period (Strahler et al., ATBD, 1996). Results show that the simple assumption for BRDF is sufficient and that the results are greatly improved versus the lambertian correction. This BRDF is expected to depend on vegetation index and thus we can fit a $F(\bar{\rho}^*, \bar{\rho}'^*, \bar{\rho}^{\bar{\bar{*}}}, \bar{\rho})$ curve through five selected points in each group of sixty-four 1 km squares defined by our

larger 8 km by 8 km grid. These five points will be selected to span the range of vegetation index values found in the larger grid square eliminating the need for extrapolation. Thus, for any value of vegetation index encountered in the larger grid square, a value of the coupling term, $F(\overline{\rho^*}, \overline{\rho'^*}, \overline{\rho^*}, \overline{\rho})$, can be determined using the derived equation for the curve fit. In this way, both the atmospheric correction and the correction for the Lambertian assumption can be applied to each individual pixel within the correction grid square, including pixels at the 250 m resolution.

The second solution is to use a generic BRDF model look-up-table based on runs from the Mymeni et al. three-dimensional canopy model (1992). The BRDF is depending on the land cover categories used in the MODIS LAI/FPAR product (Running et al., 1994). BRDF and coupling terms are stored in tables as a function of zenith angles, aerosol optical thickness, biome type and LAI. The biome is determined by the land cover map, and the LAI is selected by minimizing the difference between the spectral dependence of observed and modeled reflectance in MODIS bands 1,2,3 and 4.

Algorithm Summary

1) On a scale of 5 km by 5 km, we use $\mu_s, \mu_v, \phi, \tau_a$ (the aerosol optical thickness), τ_s (the optical thickness of the stratosphere), τ_r (the Rayleigh optical thickness), an aerosol model and look up tables to generate $\rho_R(\mu_s, \mu_v, \phi), \rho_O(\mu_s, \mu_v, \phi), t_d(\mu), S$. Use elevation to adjust Rayleigh component of the look-up variables.

-at launch: τ_a taken climatology;

τ_s taken from SAGE data.

-post launch: τ_a taken from MODIS algorithm where available and climatology where not; τ_s taken from MODIS algorithm.

2) For every 5 km by 5 km grid square, compute gaseous absorption correction using precipitable water vapor calculated from MODIS algorithms and Eqs. (8-9).

3) For every 5 km by 5 km grid square, look up the equation for $F(\overline{\rho^*}, \overline{\rho'^*}, \overline{\rho^*}, \overline{\rho})$ the bidirectional coupling reflection function, dependent on vegetation index.

-at launch: using land cover approach (To be confirmed)

- post launch: function determined dynamically from MODIS and MISR products. (in collaboration with Alan Strahler)
- 4) For every pixel, use the equation found in step 3 to calculate $F(\overline{\rho^*}, \overline{\rho'^*}, \overline{\rho^*}, \overline{\rho})$, then use Eqs (16) to correction for BRDF/ATM coupling effect (if using dynamic BRDF)
 - 5) For every pixel, adjust for cirrus effect, using values at 1.38 μm .
 - at launch: Use Eq. (10)
 - post launch: more sophisticated technique
 - 6) For every pixel, solve Eq. (15) for $\rho(\mu_s, \mu_v, \phi)$, the surface reflectance.
 - 7) For every pixel, adjust for adjacency effect.
 - at launch: no correction
 - post-launch: implemented when other corrections are tested.
 - 8) Results are surface reflectances for seven wavelengths at every pixel.

3.1.3 Uncertainty Estimates

Uncertainty arises in the atmospheric correction procedure from many different sources. Each of these sources of error will be discussed separately. An error budget is presented for 6 different land cover type, those results were obtained using the input parameters uncertainties estimate and running the 6S code (Vermote et al., 1997). The code is available on anonymous ftp (address:kratmos.gsfc.nasa.gov). The six different land cover type were simulated using a spectral directional model available in 6S (Kuusk, 1994). The parameters of the surface model used in the simulation are given in table 2. The complete set of results is given in appendix B.

	Cropland/Grasses	Shrubs	Broadleaf Crops	Savanna	Leaf Forest	Needle Forest
LAI	3.0	3.0	3.0	3.0	3.0	3.0
C _{AB}	30.0	30.0	30.0	30.0	30.0	30.0
C _w	0.02	0.01	0.03	0.015	0.03	0.015
Sl	1.0	0.1	0.5	1.0	0.01	0.01
N	1.225	1.225	1.225	1.225	1.225	1.225
cn	1.0	1.0	1.0	1.0	1.0	1.0
s1	0.4	0.8	0.1	0.4	0.4	0.4
θ_m	70.0	40.0	40.0	70.0	10.0	10.0
ϵ	0.9	0.05	0.05	0.1	0.1	0.1

Table 2: Parameters of the surface model (Kuusk, 1994) used in the error sensitivity study. LAI is the Leaf Area Index, C_{AB} is the leaf pigment concentration in unit of $\mu\text{g}/\text{cm}^2$, C_w is the leaf liquid content in unit of cm, Sl is the ratio of the mean chord lengths of the leaves by the height of the canopy, N is the effective number of elementary layers inside a leaf, cn is the ratio of refractive indices of leaf surface wax and internal material, s1 is the weight of the price function for soil albedo (s1=0.1 for dark soil, 0.8 for bright soil), θ_m and ϵ describe the angular distribution of leaves according to an elliptical distribution model where θ_m is the modal leaf inclination and ϵ is the eccentricity of the elliptical distribution of the leaf normals.

Radiative Transfer

The 6S code was compared to other radiative code like Dave and Gazdag (1970) code. The 6S that does not have the errors associated with molecular-aerosol coupling that some approximation models have (Herman et al., 1971). It is extremely accurate up to the limits of the plane parallel approximation (about 80°). Angles of this magnitude will only be encountered in the polar regions. The current version doesn't account for polarization that is important at short wavelength (band 3,4), but the version we plan to use for generating the table for atmospheric will account for polarization. Figure 12a,b shows the importance of the atmospheric effects on different MODIS bands (gaseous absorption excluded), (a) shows the surface reflectance that should be compared to (b) the top of the atmosphere reflectance for a clear atmosphere.

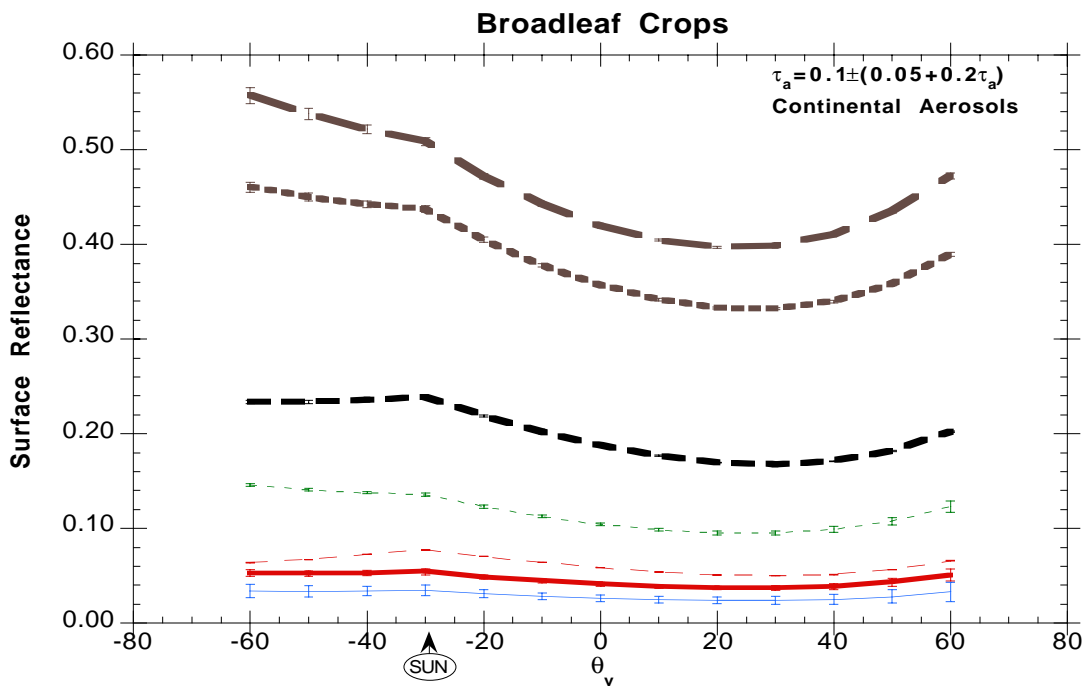


Figure 12a

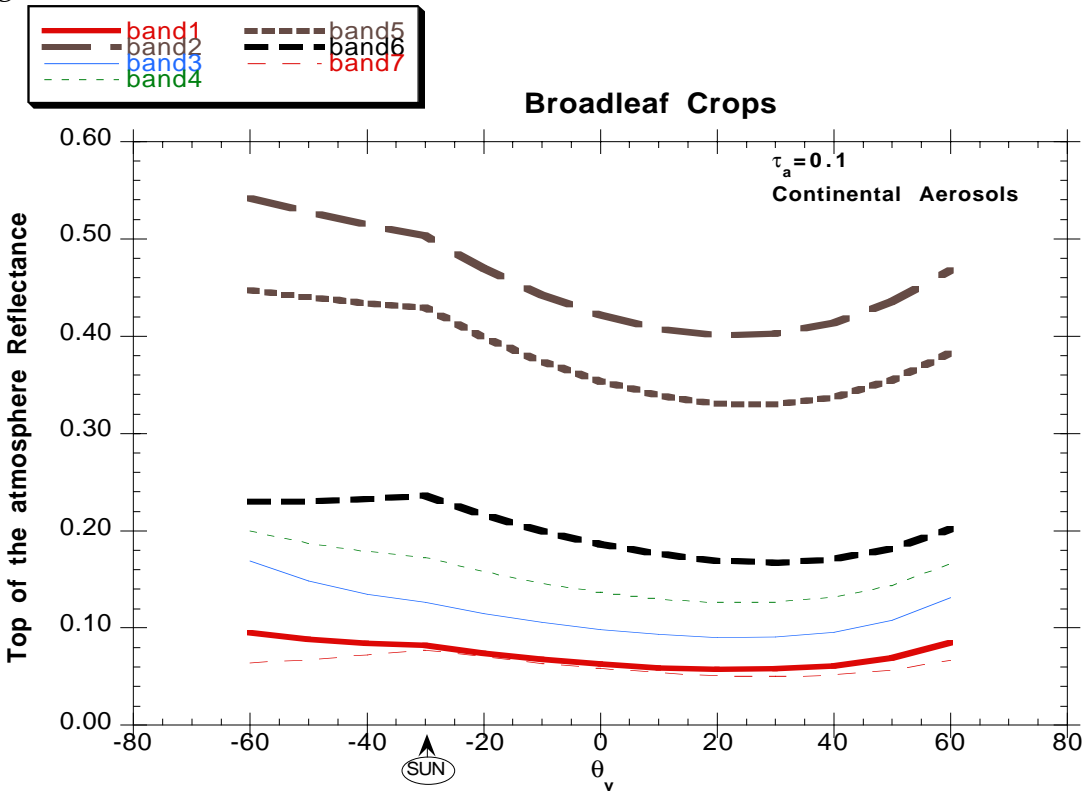


Figure 12b

Absolute Calibration

Uncertainty on absolute calibration will affect the accuracy of the reflectance at the top of the atmosphere and therefore the corrected reflectance. We simulate an error of $\pm 2\%$ on the top of the atmosphere reflectance in case “average” aerosol loading (optical depth of 0.3 at 550nm for a continental model) and compute the resulting error on surface reflectance which we report as error bars. As shown on figure 13, the relative error of 2% could translate to higher error on surface reflectance for bands where atmosphere contribution is much larger than surface contribution, typically under high view zenith angle ($>40^\circ$) and in the shortest wavelengths (band 1,3,4).

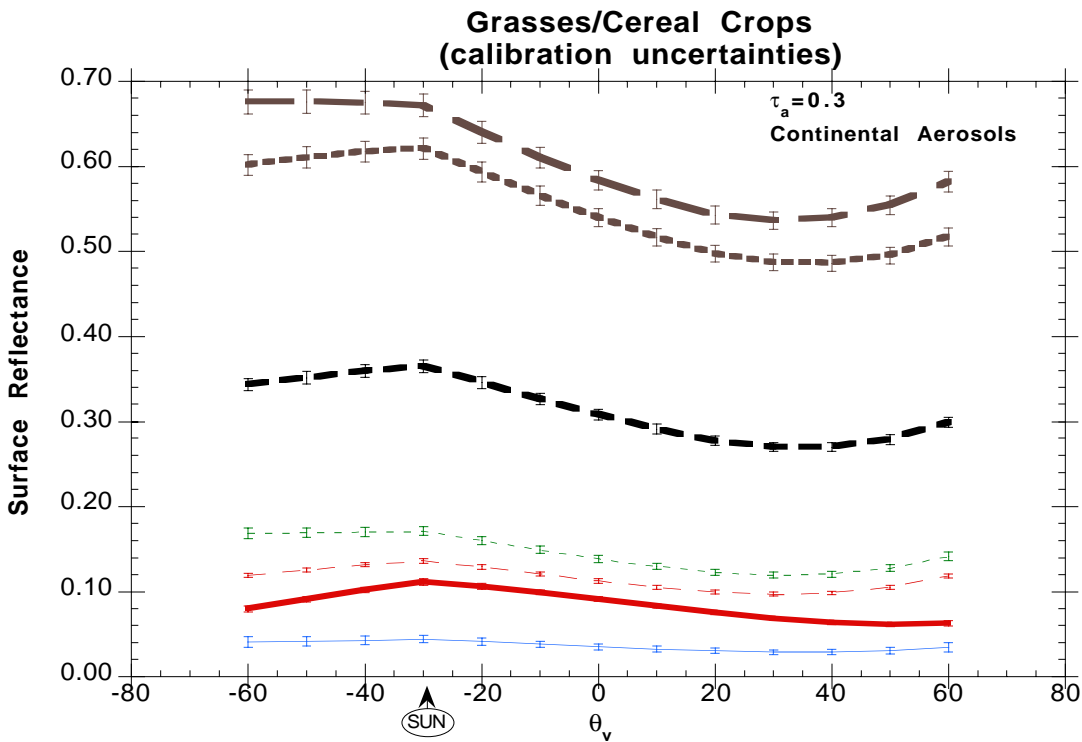


Figure 13

For a 2% calibration uncertainty, typical relative and absolute errors are:

band	rel. error %	abs. error
1	4	0.003
2	2	0.015
3	14	0.004
4	3.5	0.004
5	2	0.015
6	2	0.008
7	2	0.003

Impact of a calibration error

Input Parameter: τ_a

The accuracy of the input parameter, τ_a is discussed in Kaufman and Tanré (1996). We expect an uncertainty of 0.05 for τ_a derived from MODIS products for small optical thicknesses and 20-30% for large optical thicknesses. We present Figure 14 some simulations of the impact of uncertainties in the aerosol input product.

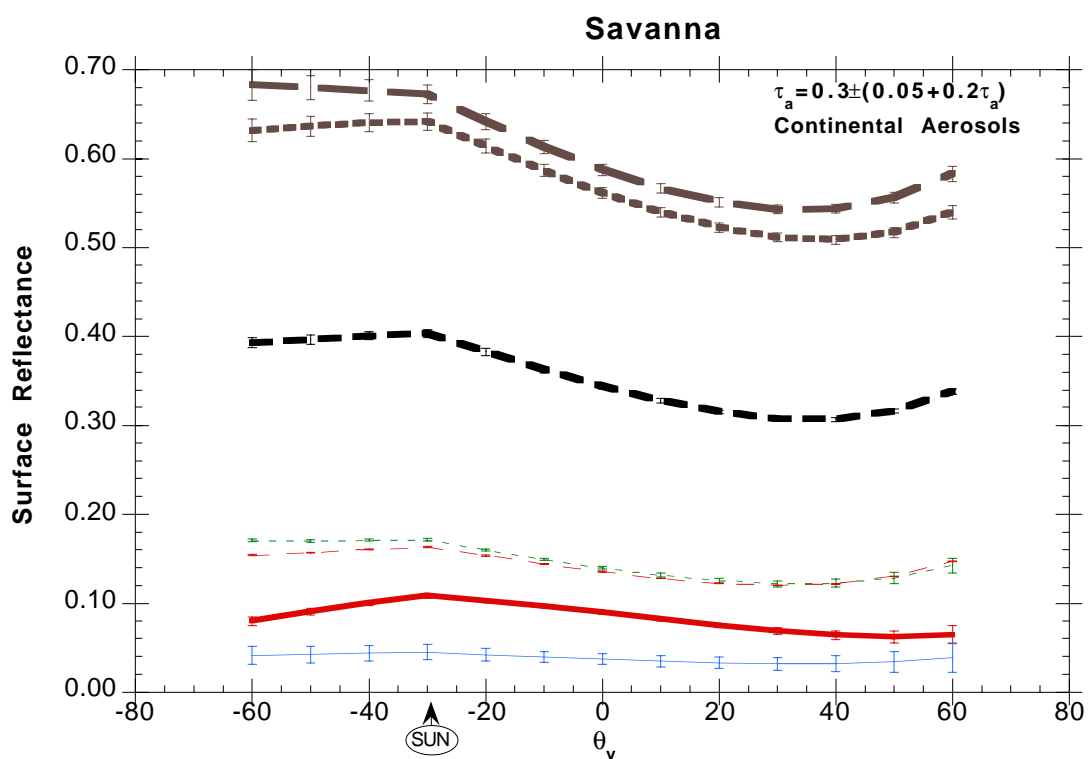


Figure 14

The impact of the uncertainty on surface reflectance retrieval will lead to typical errors :

band	abs. error of SR for $\delta_A(.55\mu\text{m})=0.1$	abs. error of SR for $\delta_A(.55\mu\text{m})=0.5$
1	0.003	0.008
2	0.008	0.018
3	0.006	0.013
4	0.003	0.007
5	0.007	0.016
6	0.003	0.007
7	0.002	0.004

Impact of AOT uncertainty on surface reflectance retrieval (reflectance units)

Aerosol Model

The choice of aerosol model which will determine the phase function, $P_a(\theta)$, and single scattering albedo, ω_{0a} , used by the radiative transfer code is an important source of uncertainty. Presently we can assign aerosol models only according to geographical location, season or aerosol loading. These criteria do not necessarily produce accurate representations of the aerosol size distribution or aerosol absorption. Uncertainty in the input phase function, $P_a(\theta)$, can cause uncertainty in the correction by as much as 0.02 in reflectance units for a surface reflection of 0.05 as described by Fraser et al. (1989) and Fraser et al. (1992). Uncertainty in the input ω_{0a} caused smaller uncertainties, less than 0.005. For the MODIS aerosol algorithms, τ_a is obtained from path radiance estimations (L_0). In this case the accuracy of the correction will be better than the accuracy reported above due to a self compensating error. We performs sensitivity study to determine the impact of an error on the aerosol model, by correcting with a continental model when the actual aerosol was dust (background desertic model in 6S) or smoke (biomass burning model in 6S). The three models (continental,dust,smoke) have different phase functions, single scattering albedos and spectral dependence of extinction coefficients which are expected to cover the range of actual conditions. The compensation process was taken into account, as it can be seen on Figure 15a,b, the error on correction of channel used to derive aerosols (band 1,3) is relatively small, error in other channels can be much higher (band 2).

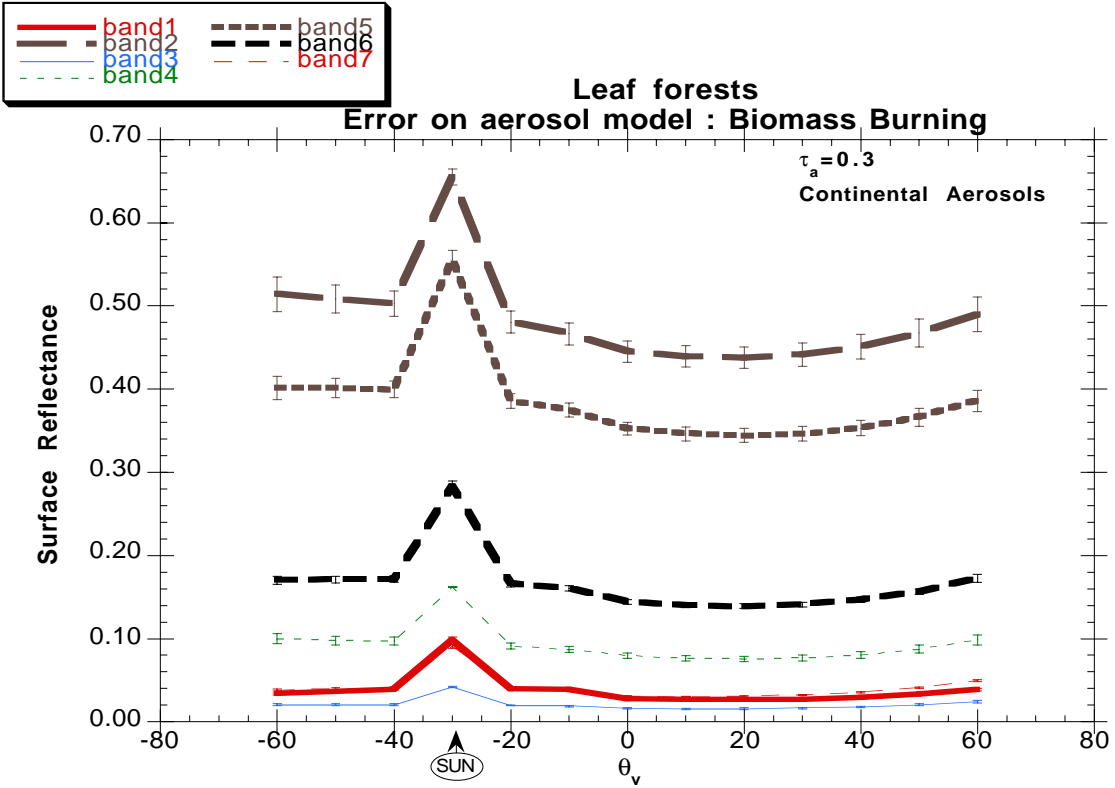


Figure 15a

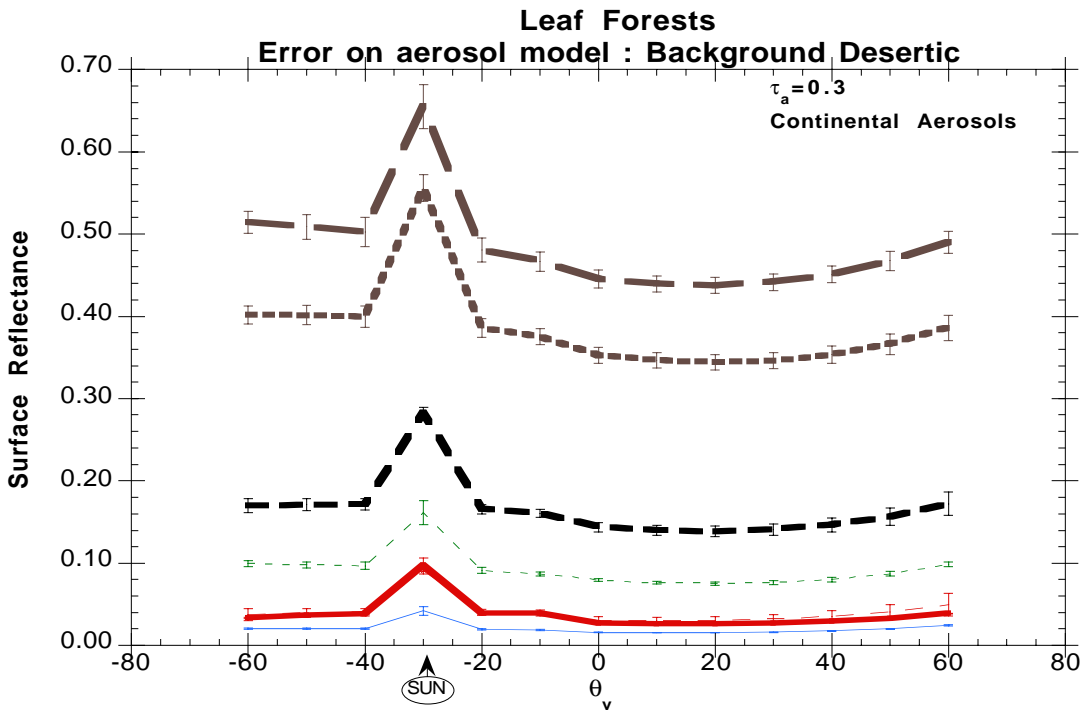


Figure 15b

The typical errors estimated are (for $\delta_A(.550 \mu\text{m})=0.3$ and sun zenith angle of 30°) :

band	abs. error
1	0.002
2	0.017
3	0.002
4	0.005
5	0.016
6	0.009
7	0.006

Impact of aerosol model uncertainty

Lambertian Approximation Error

This error results from assuming a Lambertian surface and using an equation similar to Eq. (2) in place of Eqs. (15,16). The Lambertian approximation error may be the most important error in the atmospheric correction process. Lee and Kaufman (1986) quantify the error due to Lambertian approximation based on radiative transfer simulation at 0.65 and $0.85 \mu\text{m}$ using ground boundary conditions for pasture, forest and savanna as measured by Kriebel et al. (1978). In the backscattering direction (hotspot) the error ranges from 0.02 to 0.06 in reflectance units for a clear atmosphere to 0.03 - 0.11 for a hazy atmosphere ($\tau_a=0.5$) for a solar zenith angle of 60° . The error is smaller outside of the backscattering direction and is expected to be larger at short wavelengths and with increasing solar zenith angle. Figure 16 shows for one case the error produced by the lambertian approximation. Figure 16 also shows the error done (error bars) if we use equations (15,16) with the a first guess BRDF model, in that case we use a broadleaf BRDF to correct the grasses case. The error is substantially lower than the lambertian approximation.

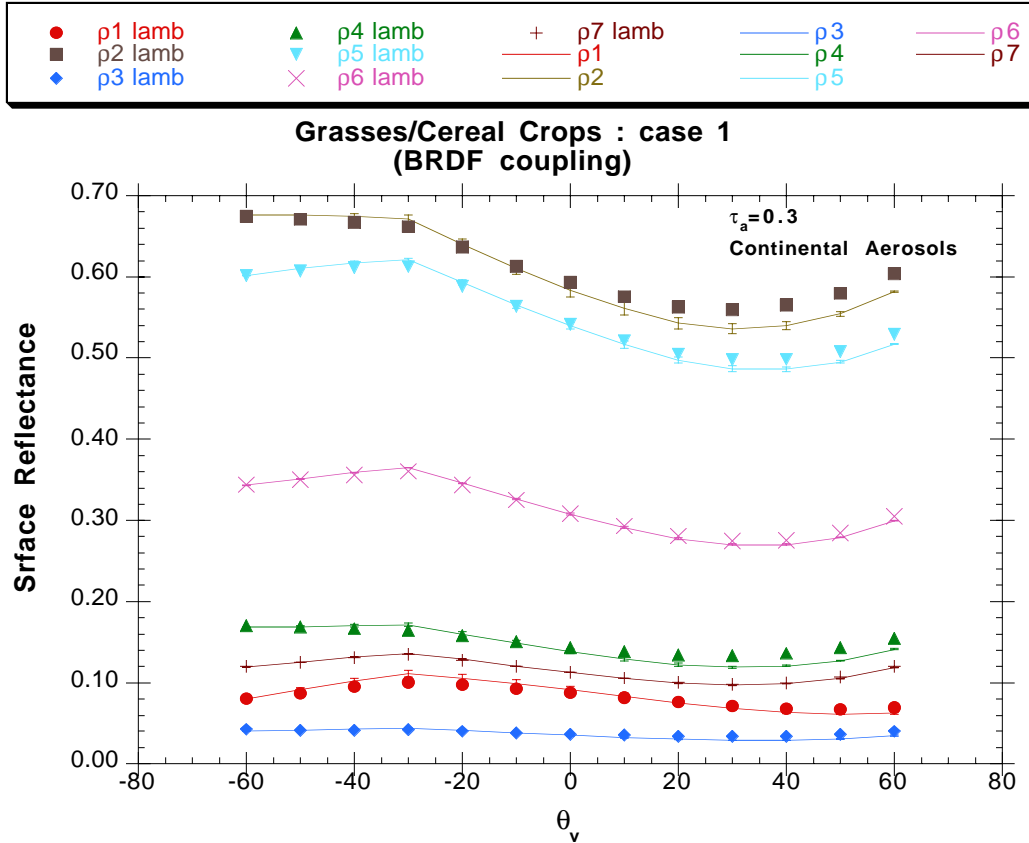


Figure 16

In the backscattering direction, relative and absolute errors resulting from BRDF uncertainty (Atmospheric correction over shrubland cover corrected assuming leaf forest BRDF) are:

band	rel. error (%) and abs. error backscattering direction	
1	9	0.003
2	2	0.011
3	8.5	0.002
4	4.5	0.003
5	1.5	0.007
6	1	0.003
7	1	0.001

Impact of BRDF uncertainty

Total theoretical typical accuracy :

band	abs. error	rel. error % (range)
1	0.005	10-33
2	0.014	3-6
3	0.008	50-80
4	0.005	5-12
5	0.012	3-7
6	0.006	2-8
7	0.003	2-8

Gaseous Absorption, Polarization, Vertical Distribution

Errors caused by uncertainties in gaseous absorption, polarization, and vertical distribution of aerosols were all found to be less than 0.005 in reflectance units for a surface reflectance of 0.05 by Fraser et al. (1989) and Fraser et al. (1992).

Adjacency Effect

The adjacency effect correction gives an approximation which is an exact solution in the case of a homogeneous background. Application of the correction to SPOT data for a target with reflectance of 0.20 surrounded by a dark background reduces the error from adjacency effect at 550 nm from 0.005 to less than 0.001 in reflectance units (Vermote, 1990). Because pixel size is larger for MODIS than for SPOT we expect errors from this effect to be even smaller and the final values after correction to have even less error. A complete sensitivity study to address that error is being done.

Cirrus Effect

We presently do not know the uncertainties involved with using Eq. (10) to

correct for cirrus contamination; however, this procedure will translate a systematic bias to random error in the following manner. Ignoring thin cirrus will cause a universal brightening of surface reflectances. By subtracting the 1.38 μm reflectance from the apparent reflectance the surface reflectances are now sometimes too bright or too dark, but the average value is closer to their actual value without the cirrus contamination.

Look-Up Table Interpolation

As explained in section 3.1.2, we created look-up tables with the 6S code to supply the needed $\rho_0(\mu_s, \mu_v, \phi)$, $t_d(\mu)$, S for a variety of sun-view geometries and aerosol loadings. Similar look-up tables are described in Fraser et al.(1989, 1992). Fraser et al. (1992) report that errors in the derived surface reflectance resulting from interpolation between entries in the look-up table are large only when either sun angle or view angle are extreme ($>70^\circ$). Uncertainty caused by interpolation from the look-up table were found to cause errors in the corrected reflectance of less than 0.005 for surface reflectance of 0.05 (Fraser et al., 1989; Fraser et al., 1992). This look-up table consisted of values for 9 solar zenith angles, 13 view angles, 19 azimuthal angles, and 4 aerosol optical thicknesses. A finer resolution table consisting of 22 solar and view zenith angles, and 73 relative azimuth angles reduces the interpolation error to 0.002 in reflectance units.

3.2 Practical Considerations

3.2.1 Numerical Computation Considerations

Nothing to report

3.2.2 Programming/Procedural Considerations

The atmospheric correction algorithm is a mid-level point in the data processing. The atmospheric correction algorithm is a completely automated procedure. The code is written to handle exceptions and errors as they occur.

Estimation of the processing time are given on figure 5.

3.2.3 Data dependencies

The atmospheric correction algorithm uses MODIS products as inputs and produces new products which are in turn used by other MODIS algorithms. The MODIS-derived products used as inputs include: geographically registered and calibrated radiances (MOD02, MOD03) cloud mask (MOD35), spectral aerosol optical thickness (MOD04), precipitable water (MOD05), ozone (MOD07) and surface BRDF product from the 16-D prior period (MOD43). Ancillary data include a Digital elevation Model, Data Assimilation Office (DAO) for surface pressure, water vapor, and ozone, climatological data for water vapor, ozone and aerosol optical thickness.

The algorithm makes use of a look-up table which supply the needed $\rho_o(\mu_s, \mu_v, \phi)$, $t_d(\mu)$, BRDF coupling terms, and s for a variety of geometries and aerosol properties. In this way we avoid the need to run the radiative transfer code for every pixel, an impossible task in terms of CPU. We calculate $\rho_o(\mu_s, \mu_v, \phi)$, $t_d(\mu)$ and s on a grid of 5 km by 5 km, but will provide the corrected reflectance at every pixel. This further reduces the calculation time.

3.2.4 Output product

L2 product:

The MOD09 implemented algorithm will process daily the 7 land bands at 250 m (bands 1 and 2) and 500 m (bands 3-7) (standard DAAC production). The output product contains the estimates of the surface reflectance, QA bit fields and QA metadata for each data granule. The HDF file for the L2 contains the following SDS :

- 1-250 m Surface Reflectance Band 1
- 2-250 m Surface Reflectance Band 2
- 3-500 m Surface Reflectance Band 3
- 4-500 m Surface Reflectance Band 4
- 5-500 m Surface Reflectance Band 5
- 6-500 m Surface Reflectance Band 6
- 7-500 m Surface Reflectance Band 7
- 8-250 m Reflectance Band Quality
- 9-500 m Reflectance Band Quality
- 10-1 km Reflectance Data State QA

L2G and L3 products:

A level 2G (daily) and a level 3 land (8-day) surface reflectance will be based upon the Level 2 data. The level 3 is a 8-day composite. The compositing technique suggested is based on the minimum-blue criterion that selects the clearest conditions over the period (See prototyping activities).

The surface reflectance is the input for the production of the MODLAND group's surface products: vegetation index, BRDF/surface albedo, land cover change and LAI/FPAR.

3.2.3 Validation

Validation activities can be divided into pre-launch validation of the algorithm and post-launch validation of the product. Various approaches can be adopted for validation. The Surface Reflectance Product validation will use a combination of ground based measurements, airborne measurements, comparison with other sensor data and image analysis.

The mainstay of the pre-launch validation of the algorithm will be the use of sun photometer data collected at a series of test sites with known land cover characteristics in conjunction with data from existing sensor systems e.g. TM, MAS and AVHRR. We will build on the experience developed using the LTER/Sunphotometer atmospheric correction validation project (figure 17). The proposed algorithm will be prototyped using AVHRR 1km data.. An assessment will be made of the algorithm performance and the impact of errors in the aerosol input product and in using the aerosol climatology. MAS data acquired by the ER2 will be used to provide additional validation in bands unavailable on the AVHRR (see figure 18). Flights will be coordinated with other members of the MODIS team and will require contemporaneous sun photometer data. The existing sun photometer network is shown in figure 18. Ideally this network will be expanded by the EOS Validation Program to include sufficient sites to represent the range of atmospheric conditions and surface types. Advantage will be taken of data suitable for the algorithm validation collected as part of the NASA intensive field campaigns (e.g. BOREAS and LBA) or through EOS coordinated field validation programs (e.g. SCAR campaigns). In the pre-launch period, we will also assist in defining and testing generic image validation tools suitable for use by the MODIS

Science Team planned for development by MODIS SDST, ECS or other instrument teams e.g. time series video looping.

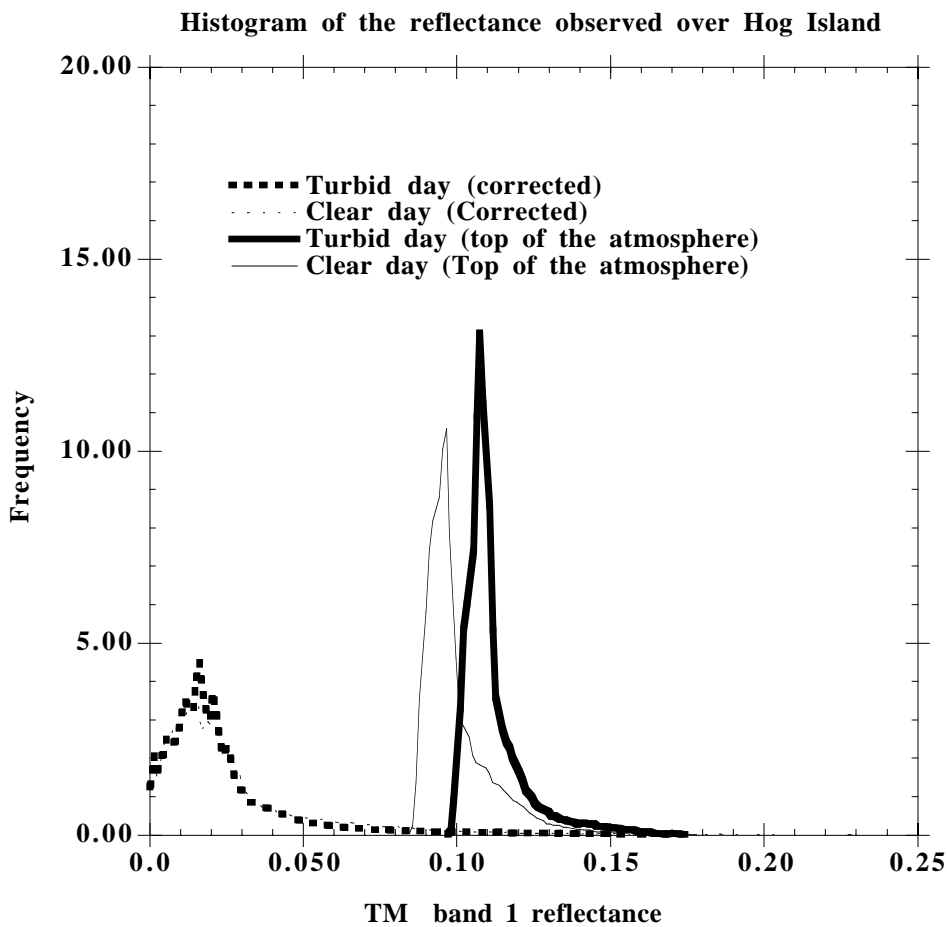


Figure 17: test of the result of the atmospheric correction procedure (including aerosol retrieval and atmospheric point spread function correction) for a 1000x1000 TM pixels area of the Hog Island site for the clear and hazy day for TM band 1.

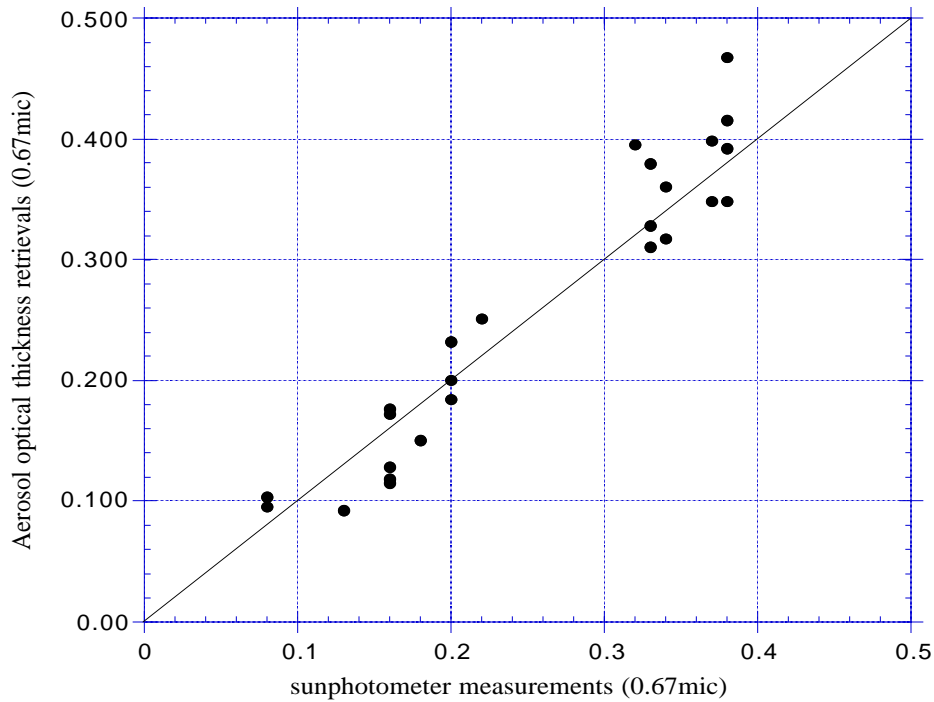


Figure 18: Retrieval of aerosol optical depth using the dark target technique with the 2.14 μ m from MODIS Airborne simulator data during the SCAR-A experiment (Roger et al, 1994)

In the post-launch period emphasis will be given to product validation including automated assessment of the quality flags, statistical analysis of time series data and visual inspection of sample imagery. Initial attention will be given to understanding the quality of the instrument calibration and the 1B product, which will be used as input to the surface reflectance product. A close link will be developed with the MODIS Calibration Support Team (MCST) and the MODIS Calibration Scientist. We will contribute to the MODIS post-launch vicarious calibration by applying the technique developed for the AVHRR (Vermote and Kaufman, 1995).

The technique relies on using using high altitude (12 km and above) bright clouds as "white" targets for intercalibration between channels in the visible, near infrared range. Ocean glint can be used at larger wavelengths . Using intercalibration between a shorter wavelength channel and near infrared, an absolute calibration of first channel can be deduced using ocean off-nadir view (40°-70°) in channel 1 and 2 and correction for the aerosol effect. In this process the second channel to correct aerosol effect in the first channel 1. Figure 19 shows the results of intercalibration of channel 1 and 2 for NOAA7,9,11 using the cloud technique. Figure 20 shows for the results of the absolute calibration derived for channel 1.

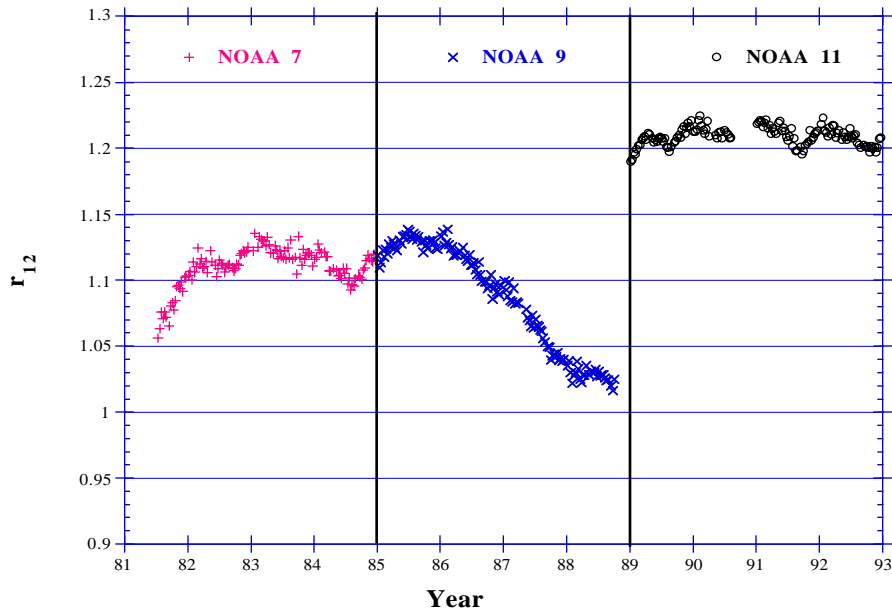


Figure 19: Intercalibration between AVHRR channel 1 and 2, r_{12} as observed over high reflective clouds for NOAA7-9-11 (Vermote and Kaufman, 1995).

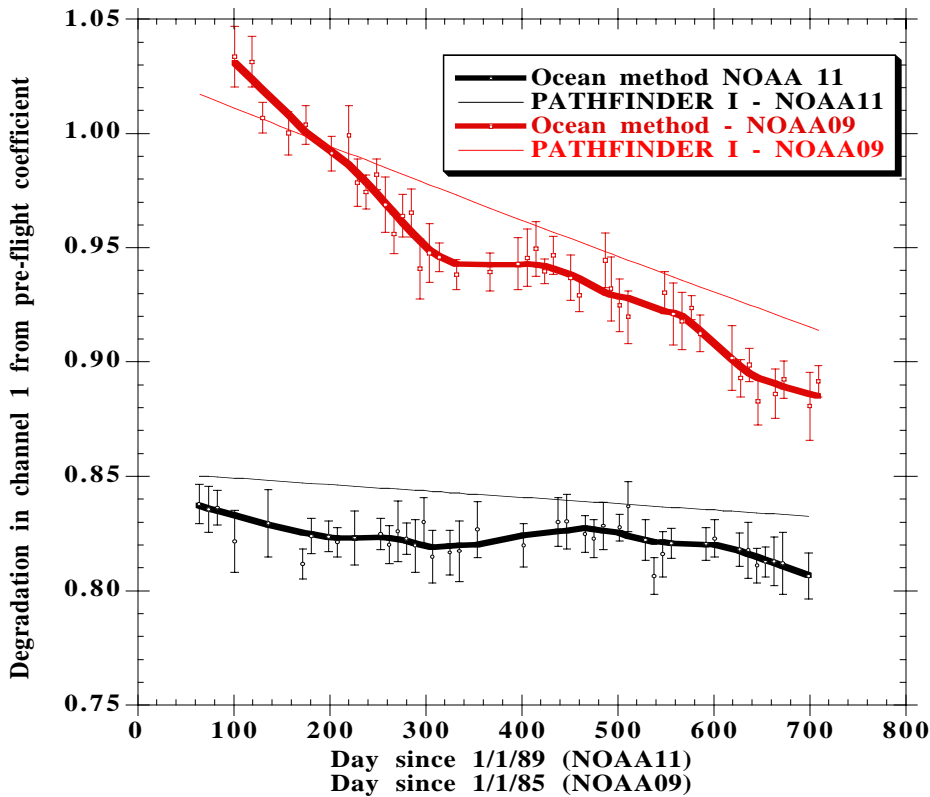


Figure 20: Absolute calibration of NOAA-9,11 AVHRR channel 1 using the ocean method, The results are normalized to the by NOAA pre-flight calibration (Vermote and Kaufman, 1995). Also shown is the Pathfinder recommended calibration

In a post launch phases, validation of the MODIS surface reflectance products will be done at a field campaign level and at a more continuous level through validation sites. Prototype of the validation site are being designed now. Although details of the validation plan are included in the MODIS Land Validation plan available on the WWW from the EOS Validation Office, several key points are outlined here. The MODIS land products will be validated at test sites grouped according to a five-tier system. The system is based on the instrumentation and activities occurring at the sites, and include: 1) intensive field campaign sites (e.g., FIFE, BOREAS, LBA), 2) fully instrumented sites (e.g., ARM/CART), 3) biome tower sites (e.g., Harvard Forest LTER), 4) globally distributed test sites (e.g., NOAA CMDL), and 5) instrument calibration sites (White Sands). The number of sites increases from only a few tier 1 and 2 sites to perhaps 60 tier 4 sites, while the instrumentation

and investment per site decreases from tiers 1 and 2 to tier 4.

Full atmosphere and surface characterization generally will be available for the tier 1 and 2 sites as these typically involve simultaneous sun photometer measurements, aircraft overflights, and full surface and atmosphere radiometry. Although we will extensively use data from the CIMEL sunphotometer (see below), other instrumentation such as spectrometers and shadow-band radiometers normally are available at these sites. In addition, vegetation biophysical variables are typically well sampled. Although expense prevents a large number of tier 1 and 2 sites from being developed or operated over long periods, these sites will present the best opportunities for end-to-end product validation and error analysis. Thus, we expect our most comprehensive algorithm testing will be completed at these sites, and we will participate as opportunities exist.

Because the few tier 1 and 2 sites will not be able to represent the broad range of climate/land cover combinations encountered globally, we will rely on the more instrument-limited tier 3 and 4 sites for continuous global validation. Currently, we plan to collaborate with existing tower sites maintained under various “network” studies (e.g., EUROFLUX, LTER, AMERIFLUX, AERONET). To minimize costs, and thus increase the number of sites, we propose that each tower site include a CIMEL sunphotometer (~\$20,000) mounted well above the canopy top. With the current software used in the AERONET sunphotometer network, CIMEL data allow retrieval of the aerosol optical depth and phase function. Augmented with new surface BRDF software being developed by the CIMEL company and tested by MODLAND, the sunphotometer will measure the surface-leaving radiance over a large range of view angles—including the MODIS-view angles. Again using the AERONET model, the data will be uplinked in real-time to a satellite and received at our SCF. This abundant data resource will allow continuous evaluation of the aerosol optical depth input to our algorithm, and the BRDF-atmosphere coupling terms (including the bihemispherical reflectance distribution function [BHRF] and the hemispherical directional reflectance distribution [HDRF], which represents the convolution of the total irradiance with the surface BRDF). Note the deconvolved surface reflectance product cannot be measured independently, and therefore we must rely on ground-measured HDRF values to validate our algorithm and product.

The tier 3 and 4 tower configuration, complete with the modified CIMEL sampling program, will be rigorously tested in 1997 during two MODLAND prototype validation campaigns. Although the exact sites and times are still under review, we will set up the tower and ground instrumentation for 10 day periods at both a tall canopy (e.g., forest) site and a short canopy (e.g., grassland) site. In addition, we are scheduling aircraft sensor overflights (e.g., MAS and AVIRIS) and ground biophysical characterization (LAI, fAPAR) while collecting the tower instrument data. These prototype campaigns should expose any problems in our instrumentation or sampling scenarios (time or space) in time to modify procedures, if necessary, before the actual validation sites are developed. Note that all MODLAND science teams are participating in these prototype campaigns. Both the ASTER and MISR teams have expressed interest in collaborating, and upon finalizing details we expect to involve others—including the successful proposers to the EOS Validation Office Announcement of Opportunity—in these activities.

Overall, we expect to have at least 10 tier 3 and 4 sites instrumented and operating at launch (Phase A), providing an opportunity for immediate product evaluation. Within a year post-launch, we expect to have an additional 10 sites operating (Phase B), and hope to complete a network of 80 total sites by the year 2000 (Phase C). We are currently developing a list of preferred sites for priority instrumentation, and our working closely with the EOS validation office, other AM instrument teams, and network personnel in our planning. Every effort will be made to ensure the sites are relatively homogeneous (or “constantly mixed”), large (at least 2 km x 2 km), and representative of the most spatially extensive and/or biogeochemically-important landcovers.

3.2.4 Quality Control and Diagnostics

The estimates of the surface reflectance is accompanied with quality assurance information. QA bits contain information stored at the product resolution, whereas QA metadata contain overall statistical information of a whole granule calculated from QA bits. The QA data include information on the integrity of the surface reflectance estimate, the successful completion of the correction scheme, the cloud cover, the source of aerosol, water vapor and ozone information.

QA analyses will be performed over a sample of data at different time scales and spatial resolutions. EOS validation sites will be systematically monitored.

A MODIS coarse spatial resolution of the level 2 and the level 3 surface reflectance product have been developed by the SCF for internal QA purposes. These products are not to be archived and should only be distributed to the GSFC Land SCF or the MODLAND Land Data Operational Product Evaluation Group (LDOPE). A preliminary QA will be performed every day on these coarse resolution products. It should allow a rapid global assessment of the data quality. With the metadata stored LDOPE QA database, it will help the selection of granules or tiles to be ordered for detailed QA.

The algorithm products will be reviewed post-launch to determine whether the corrected surface reflectances are dependent on other variables and in what manner. This may give us insights into possible improvements in the algorithm. For example, an ideal atmospheric correction should produce surface reflectances not dependent on τ_a . However, the algorithm we are proposing for bidirectional effects may not be accurate enough to correct for the dependence between τ_a and surface reflectance due to shadows. This effect is stronger in the forward scattering direction but almost negligible in the backscattering direction (Deering, 1989). For this reason we will look at data only from the backscattering direction in evaluating the algorithm's dependence on τ_a . Dependence of corrected surface reflectance on τ_a in the backscattering direction points to errors in the aerosol phase function or to errors in the single scattering albedo (Fraser and Kaufman, 1985).

We developed an "investigative tool" that can detect such data dependency. This tool is based on the 6S radiative code and will be used as a "flexible MOD09". It allows modifying some of the input (e.g. aerosol optical thickness, aerosol model). It will be very useful to verify that the processing of the L1B data is working correctly (DAAC benchmarking).

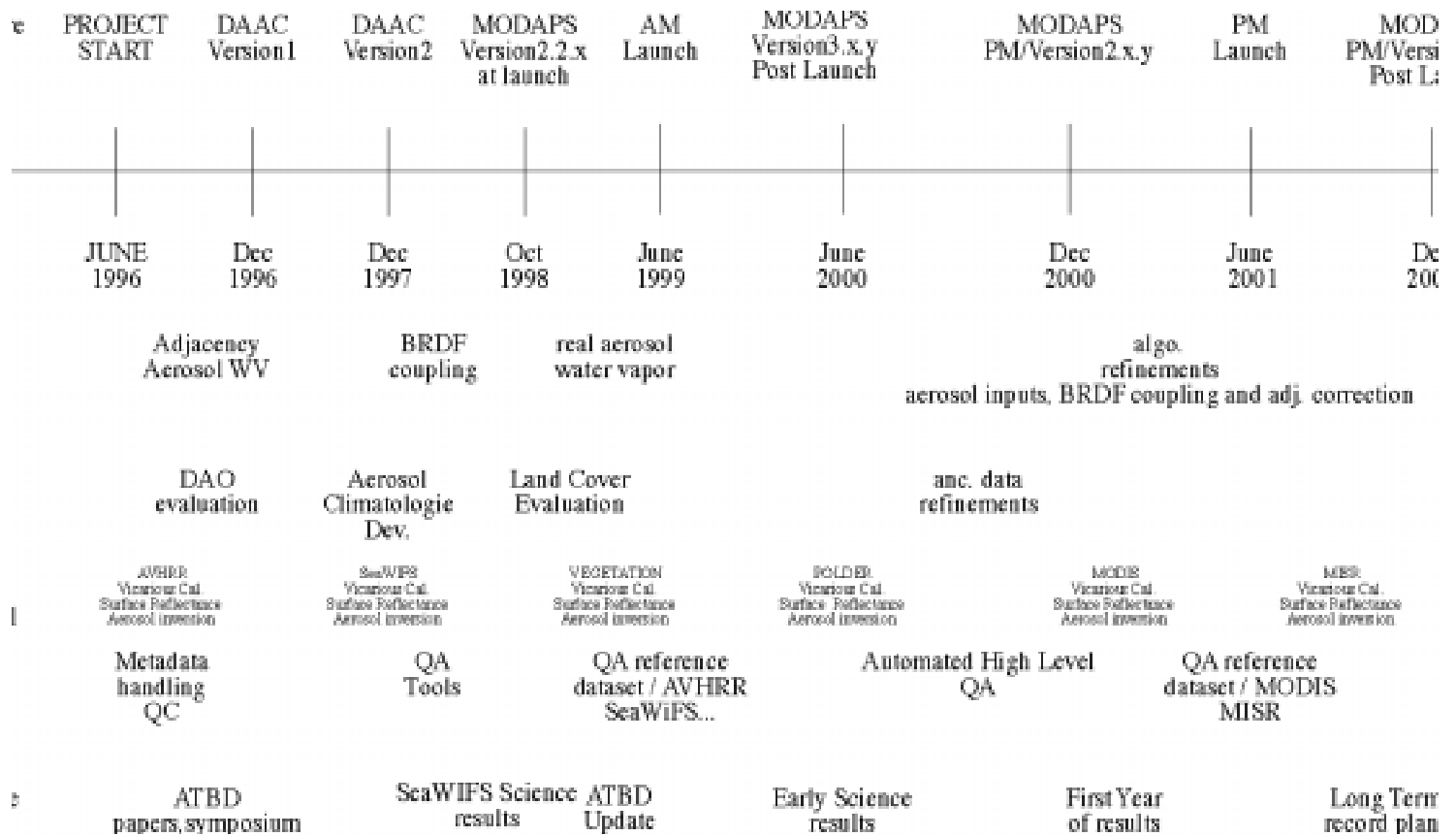
3.2.5 Exception Handling

Exception handling will be built into the code. Extreme angles and extreme input parameters will be flagged. Cloud and cirrus contamination will be noted. Missing data will also be noted.

4. Constraints, Limitations and Assumptions

This algorithm is constrained to land areas and will be most accurate in regions where the aerosol optical thickness is derived from MODIS products. These are areas with sufficient dense, dark vegetation. "Clear" climatological values of optical thickness still need to be measured in most parts of the world. This fact limits the accuracy of the at-launch algorithm. Furthermore, in the case of an important volcanic eruption (e.g. Mt Pinatubo) it appears essential that the MODIS aerosol product (Kaufman and Tanre,1998) should de-couple the stratospheric and tropospheric aerosol contribution. Errors in de-coupling this product will limit the accuracy of the derived surface reflectance during volcanic events. Extreme angles, which may be encountered in polar regions may cause large errors.

5. Research Agenda



REFERENCES

F. J. Ahern, R. P. Gauthier, P. M. Teillet, J. Sirois, G. Fedosejevs and D. Lorente, 1991: An investigation of continental aerosols with high spectral resolution solar extinction measurements. *Applied Optics*,**30**,5276-5287.

F. J. Ahern, D. G. Goodenough, S. C. Jain, V. R. Rao and G. Rochon, 1977: Use of clear lakes as standard reflectors for atmospheric measurements. in *Proc. 11th Int. Symp. on Remote Sens. of Environ.*, Ann Arbor MI. 731-755.

G. A. d'Almeida, P. Koekpe and E. P. Shettle, 1991: in *Atmospheric Aerosols Global Climatology and Radiative Characteristics*. Hampton. A. Deepak Publishing, 561 pp.

J. V. Dave and J. Gazdag, 1970: A modified Fourier transform method for multiple scattering calculations in a plane parallel Mie atmosphere. *Applied Optics*,**9**,1457-1466.

D. W. Deering, 1989: Field measurements of bidirectional reflectance. in *Theory and Applications of Optical Remote Sensing*, ed. G. Asrar, New York. Wiley & Sons, 734 pp.

P. Y. Deschamps, M. Herman and D. Tanre, 1983: Modeling of the atmospheric effects and its application to the remote sensing of ocean color. *Applied Optics*,**22**,3751-3758.

Descloitres and Vermote, 1999 : Operational retrieval of the spectral surface reflectance and vegetation index at global scale from SeaWiFS data. Proceedings of the International Conference and Workshops on Ocean Color, Land Surfaces, Radiation and Clouds, Aerosols, ALPS99 : The contribution of POLDER and new generation spaceborne sensors to global change studies, Land surfaces-O-02

Deuze, J. L., Herman, M. and Santer, R. (1989), Fourier series expansion of the transfer equation in the atmosphere-ocean system, *J.Q.S.R.T.* 41(6):483-494.

J. Dozier and J. Frew, 1981: Atmospheric corrections to satellite radiometric data over rugged terrain. *Remote Sens. Environ.*,**11**,191-205.

El Saleous, N.Z., Vermote, E.F., Justice, C.O., Townshend, J.R.G., Tucker, C.J., Goward, S.N., 1999, Improvements in the global biospheric record from the Advanced Very High Resolution Radiometer (AVHRR), *International Journal of Remote Sensing*.

R. S. Fraser and Y. J. Kaufman, 1985: The relative importance of scattering and absorption in remote sensing. *IEEE Trans. on Geoscience and Rem. Sens.*,**23**,625-633.

R. S. Fraser, R. A. Ferrare, Y. J. Kaufman and S. Mattoo, 1989: Algorithm for atmospheric corrections of aircraft and satellite imagery. *NASA Technical Memorandum 100751*,98 pp.

R. S. Fraser, R. A. Ferrare, Y. J. Kaufman and S. Mattoo, 1992: Algorithm for atmospheric corrections of aircraft and satellite imagery. *Int. J. Remote Sensing*, **13**, 541-557.

B.-C. Gao and Y.J. Kaufman, 1993: Water vapor retrieval from MODIS.

H. R. Gordon, J. W. Brown and R. H. Evans, 1988: Exact Rayleigh scattering calculations for use with the Nimbus-7 Coastal Zone Color Scanner. *Applied Optics*,**27**,862-871.

B. M. Herman, S. R. Browning and R. J. Curran, 1971: The effect of Atmospheric Aerosols on Scattered Sunlight. *J. Atmos. Sci.*,**28**,419-428.

B. N. Holben, 1986: Characteristics of maximum-value composite images for temporal AVHRR data. *International Journal of Remote Sensing*,**7**,1435-1445.

B. N. Holben, E. Vermote, Y. J. Kaufman, D. Tanré and V. Kalb, 1992: Aerosol Retrieval over Land from AVHRR data-Application for Atmospheric Correction. *IEEE Trans. on Geosci. and Rem. Sens.*,**30**,212-222.

Holben, B. N., Eck, T. F., Slutsker, I., Tanré, D., Buis, J. P., Setzer, A., Vermote, E. F., Reagan, J. A., Kaufman, Y. J., Nakajima, T., Lavenue, F., Jankowiak, I., & Smirnov, A. (1998). AERONET - A federated instrument network and data archive for aerosol

characterization. *Remote Sensing of Environment*, 66(1), 1-16.

R. G. Holm, M. S. Moran, R. D. Jackson, P. N. Slater, B. Yuan and S. F. Biggar, 1989: Surface reflectance factor retrieval from Thematic Mapper data. *Remote Sens. Environ.*, 27, 47-57.

M. E. James, S. N. V. Kalluri and J. R. G. Townshend, 1993: The Pathfinder AVHRR land data set: An improved coarse resolution data set for terrestrial monitoring. *Int. J. Remote Sensing*, submitted.

C. O. Justice, J. R. G. Townshend, B. N. Holben and C. J. Tucker, 1985: Analysis of the phenology of global vegetation using meteorological satellite data. *Int. J. Remote Sensing*, 6, 1271-1318.

C. O. Justice, T. F. Eck, D. Tanré and B. N. Holben, 1991: The effect of water vapour on the normalized difference vegetation index derived for the Sahelian region from NOAA AVHRR data. *Int. J. Remote Sensing*, 12, 1165-1187.

Y. J. Kaufman, 1982: Solution of the equation of radiative transfer for remote sensing over two-dimensional surface reflectivity. *J. Geoph. Res.*, 20, 4137-4147.

Y. J. Kaufman, 1987: The effect of subpixel clouds on remote sensing. *Int. J. Remote Sensing*, 8, 839-857.

Y. J. Kaufman and R. S. Fraser, 1983: Light Extinction by Aerosols During Summer Air Pollution. *J. Clim. App. Meteor.*, 22, 1694-1706.

Y. J. Kaufman, A. Gitelson, A. Karnieli, E. Ganor, R. S. Fraser, T. Nakajima, S. Mattoo and B. Holben, 1993: Size distribution and phase function of aerosol particles retrieved from sky brightness measurements. *J. Geoph. Res. - A*, submitted June.

Y. J. Kaufman and C. Sendra, 1988: Algorithm for automatic atmospheric corrections to visible and near-IR satellite imagery. *Int. J. of Remote Sens.*, 9, 1357-1381.

Y. J. Kaufman and D. Tanré, 1992: Atmospherically resistant vegetation index (ARVI) for EOS-MODIS. *IEEE Trans. Geosci. Remote Sensing*, 30, 261-270.

Kaufman, Y. J., Tanre, D., Remer, L., Vermote, E., A. Chu and Holben, B. (1997), Operational Remote Sensing of tropospheric aerosol over land from EOS moderate resolution imaging spectroradiometer, *J. Geoph. Res. Vol. 102, No14, pp17051-17067*

Y. J. Kaufman and D. Tanré, 1998: Algorithm for remote sensing of aerosol from MODIS. *MODIS Algorithm Theoretical Basis Document*.

Y. J. Kaufman, D. Tanré, B. N. Holben, B. Markham and A. Gitelson, 1992: Atmospheric effects on the NDVI - Strategies for its removal. *International Geoscience and Remote Sensing Symposium (IGARSS)*. Houston, TX. IEEE, 1238-1241.

Kimes, D. S., Newcomb, W. W., Tucker, C. J., Zonneveld, I. S., Van Wijngaarden, W., De Leeuw, J. and Epema, G. F., 1985, Directional Reflectance Factor Distributions for Cover Types of Northern Africa. *17*, 1-19.

M. D. King, Harshvardhan and A. Arking, 1984: A model of the radiative properties of the El Chichon stratospheric aerosol layer. *J. Clim. Appl. Meteorol.*,**23**,1121-1137.

K. T. Kriebel, 1978: Measured directional reflection properties of four vegetated surfaces. *Applied Optics*,**17**,253-259.

Kuusk A. A,1994 a multispectral canopy reflectance model., *Remote Sens. Environ.*, 1994, 50:75-82.

T. Y. Lee and Y. J. Kaufman, 1986: Non-Lambertian effects on remote sensing of surface reflectance and vegetation index. *IEEE Trans. Geoscience and Rem. Sens.*, **GE-24**,699-708.

J. Lenoble, 1993: *Atmospheric Radiative Transfer*. Hampton, VA. A. Deepak Publishers, 532 pp.

R. A. McClatchey, R. W. Fenn, J. E. A. Selby, F. E. Volz and J. S. Garing, 1971: *Optical properties of the atmosphere*. AFCRL-71-0279, Air Force Cambridge Research Lab, Hanscom AFB MA.

M. P. McCormick and R. E. Viegas, 1992: Sage II Measurements of early Pinatubo Aerosols. *Geophysical Research Letters*,**19**,155-158.

Y. Mekler and Y. Kaufman, 1980: The effect of earth's atmosphere on contrast reduction for a nonuniform surface albedo and two-halves field. *J. Geoph. Res.*,**85**,4067-4083.

M. S. Moran, R. D. Jackson, G. F. Hart, P. N. Slater, R. J. Bartell, S. F. Biggar, D. I. Gellman and R. P. Santer, 1990: Obtaining surface reflectance factors from atmospheric and view angle corrected SPOT-1 HRV data. *Remote Sens. Environ.*,**32**,203-214.

M. S. Moran, R. D. Jackson, P. N. Slater and P. M. Teillet, 1992: Evaluation of simplified procedures for retrieval of land surface reflectance factors from satellite sensor output. *Remote Sens. Environ.*,**41**,169-184.

Ouaidrari H., & Vermote E. F. (1999, in press). LANDSAT TM software for atmospheric correction. *Remote Sensing of Environment*.

J. T. Peterson, E. C. Flowers, G. J. Berri, C. L. Reynolds and J. H. Rudisill, 1981: Atmospheric turbidity over central North Carolina. *J. Appl. Meteor.*,**20**,229-241.

Putsay, M. (1992), A simple atmospheric correction method for the short wave satellite image, *Int. J. Remote Sensing* 13(8):1549-1558.

S. I. Rasool, 1987: Potential of remote sensing for the study of global change. *Advances in Space Research*,**7**,1-90.

J.C. Roger , Eric Vermote and Nazmi El Saleous., 1994, "Atmospheric Correction of MAS data during SCAR-A experiment", *Atmospheric Sensing and Modeling*, Rome, Italy, September 29-30, SPIE proceedings, Vol 2311, pp 83-89.

S. W. Running, C. Justice, V. Salomonson, D. Hall, J. Barker, Y. Kaufman, A. Strahler, A. Huete, J.-P. Muller, V. Vanderbilt, Z. M. Wan, P. Teillet and D. Carneggie, 1994: Terrestrial remote sensing science and algorithms planned for EOS/MODIS. *Int. J. Rem. Sens.*,submitted,

V. V. Salomonson, W. L. Barnes, P. W. Maymon, H. E. Montgomery and H. Ostrow, 1989: MODIS: Advanced Facility Instrument for Studies of the Earth as a System. *IEEE Trans. Geosci. Remote Sensing*,**27**,145-153.

E. P. Shettle and R. W. Fenn, 1979: *Models for the aerosol of the lower atmosphere and the effect of humidity variations on their optical properties*. AFGL-TR-79-0214, Air Force Geophysics Lab., Hanscom AFB, MA.

S. M. Singh, 1988: Simulation of solar zenith angle effect on global vegetation index (GVI) data. *Int. J. Remote Sens.*,**9**, 237-248.

D. Tanré, M. Herman and P. Y. Deschamps, 1983: Influence of the atmosphere on space measurements of directional properties. *Applied Optics*,**21**,733-741.

D. Tanré, M. Herman, P. Y. Deschamps and A. de Leffe, 1979: Atmospheric modeling for space measurements of ground reflectances, including bidirectional properties. *Applied Optics*,**18**,3587-3594.

Tanre, D., Herman, M. and Deschamps, P. Y. (1981), Influence of the background contribution upon space measurements of ground reflectance, *Applied Optics* 20:3673-3684.

D. Tanré, C. Deroo, P. Duhaut, M. Herman, J. J. Morcette, J. Perbos and P. Y. Deschamps, 1990: Description of a computer code to simulate the satellite signal in the solar spectrum: 5S code. *Int. J. Remote Sensing*,**11**,659-668.

Tanré, D., Holben, B. N. and Kaufman, Y. J., 1992: Atmospheric Correction algorithm for NOAA-AVHRR Products: Theory and Application. *IEEE Transaction on Geoscience and Remote Sensing*, **30**, 231-248.

J. R. G. Townshend, 1992: Improved Global Data for Land Applications: A proposal for a New High Resolution Data Set. *Global Change Report*, IGBP.

C. J. Tucker, 1979: Red and photographic infrared linear combinations monitoring vegetation. *Remote Sensing Environment*,**8**,127-150.

C. J. Tucker, 1986: Maximum normalized difference vegetation index images for sub-Saharan Africa for 1983-1985. *International Journal of Remote Sensing*, 7, 1383-1384.

E. Vermote, D. Tanré and M. Herman, 1990: Atmospheric effects on satellite imagery: correction algorithms for ocean color or vegetation monitoring. *International Society for Photogrammetry and Remote Sensing*, 28, 46-55.

Vermote, E. F., El Saleous, N. Z., Kaufman, Y. J. and Dutton, E., 1994, Stratospheric aerosol perturbing effect on the remote sensing of vegetation: Correction method for the composite NDVI after the Pinatubo eruption. *ISPRS symposium on Physical measurements and signature in remote sensing, Val d'Isère, France, January 1994* .

Vermote, E. and Kaufman, Y. J. (1995), Absolute calibration of AVHRR visible and near infrared channels using ocean and cloud views, *I.J.R.S.* 16(13):2317-2340.

Vermote E. F., Tanre D., Deuze J. L., Herman M. and Morcrette J. J., 1997 : Second Simulation of the Satellite Signal in the Solar Spectrum: an overview, *IEEE Transactions on Geoscience and Remote Sensing*, 35,3.

Young, A. T., 1980, Revised Depolarization Corrections for Atmospheric Extinction. *Applied Optics*, 19, 3427-3428.

Young, A. T., 1981, On the Rayleigh-Scattering Optical Depth of the Atmosphere. *Journal of Applied Meteorology*, 20, 328-330.

Young, A. T., 1981, Rayleigh Scattering. *Applied Optics*, 20, 4, 533-535.

Appendix A: Rayleigh Scattering

Rayleigh scattering will be calculated in the following manner. The refractive index of the air, n_s , is calculated for the wavelength, λ , where λ is in cm,

$$(n_s - 1) \times 10^8 = 6593. + \frac{3010189.3}{146 - \lambda^{-2}} + \frac{26113.82}{41 - \lambda^{-2}} \quad (A1)$$

The scattering cross section, σ_λ is given by

$$\sigma_\lambda = \frac{8\pi^3(n_s^2 - 1)^2 (6 + 3\lambda)}{3\lambda^4 N_s^2 (6 - 7\lambda)} \quad (A2)$$

where N_s is the number density of air molecules given by

$$N_s = \frac{6.02253 \times 10^{23}}{22.414 \times 10^3} \quad (A3)$$

and λ is the wavelength. The correction for pressure and temperature is given by

$$N_r(z) = N_s \frac{P(z)}{1013.25} \frac{273.85}{T(z)} \quad (A4)$$

where $P(z)$ is the profile of pressure and $T(z)$ is the temperature profile. The extinction coefficient, β_λ is

$$\beta_\lambda(z) = \sigma_\lambda N_r(z) \times 10^5 \quad (A5)$$

and the Rayleigh optical thickness, τ_R^λ can be calculated as

$$\tau_R^\lambda = \int_0^\infty \beta_\lambda(z) dz \quad (A6)$$

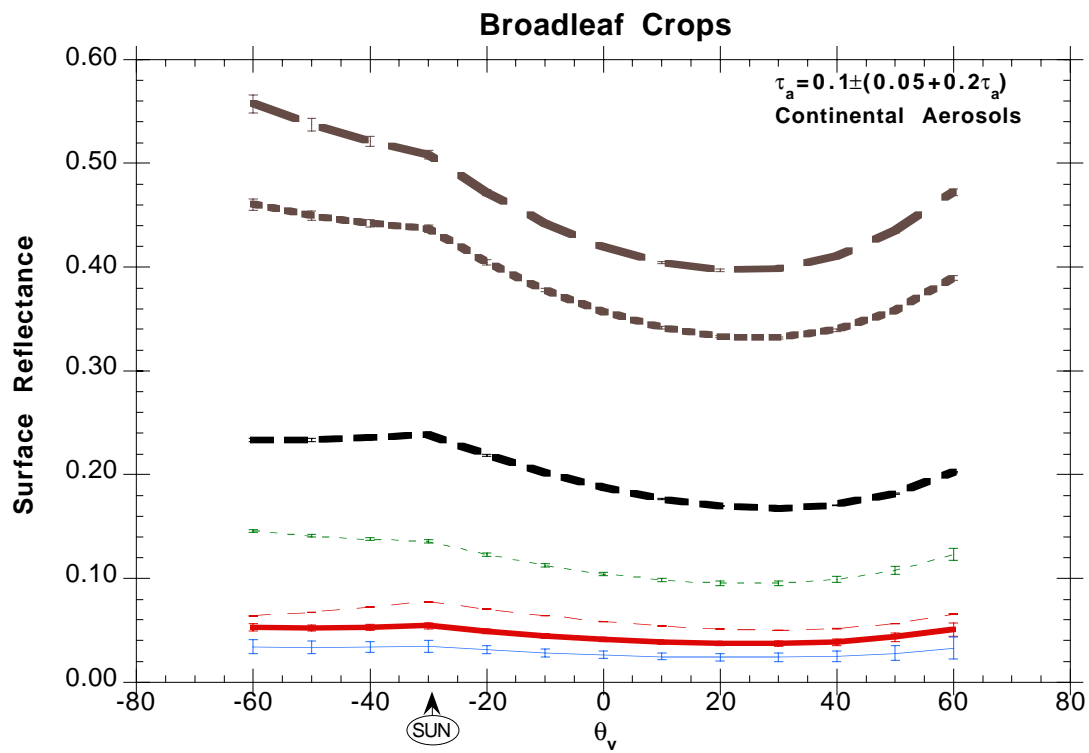
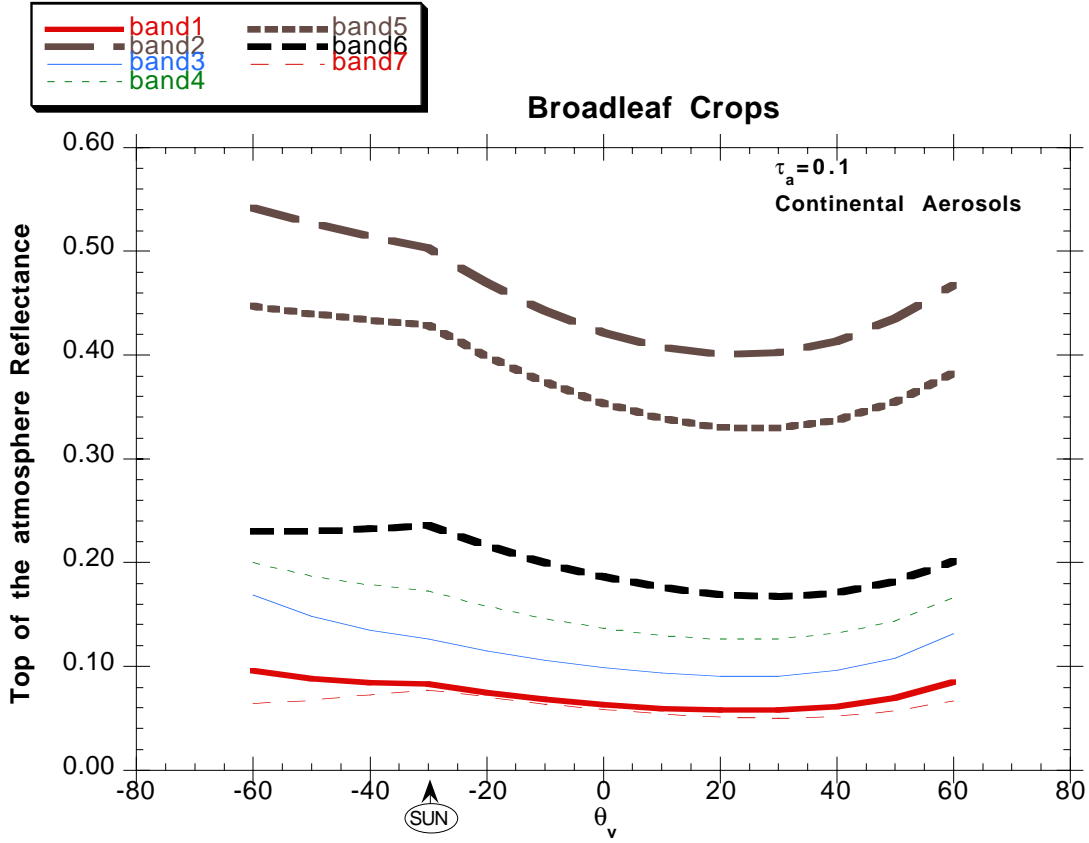
The Rayleigh phase function, $P_R(\theta)$, is calculated from

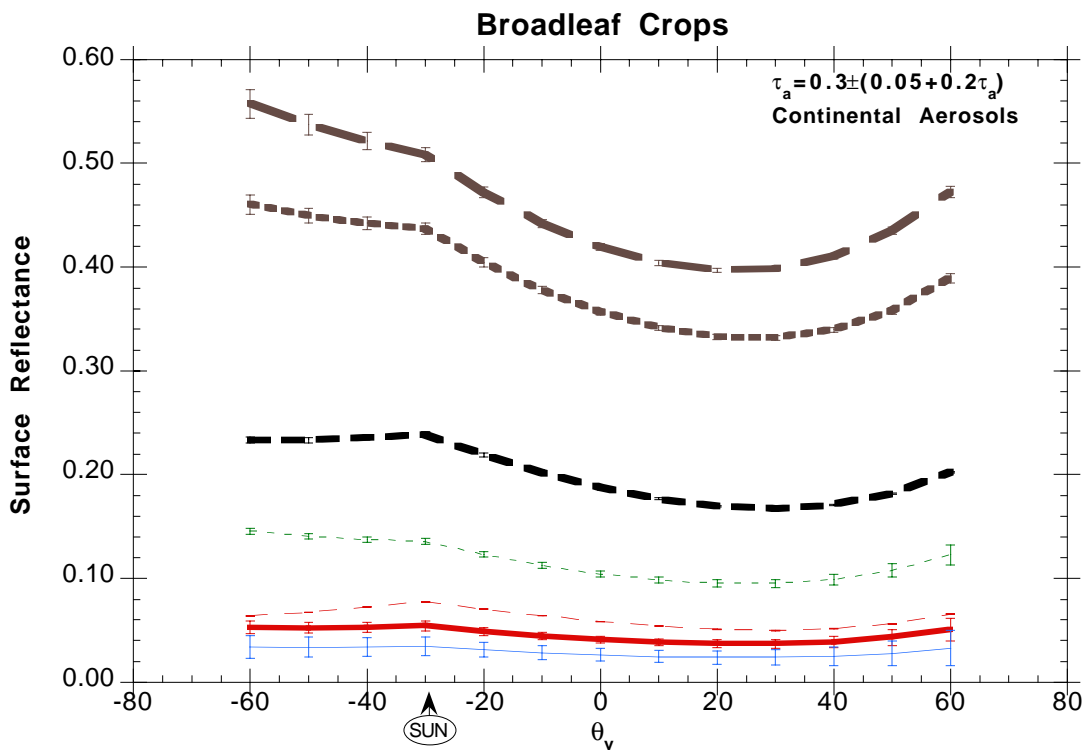
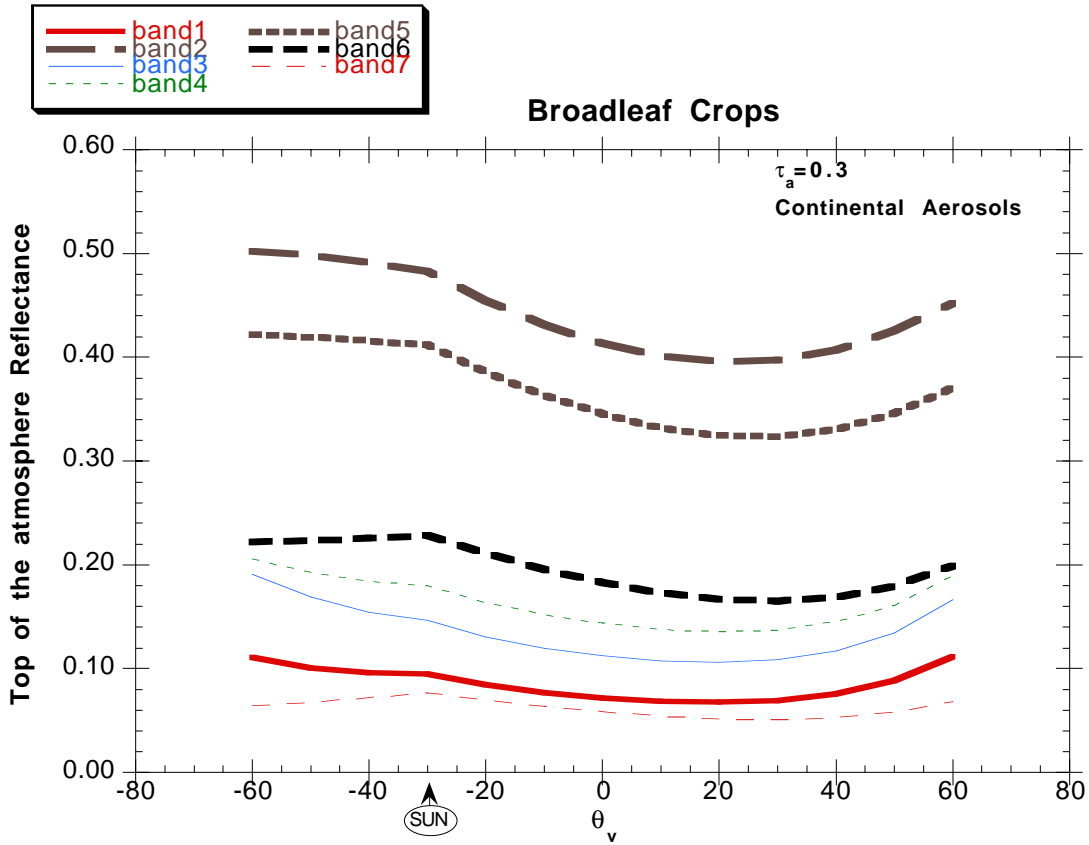
$$P_R(\theta) = \frac{3}{4}(1 + \cos^2 \theta) \left(\frac{1 - \delta_R}{1 + 2\delta_R} \right) \quad (\text{A7})$$

where θ is the scattering angle and δ_R is the Rayleigh polarization factor which we assign a constant value of 0.0279 following Young (1980,1981,1981b).

Appendix B: **Error Sensitivity study**

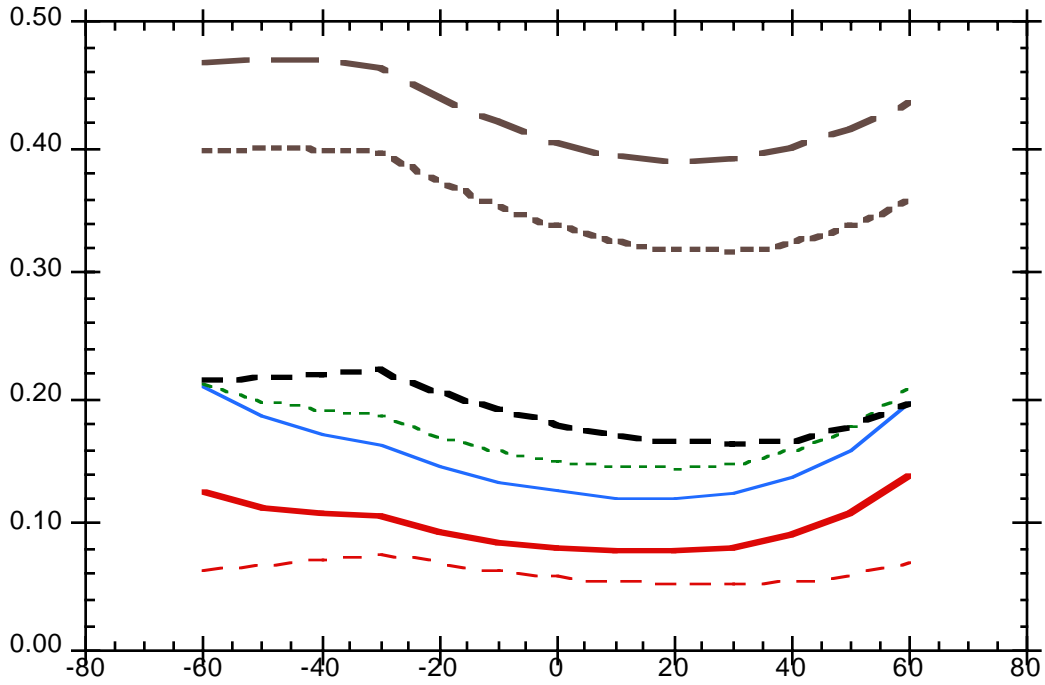
Appendix B1) Top of the atmosphere signal (at 3 optical depths at 550nm: 0.1,0.3,0.5) and sensitivity to error on optical depths (error bars) for each cover type.



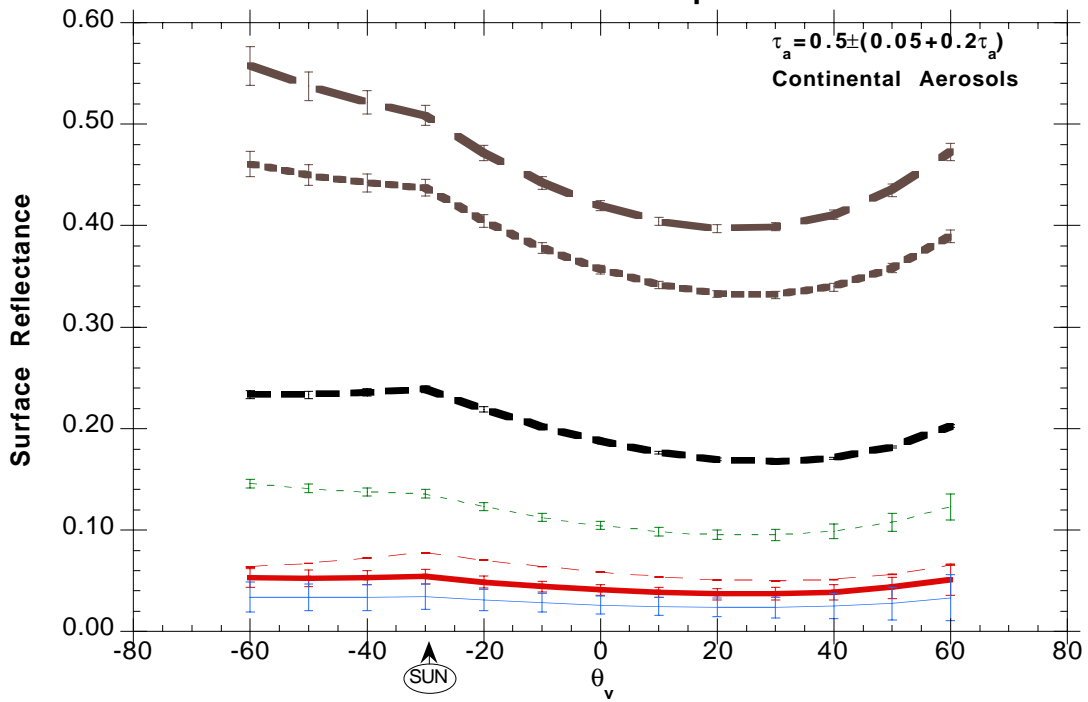


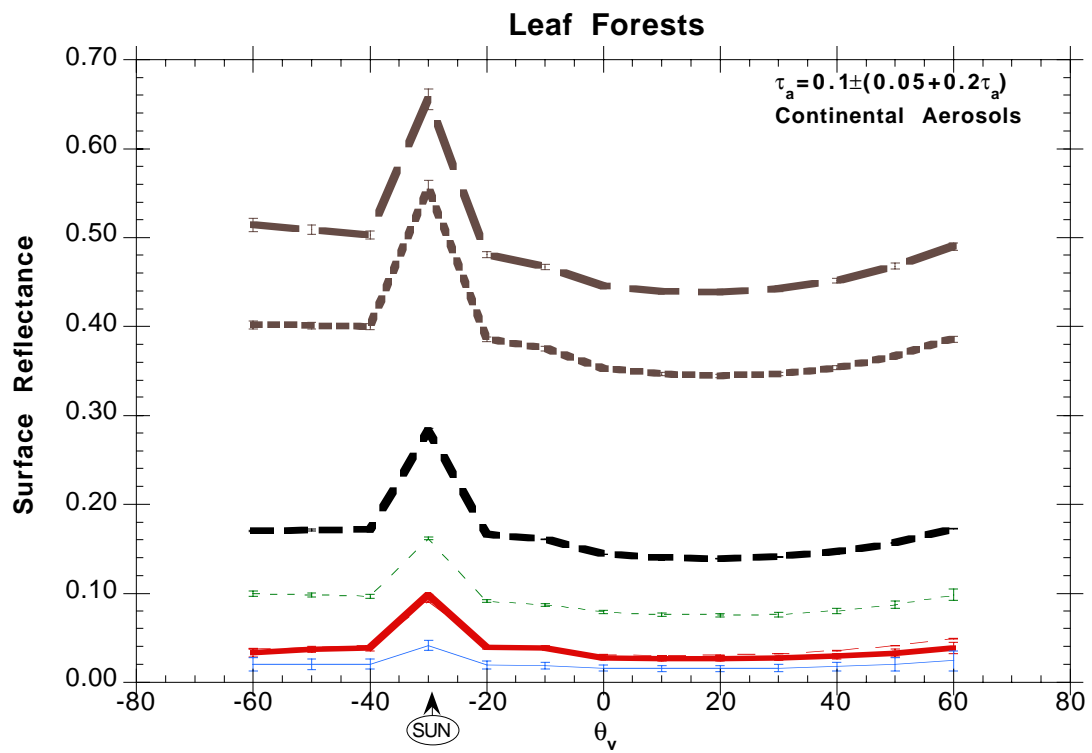
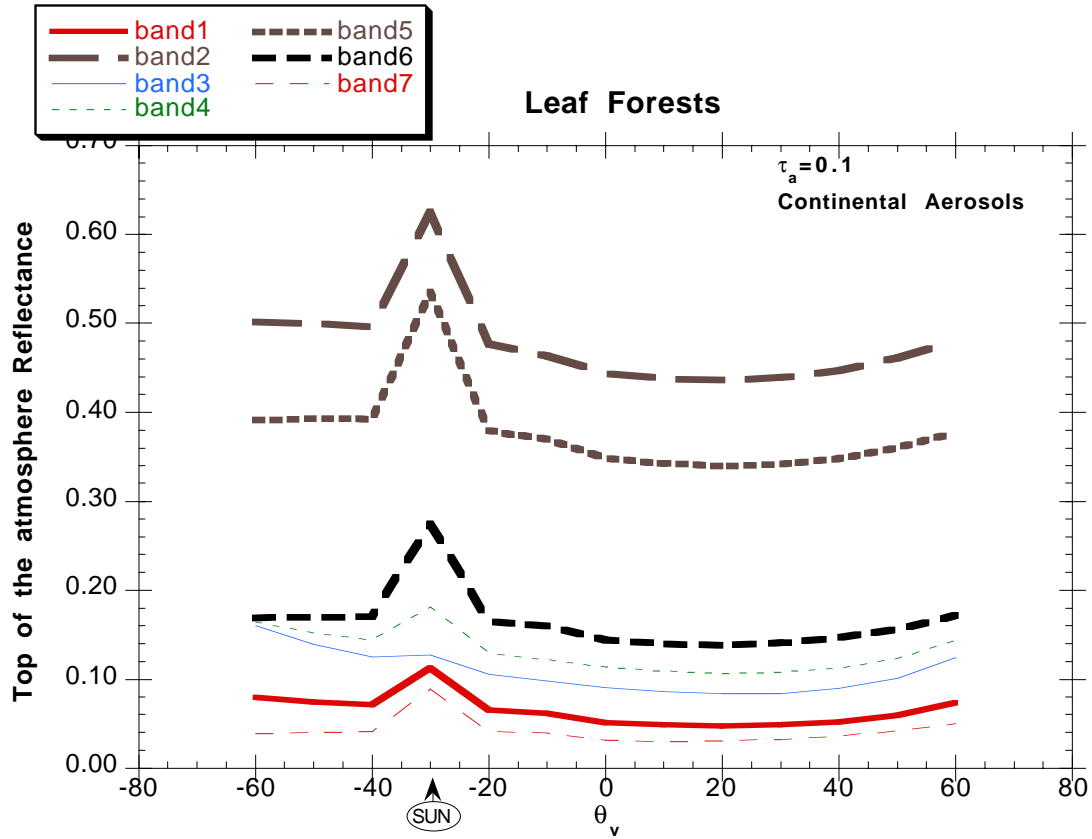


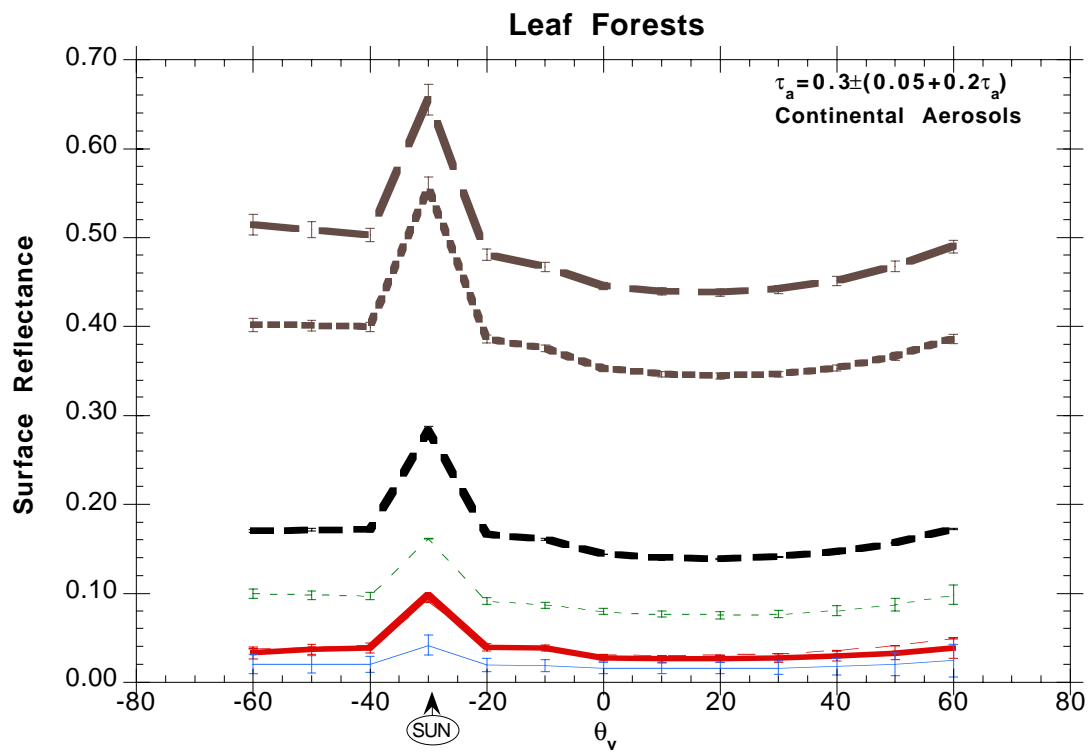
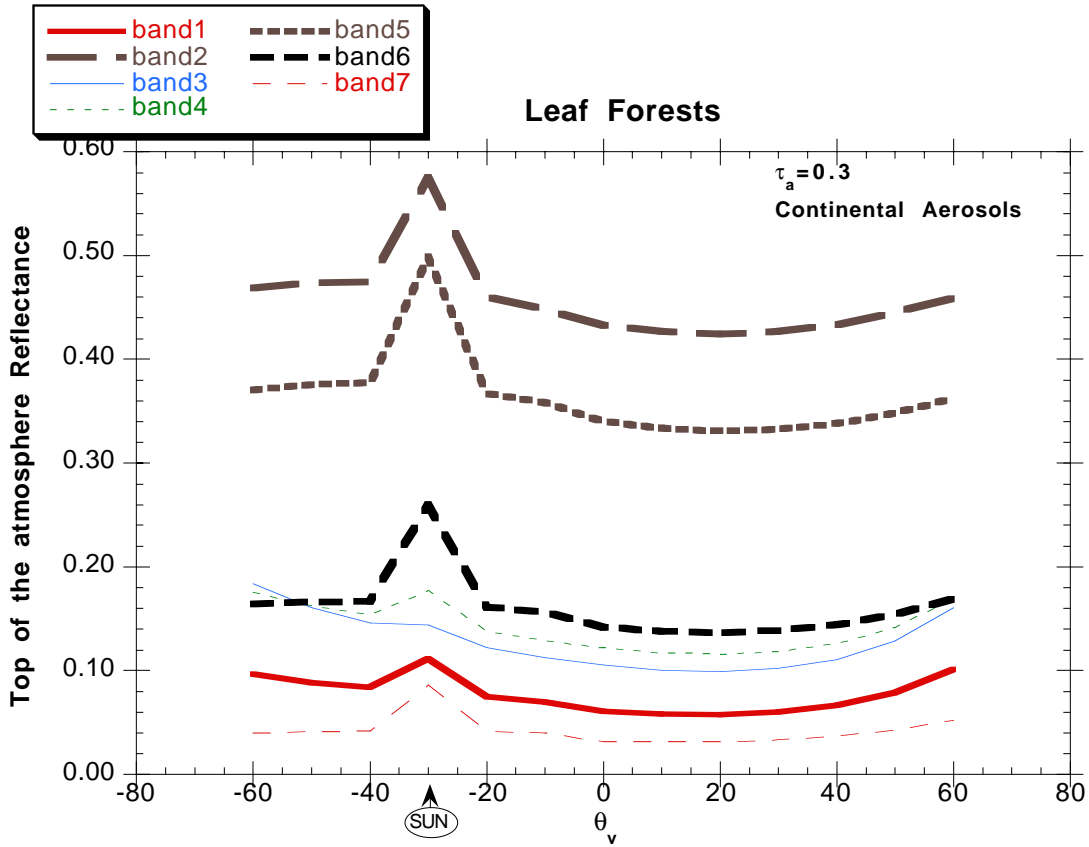
Broadleaf Crops

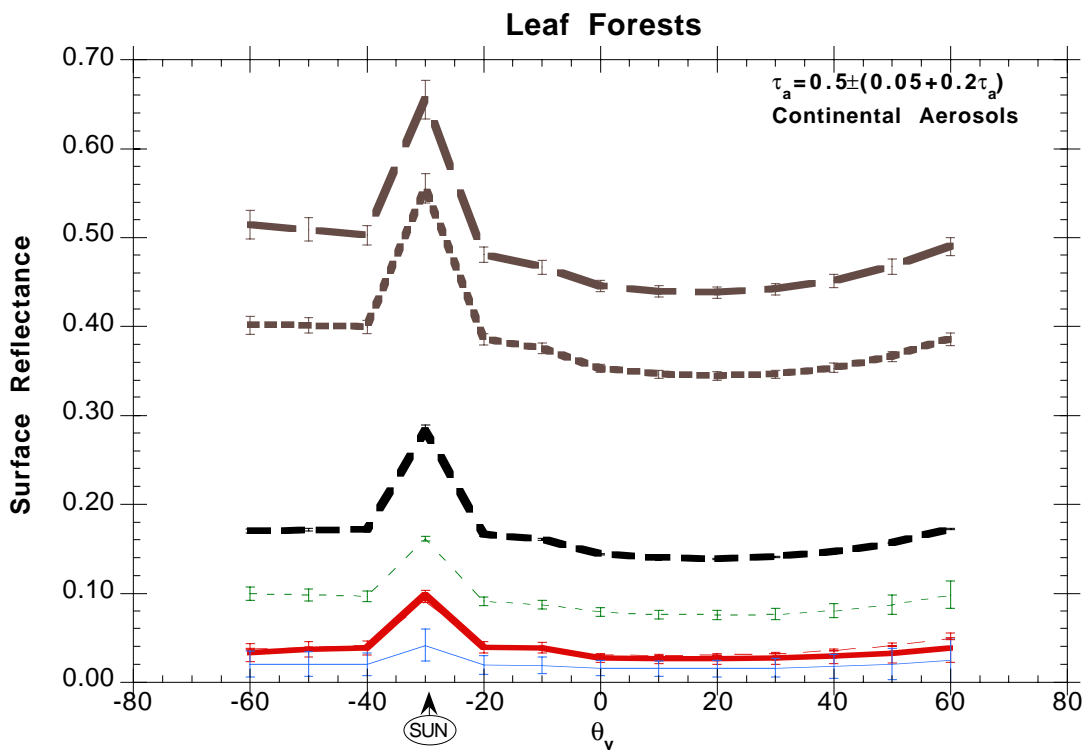
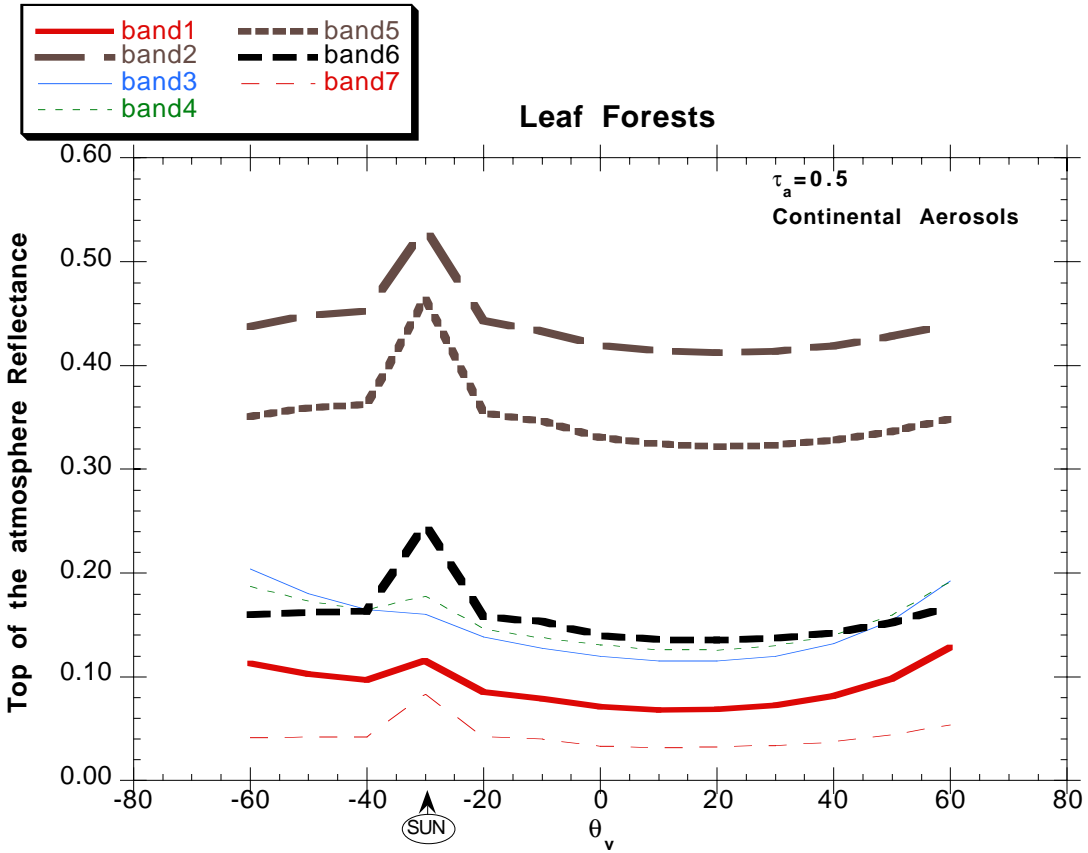


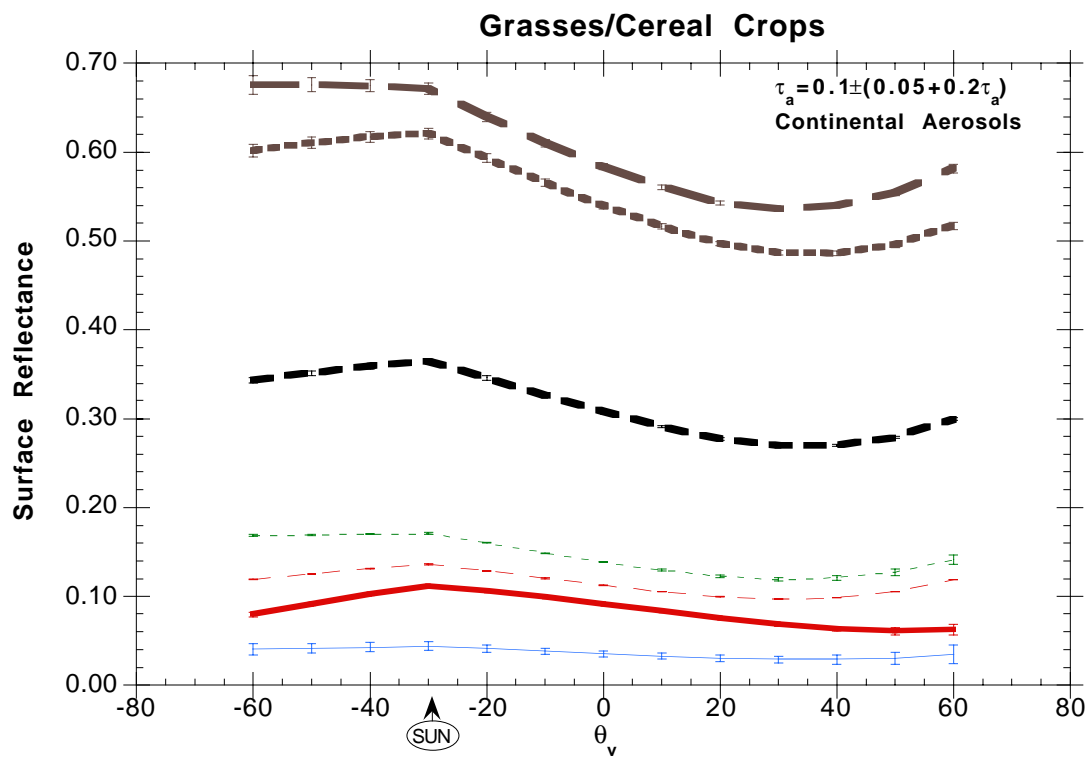
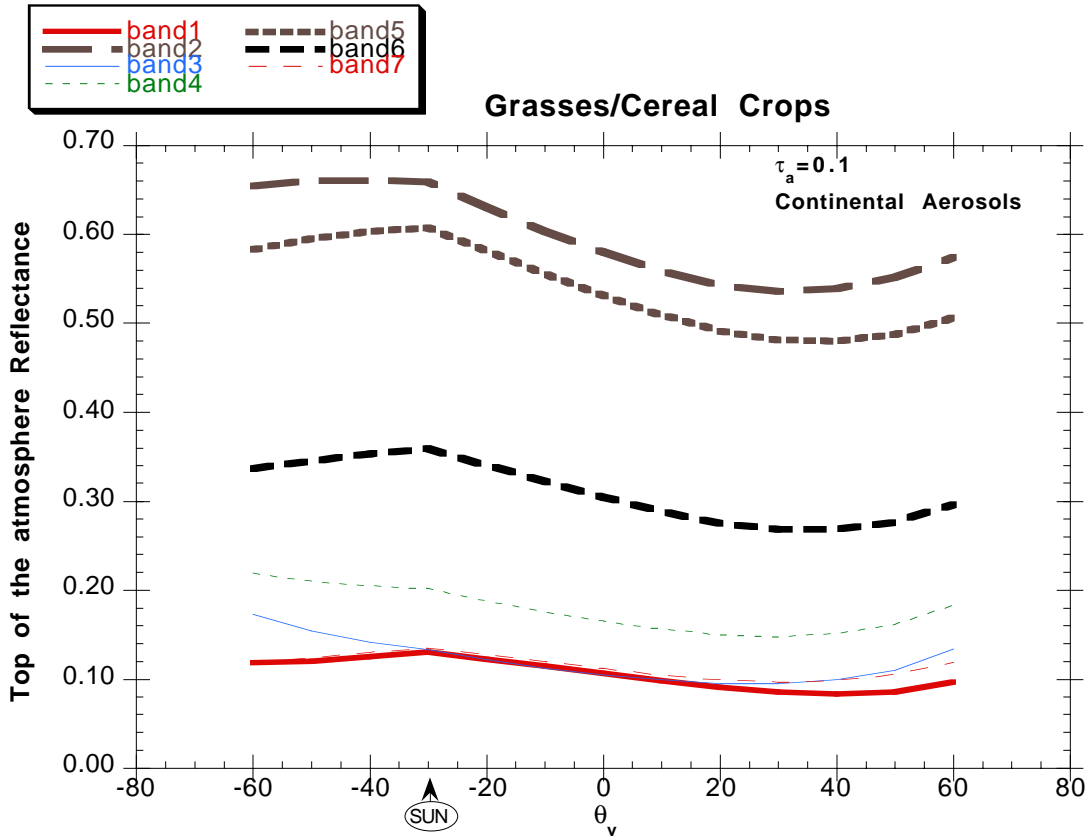
Broadleaf Crops

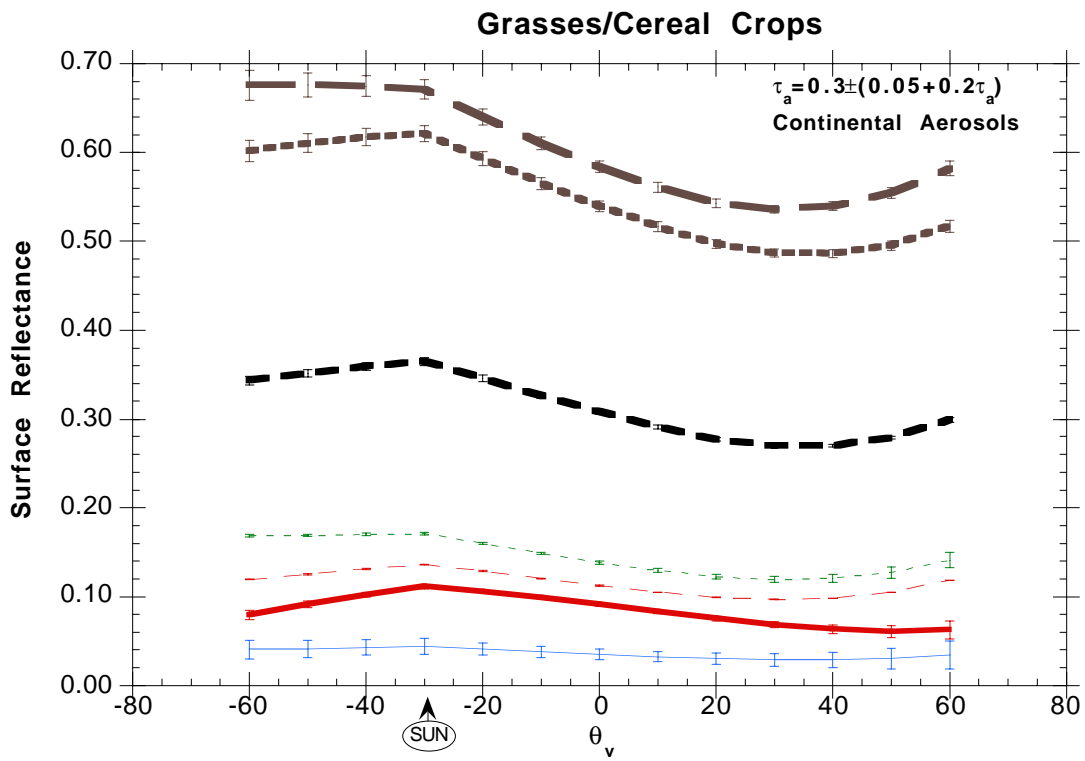
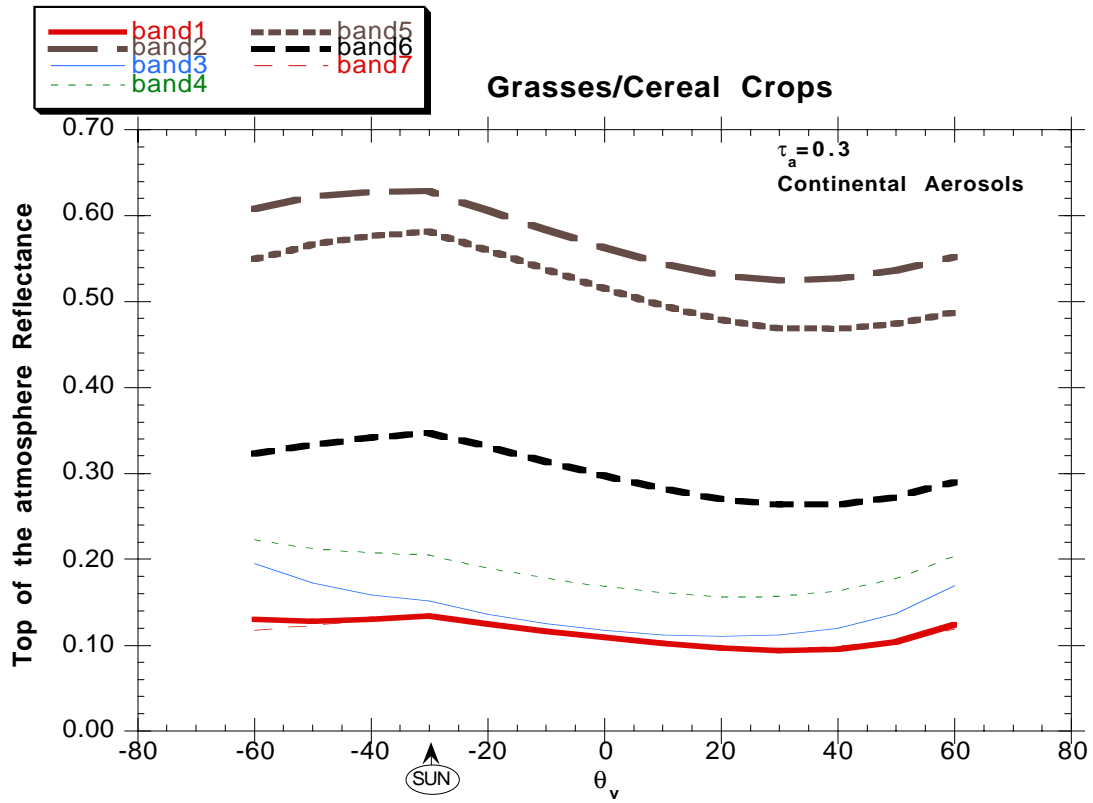


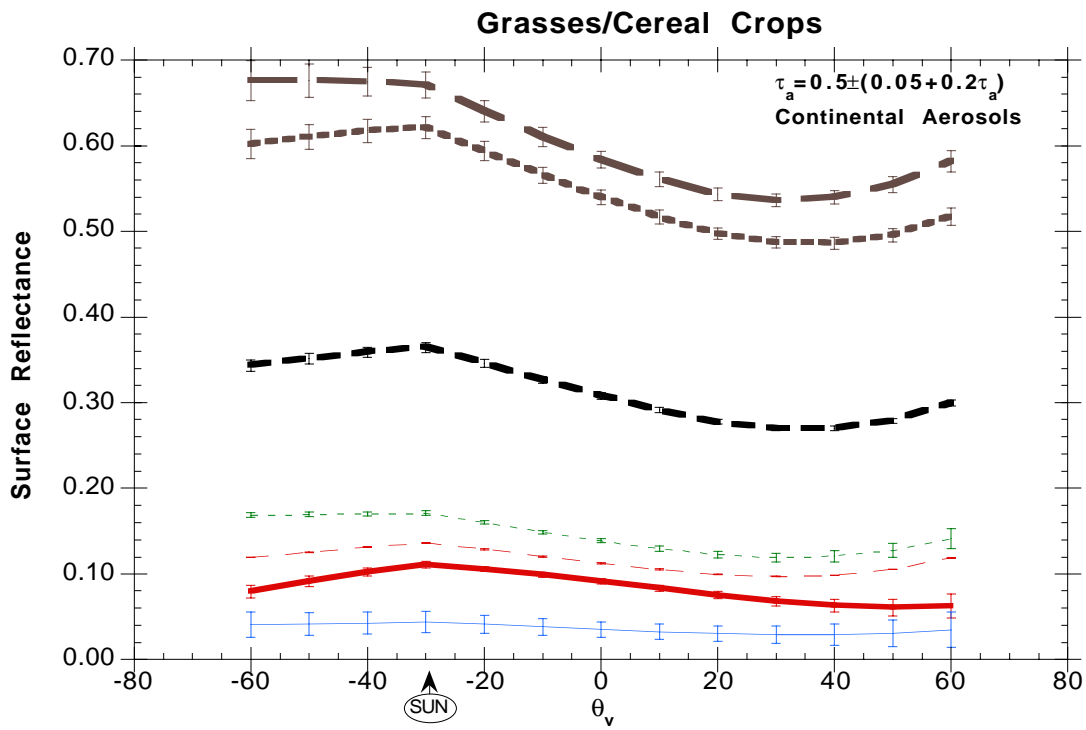
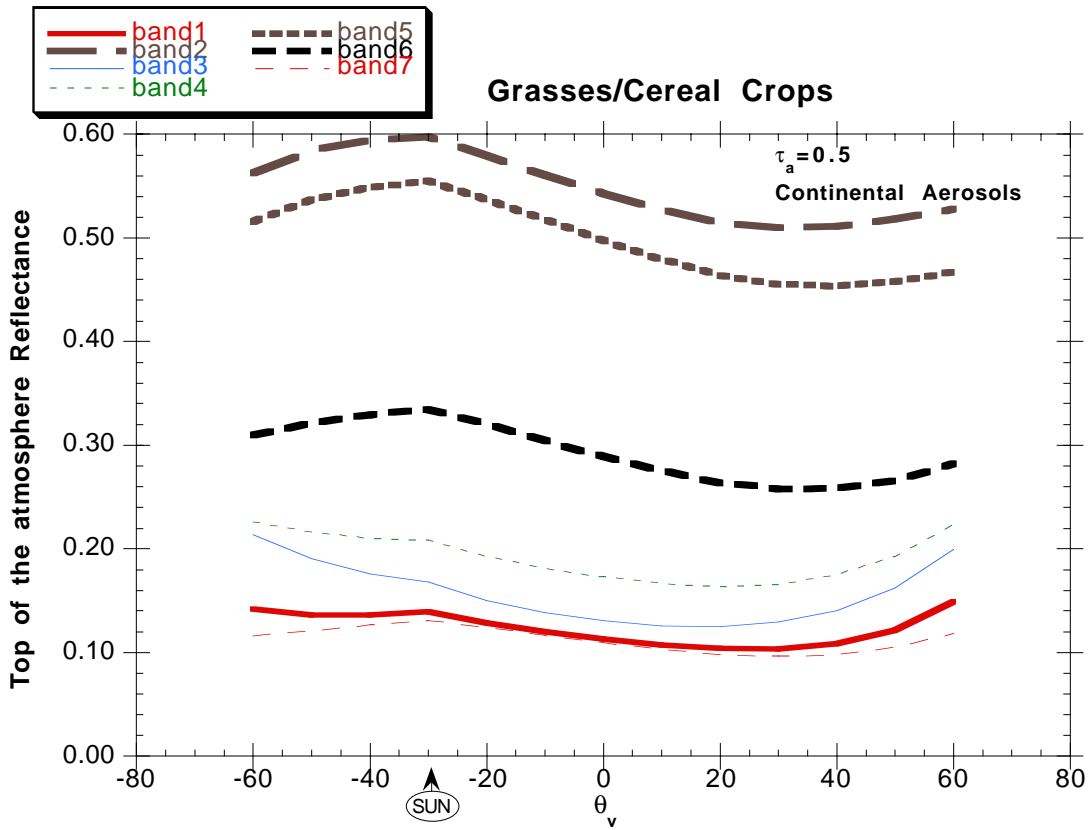


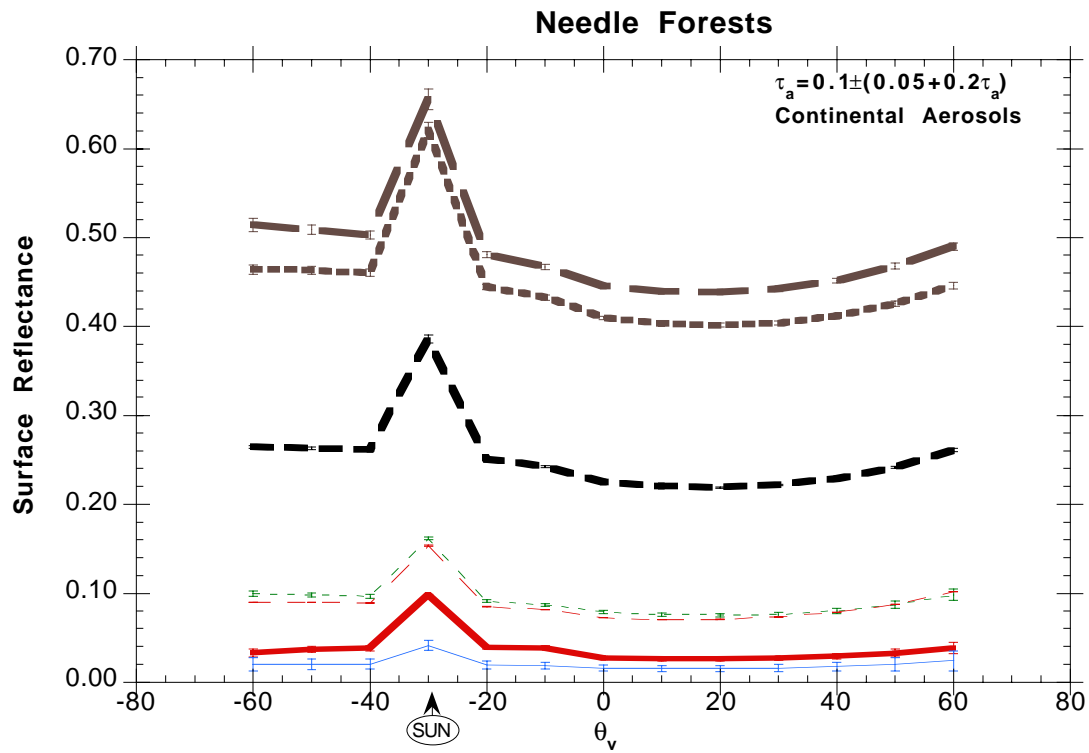
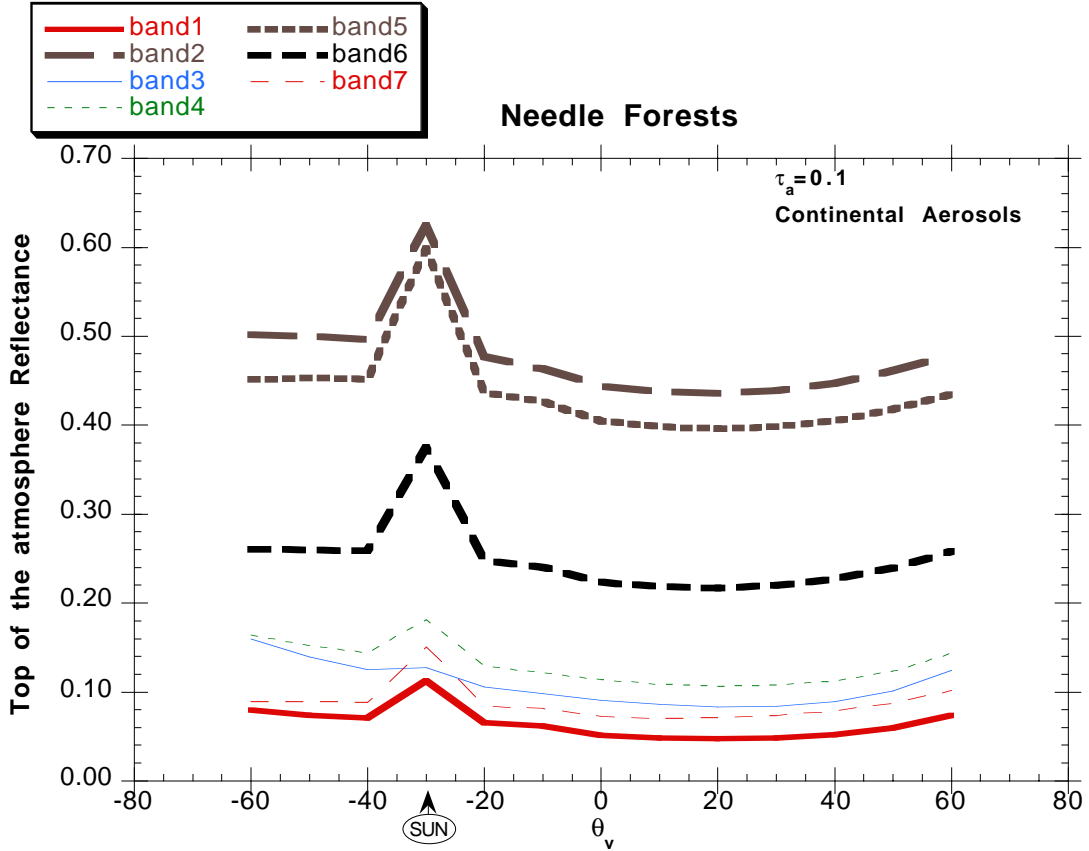


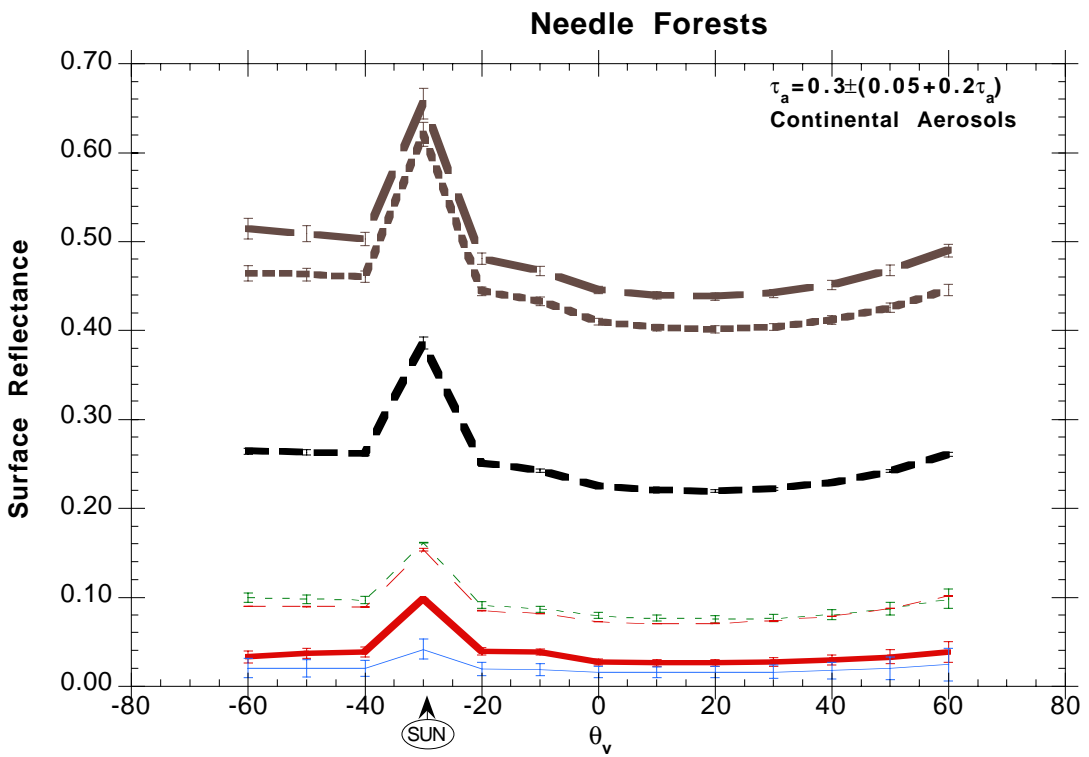
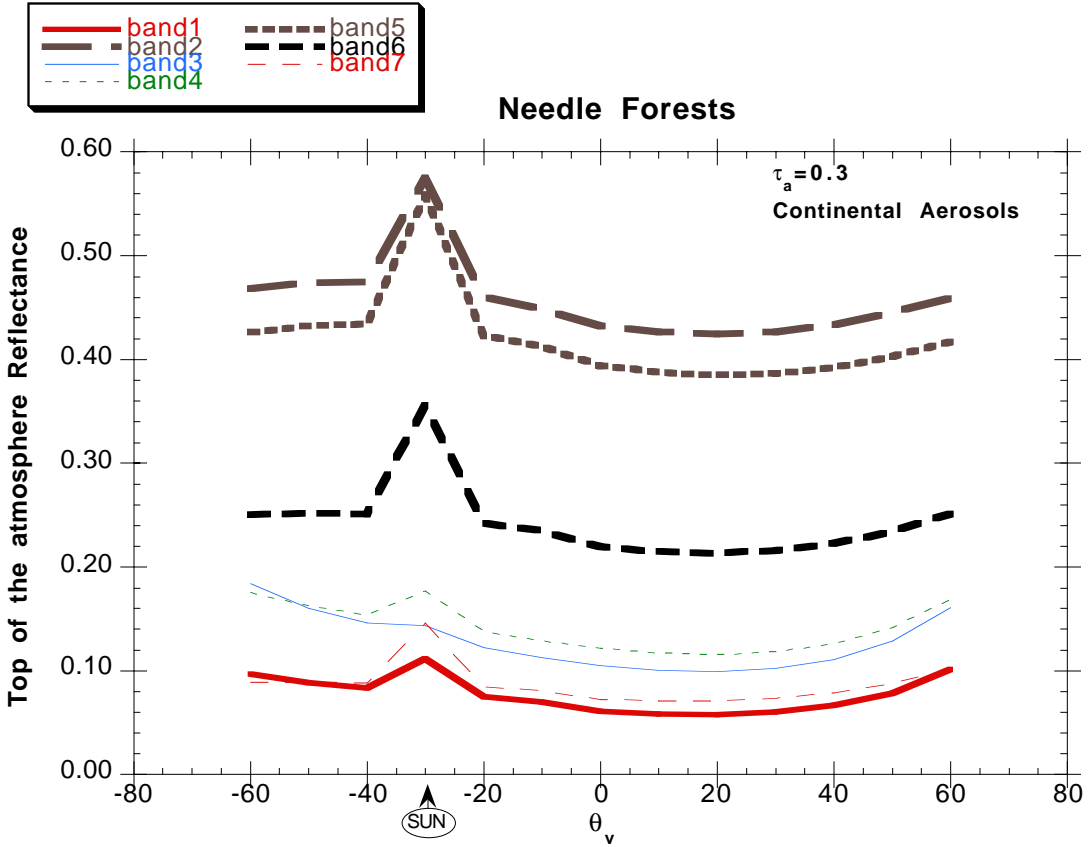


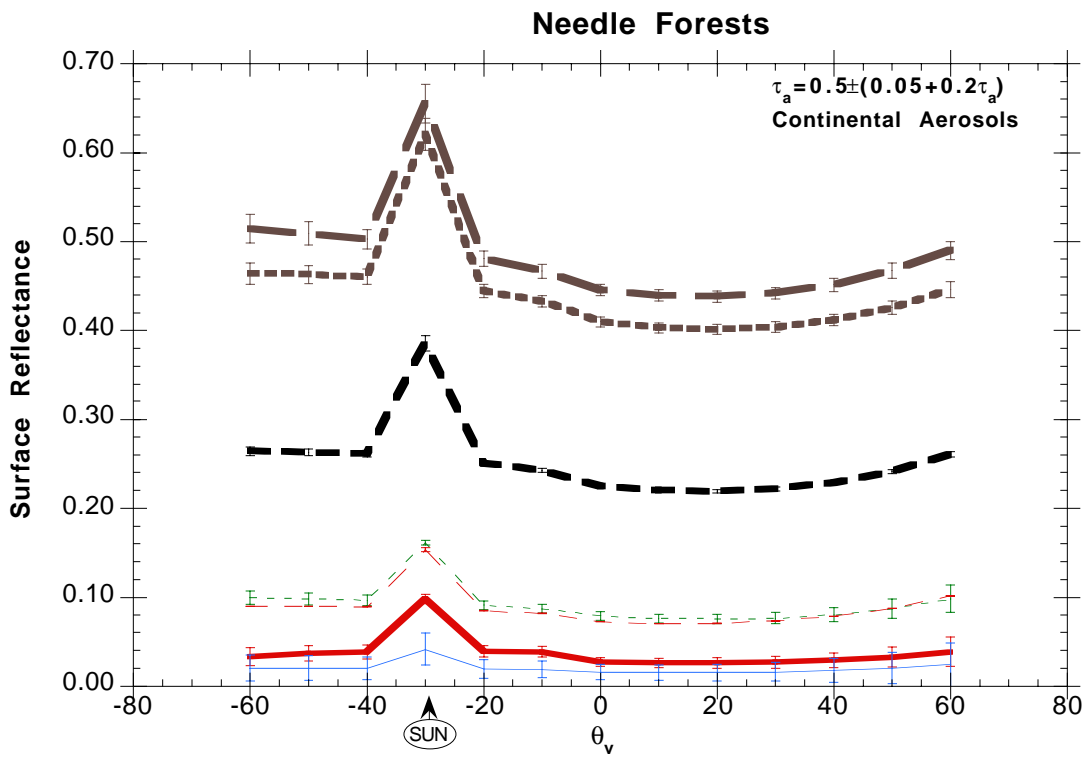
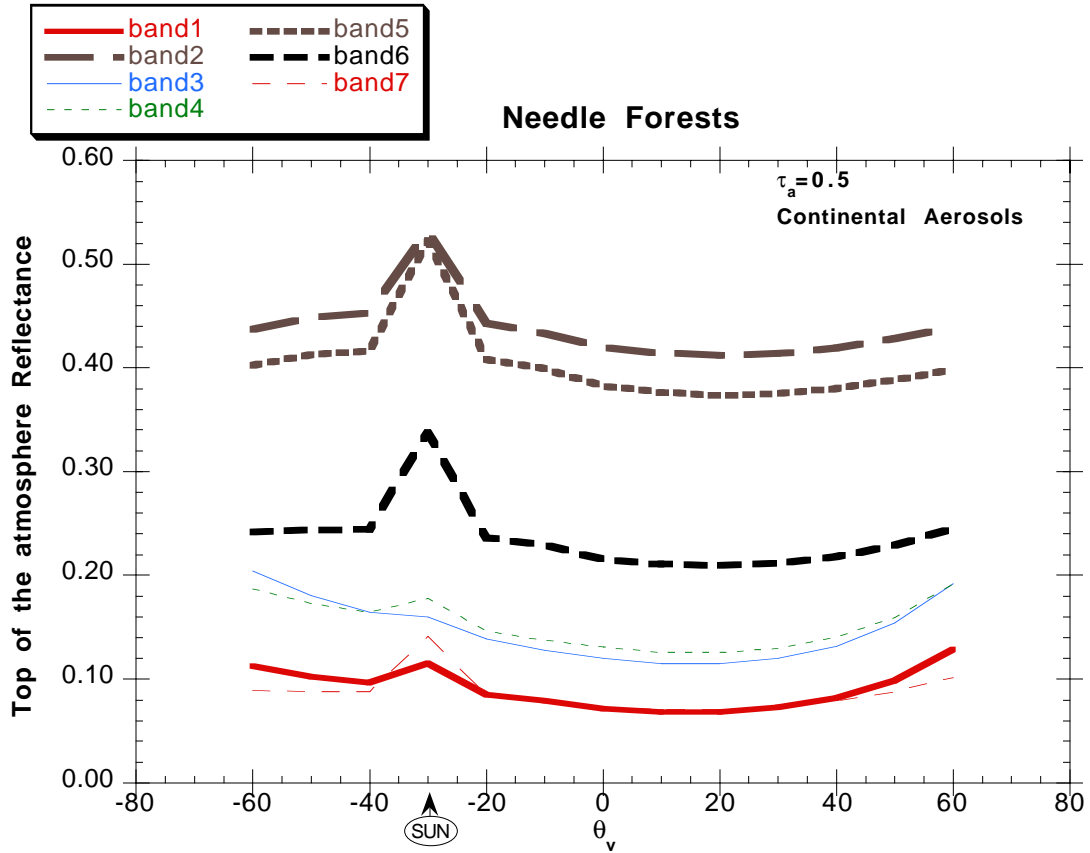


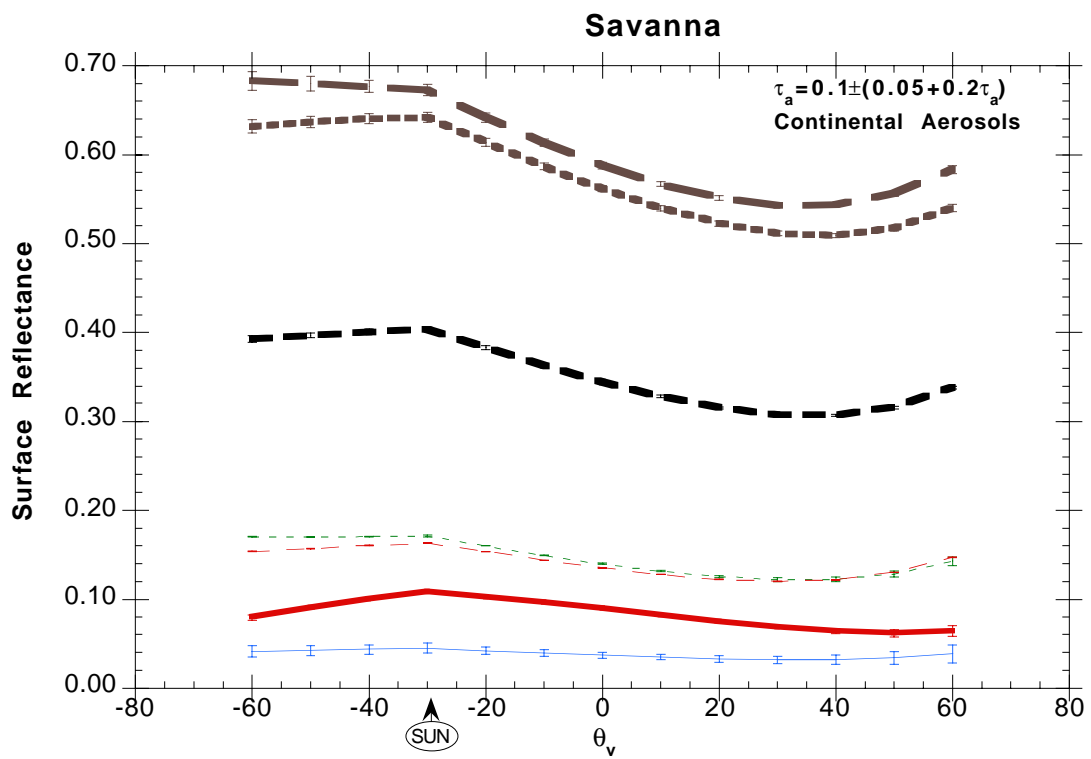
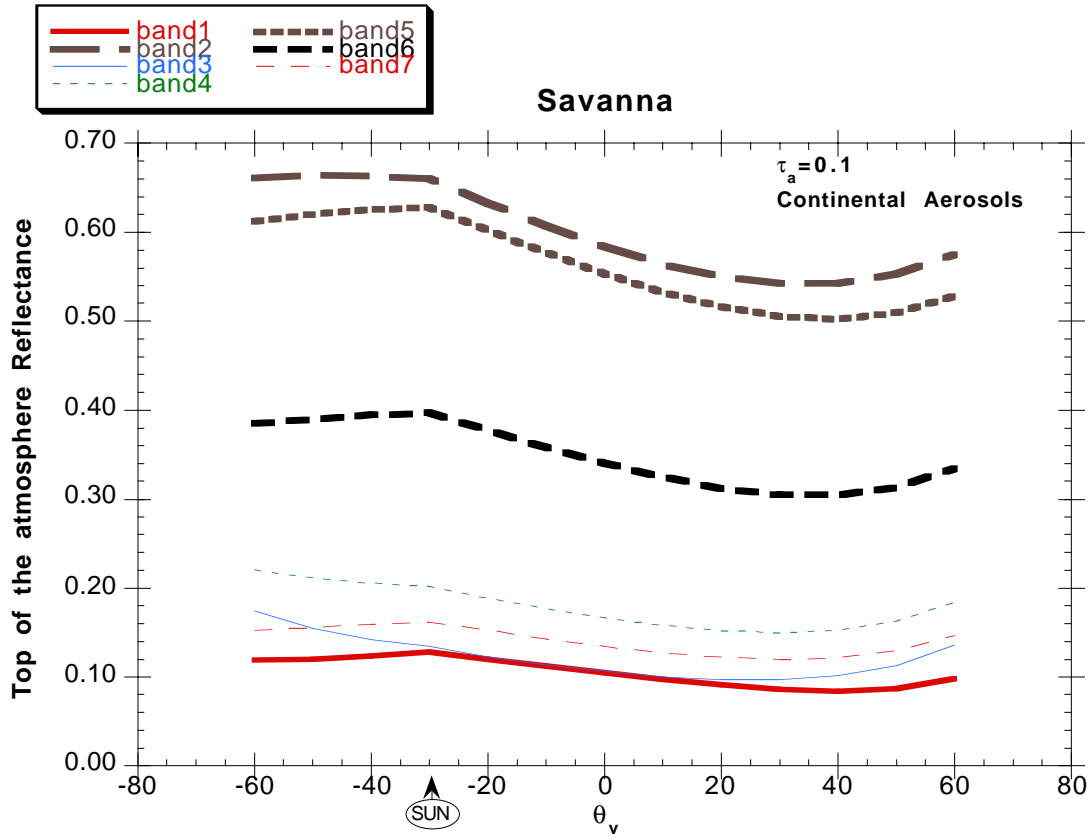


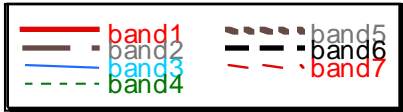




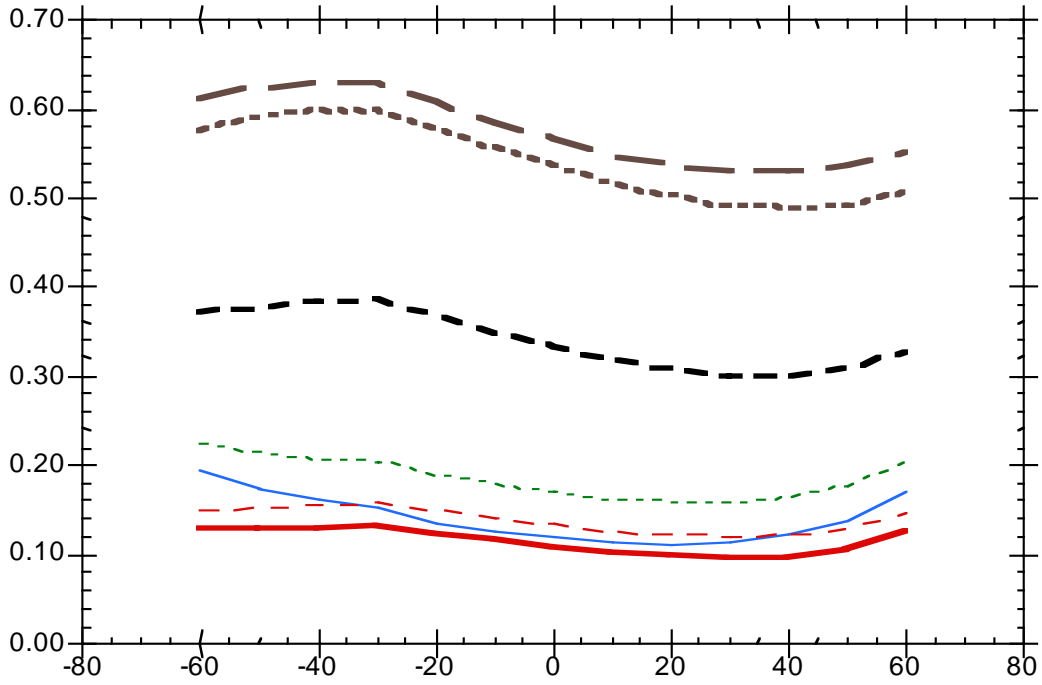




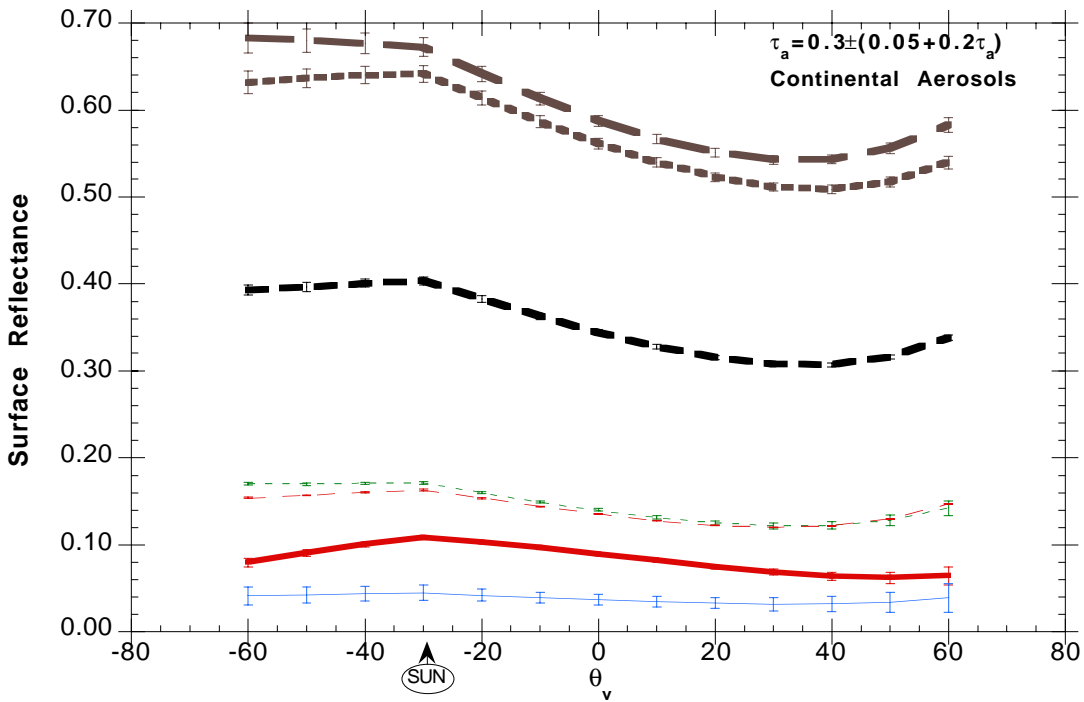


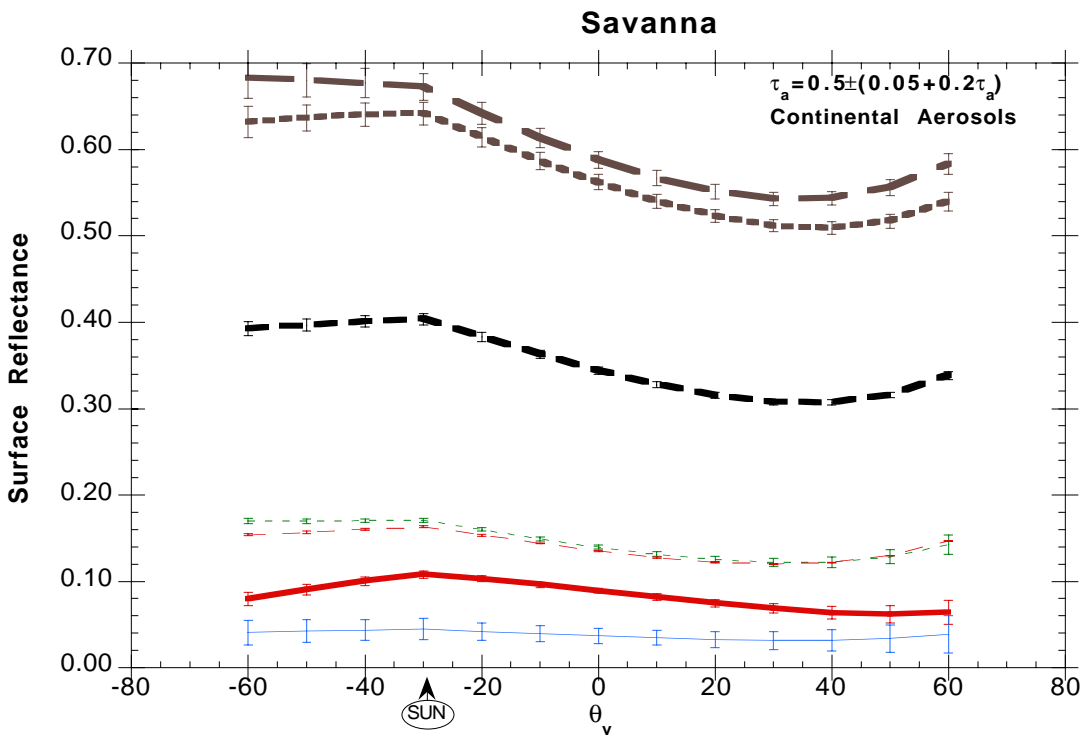
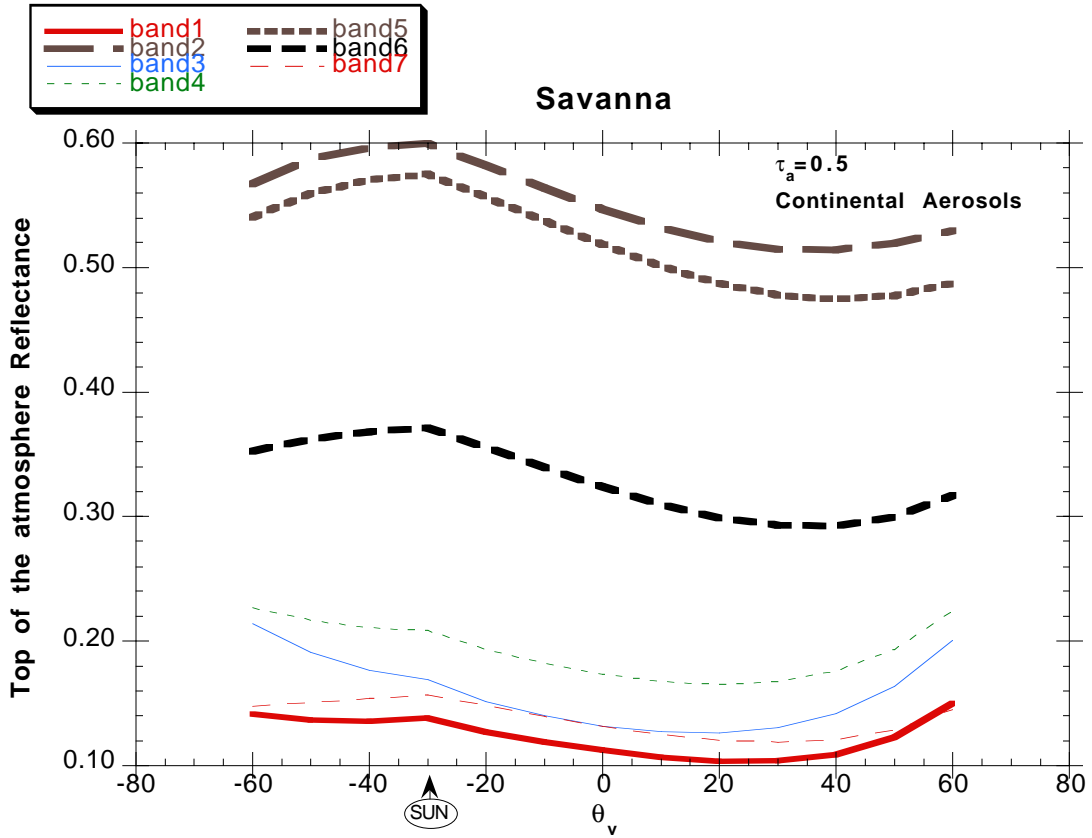


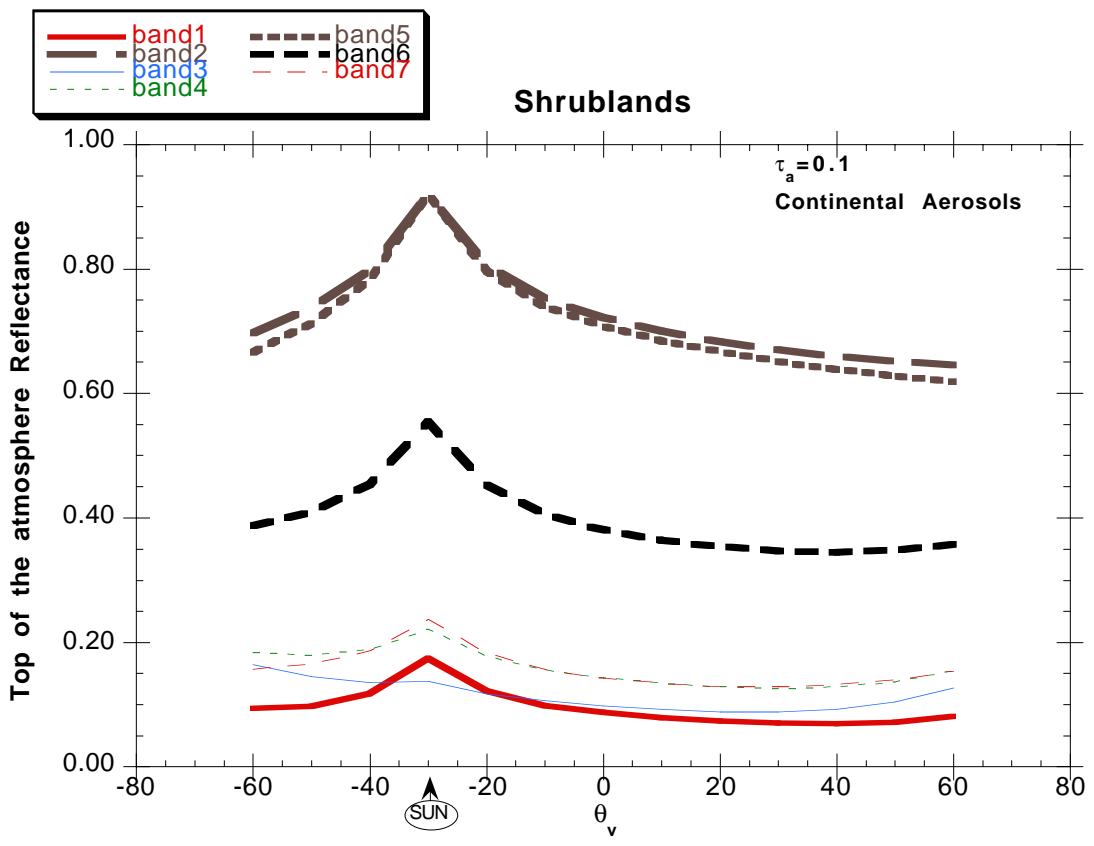
Savanna

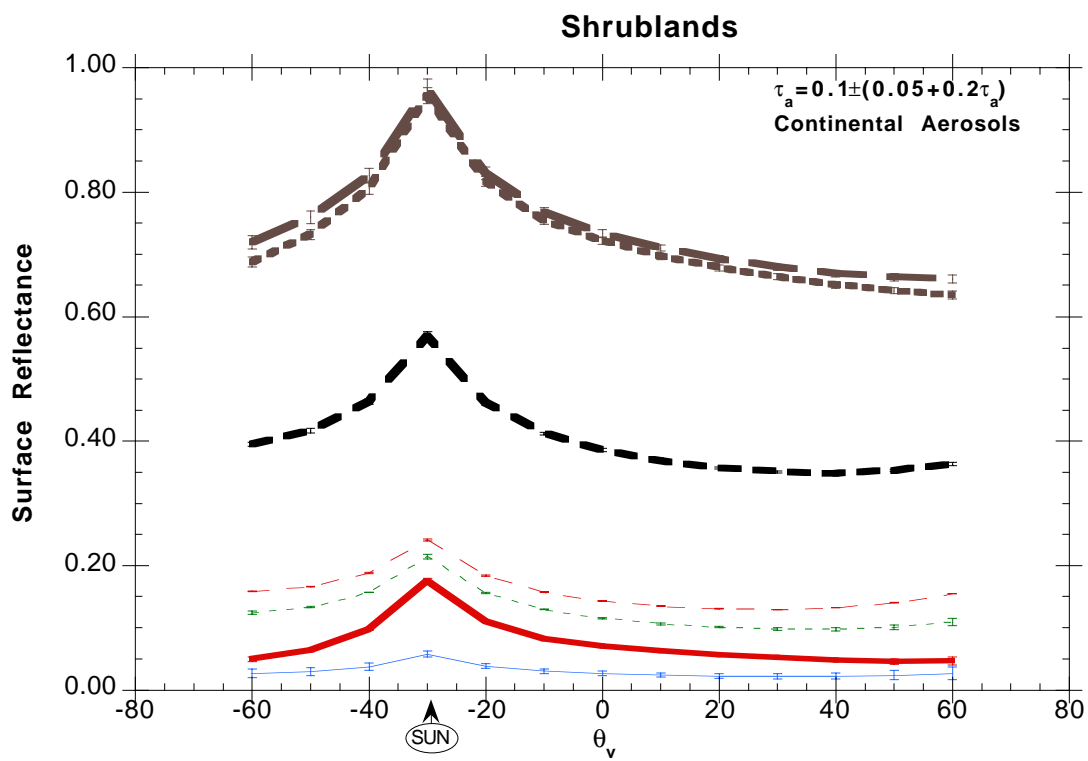


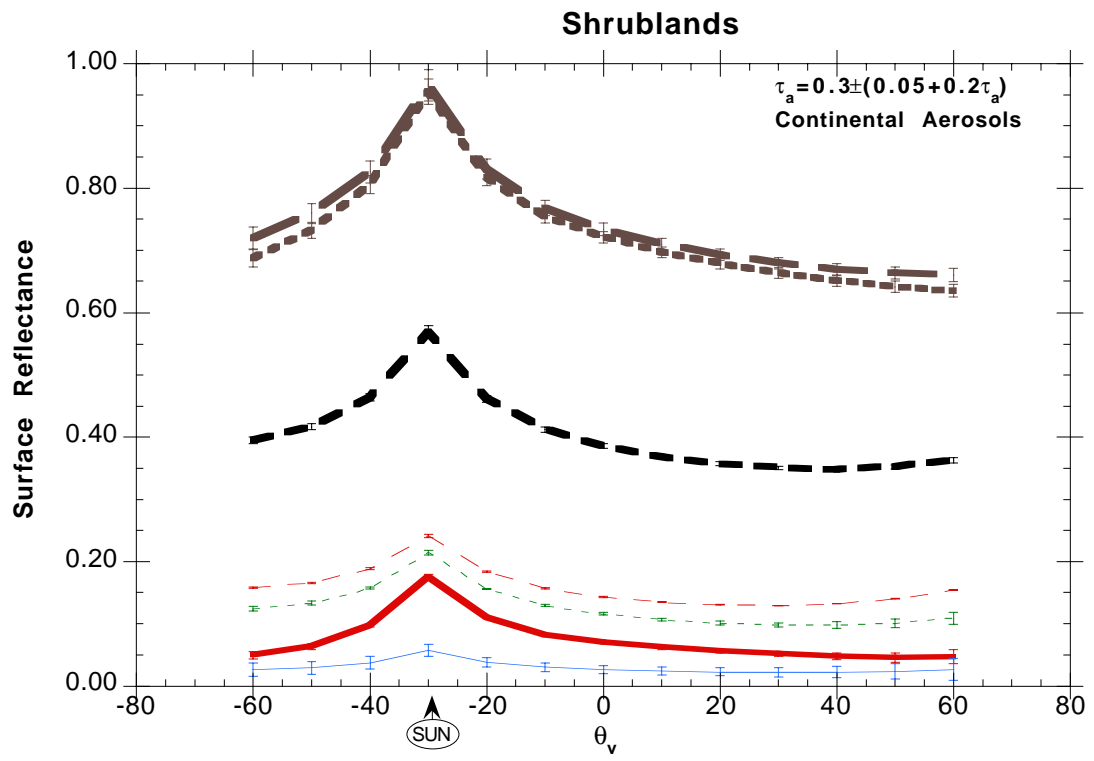
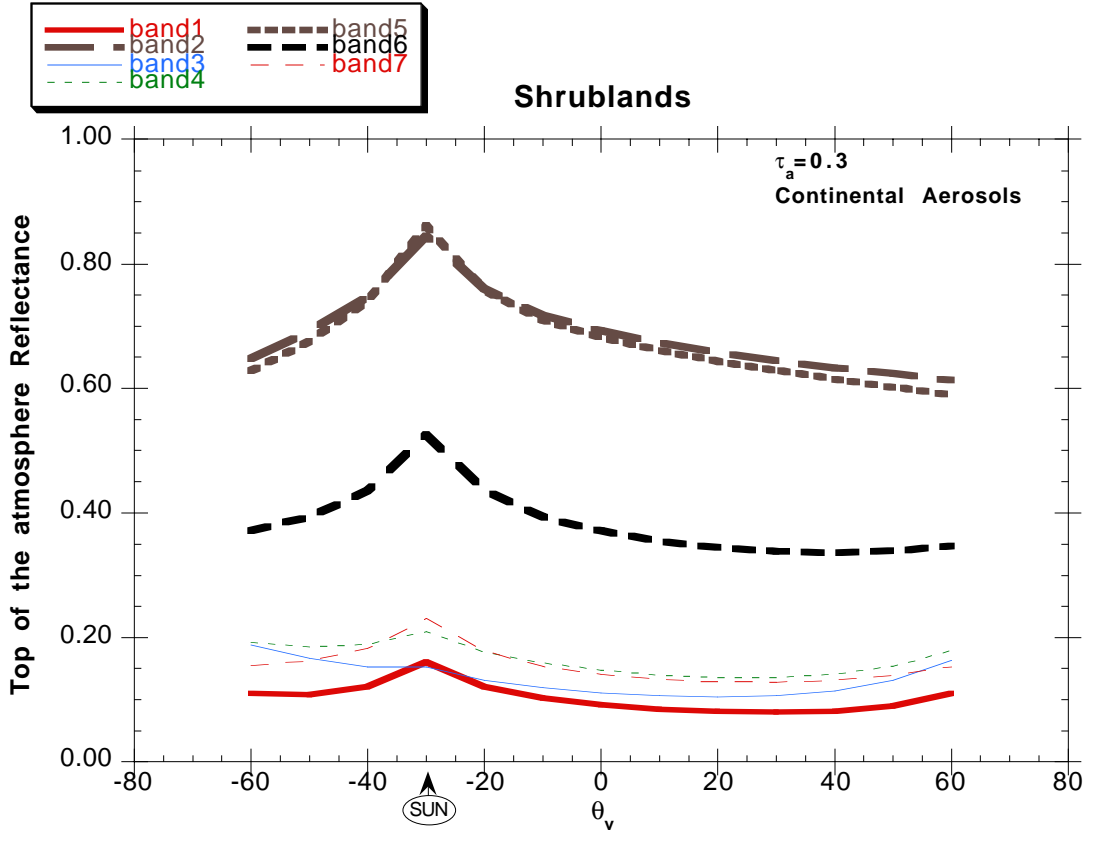
Savanna

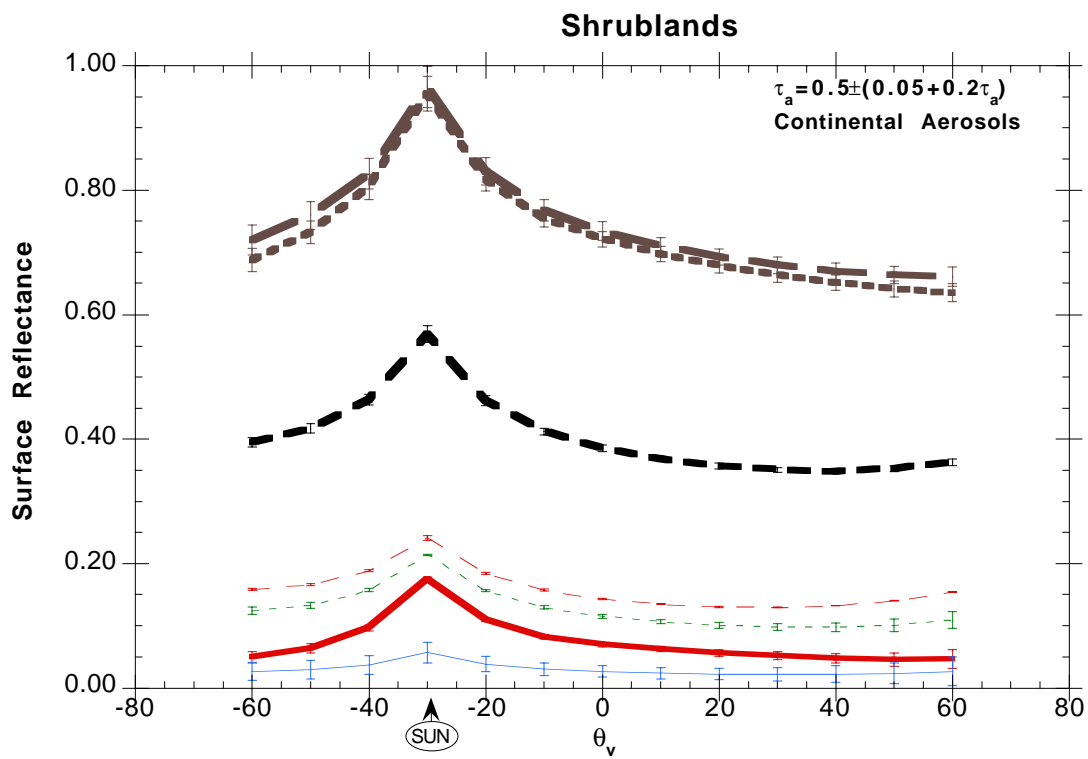
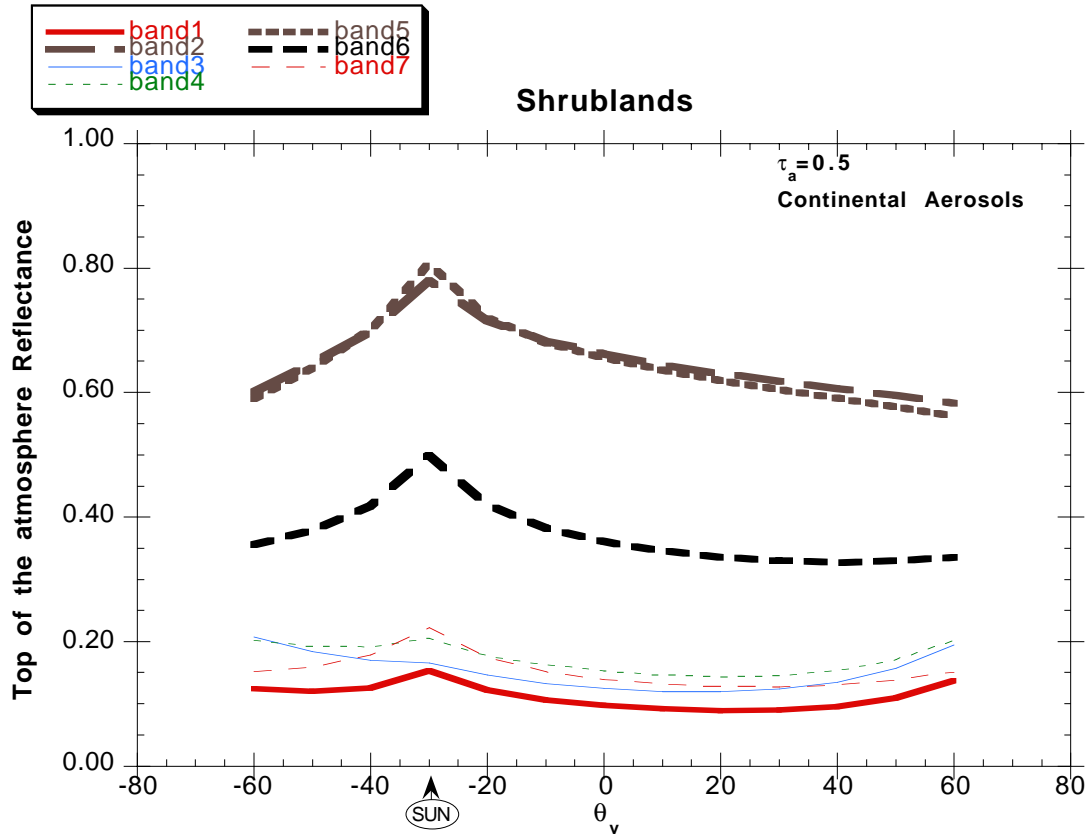




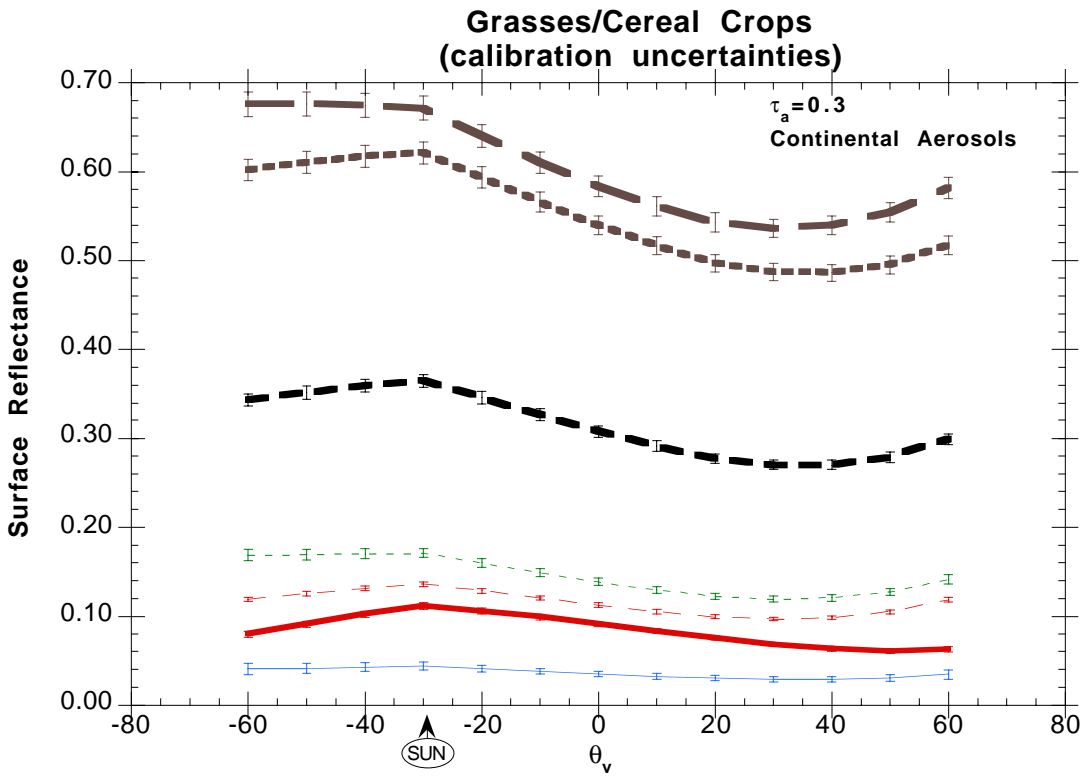
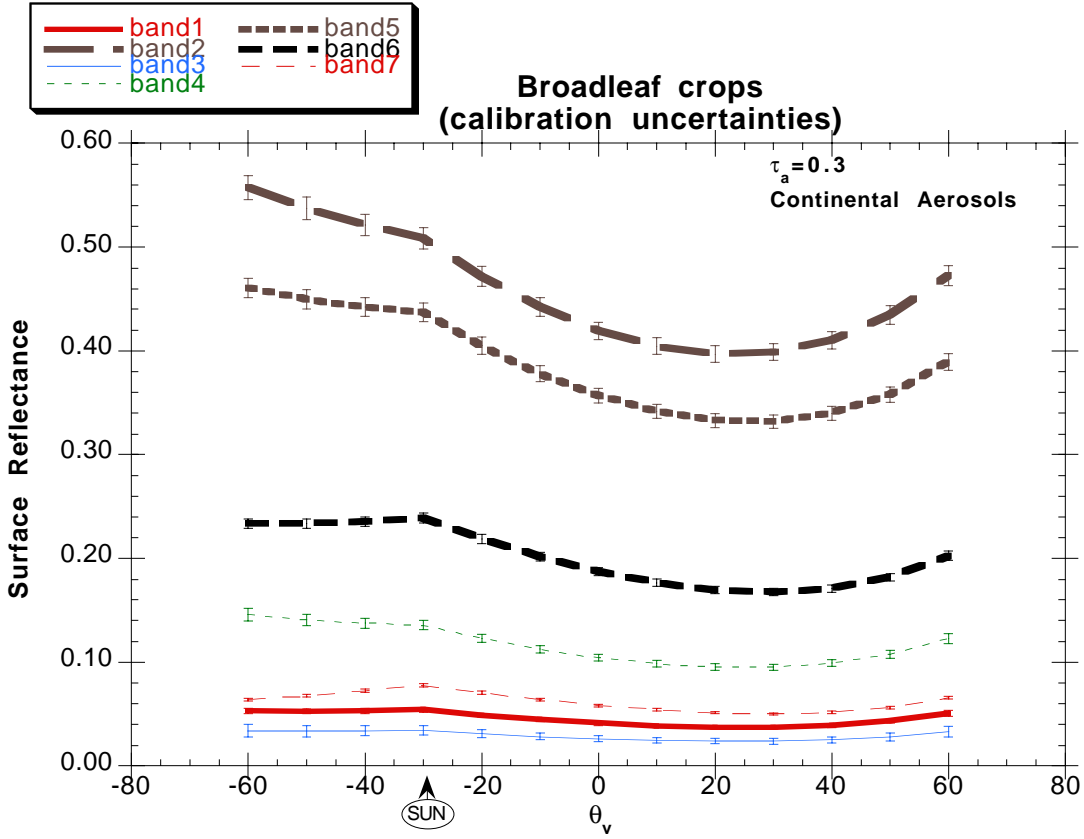


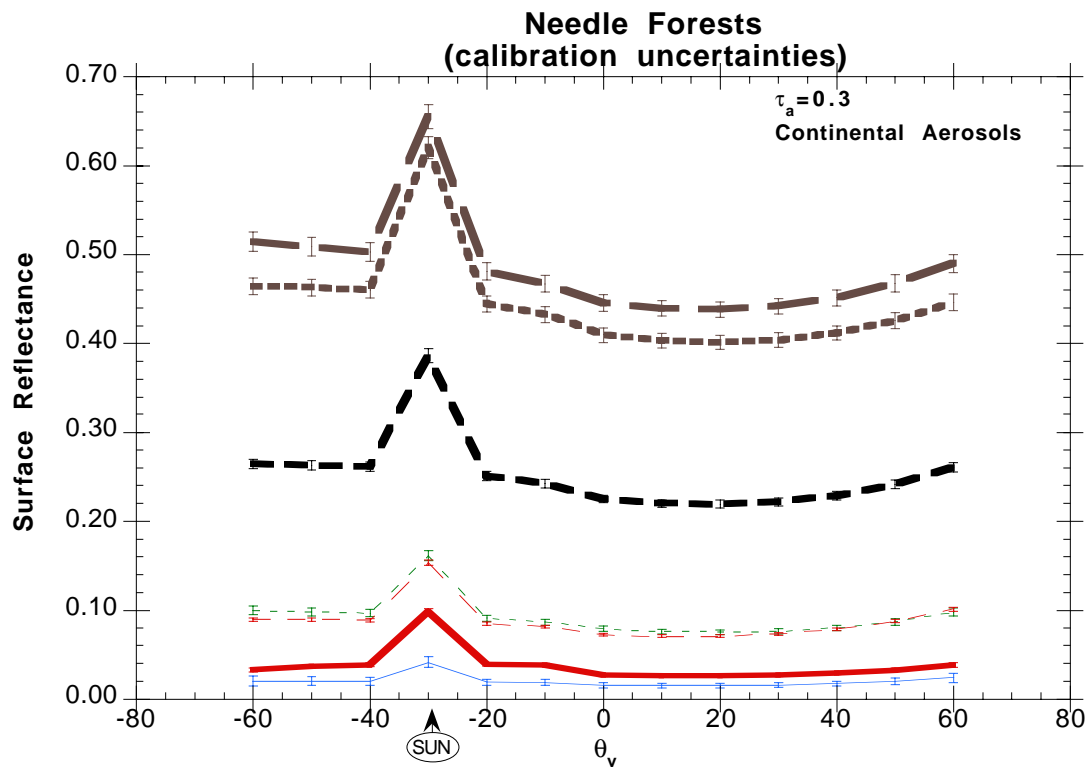
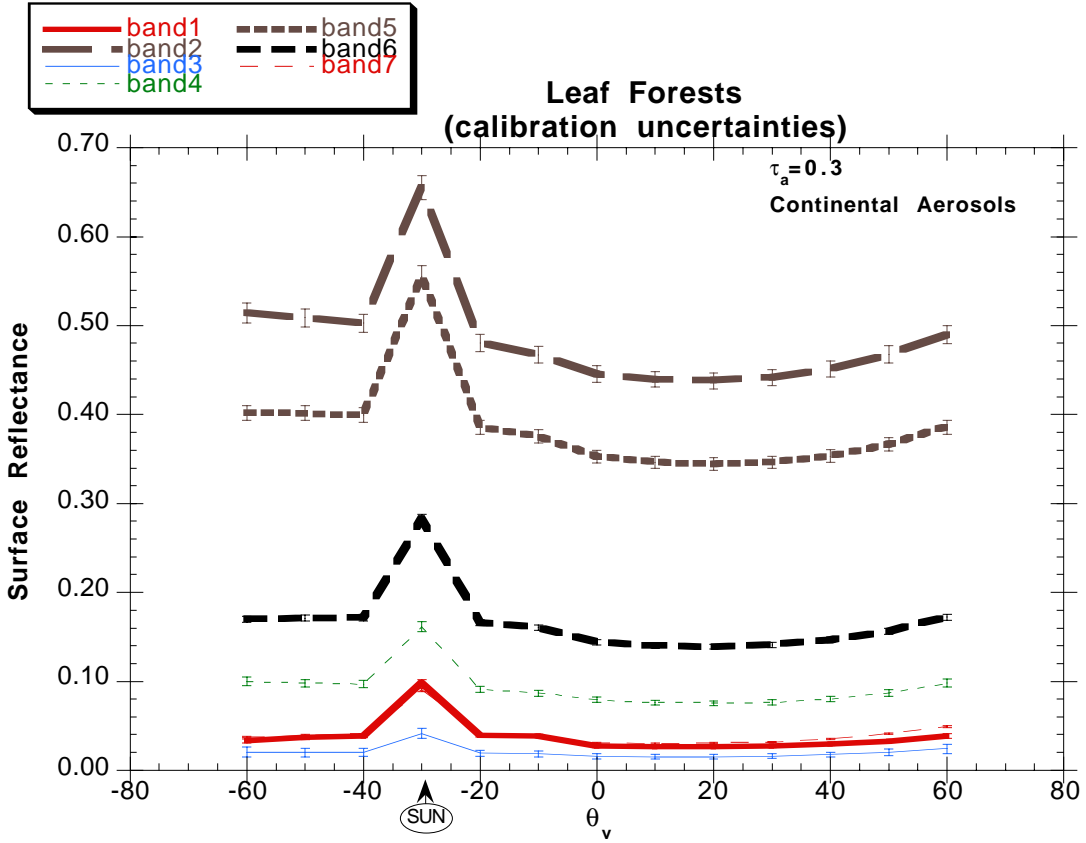


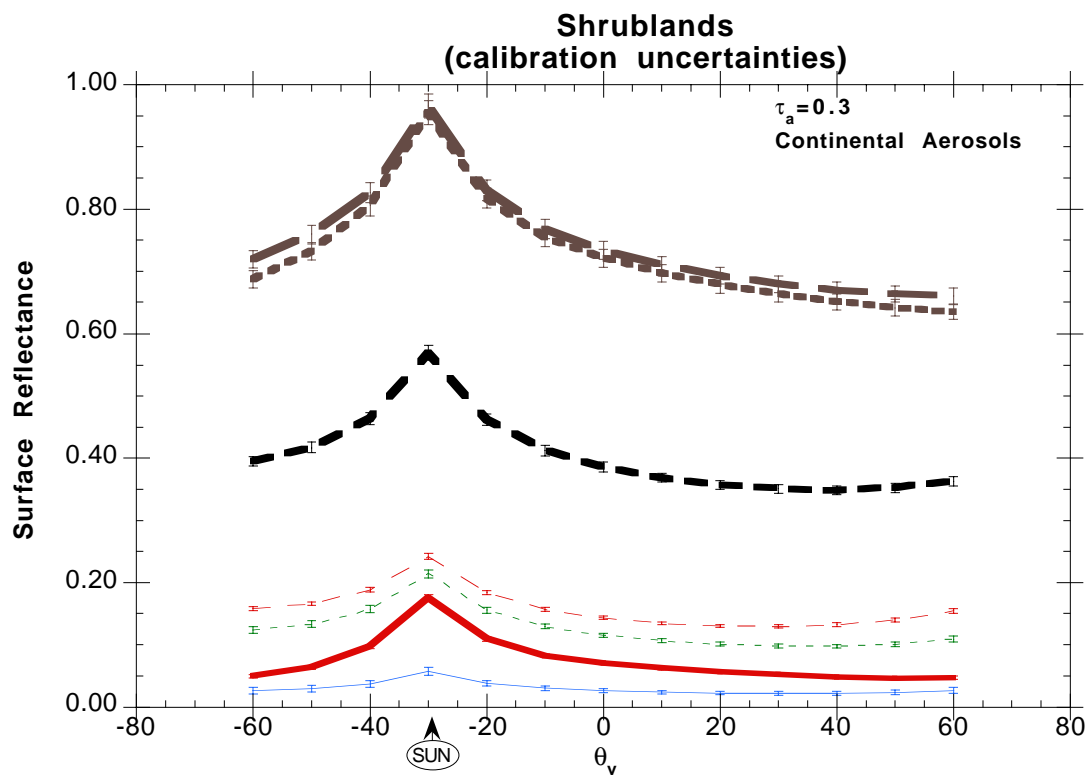
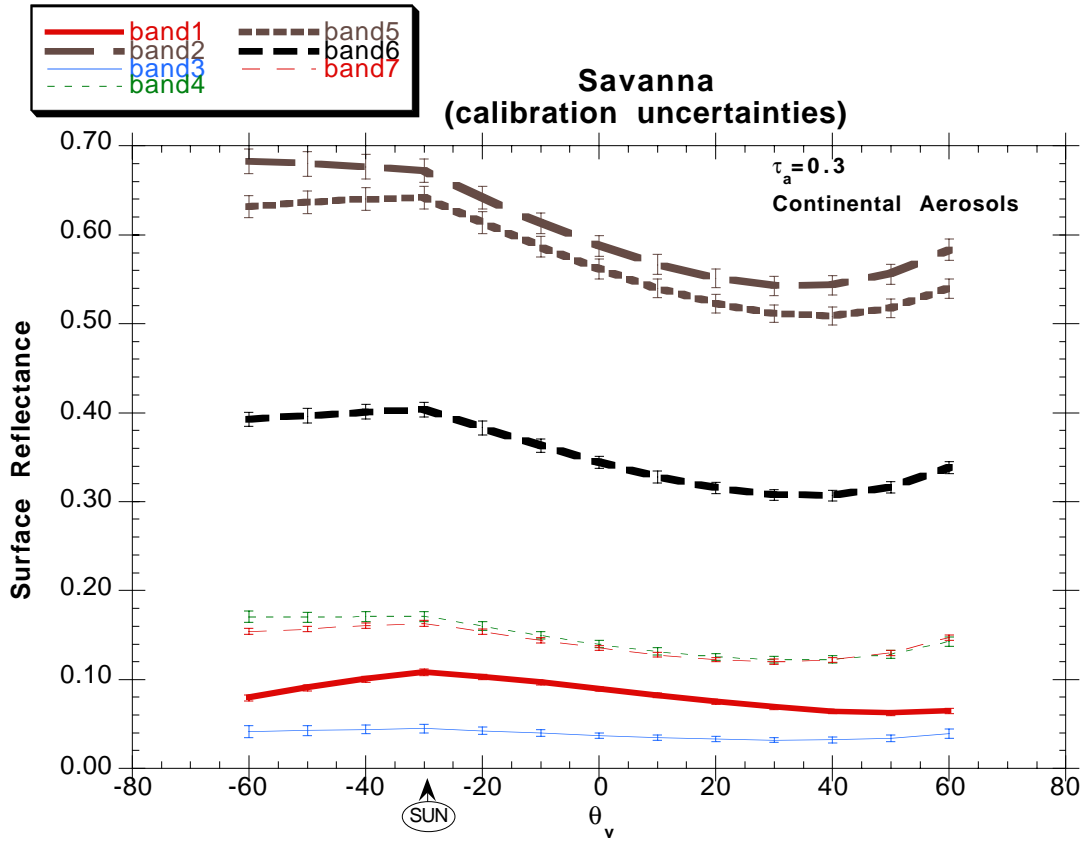




**Appendix B2) ERRORS DUE TO CALIBRATION UNCERTAINTIES
(±2%) AT OPTICAL DEPTH AT 550nm of 0.3.**

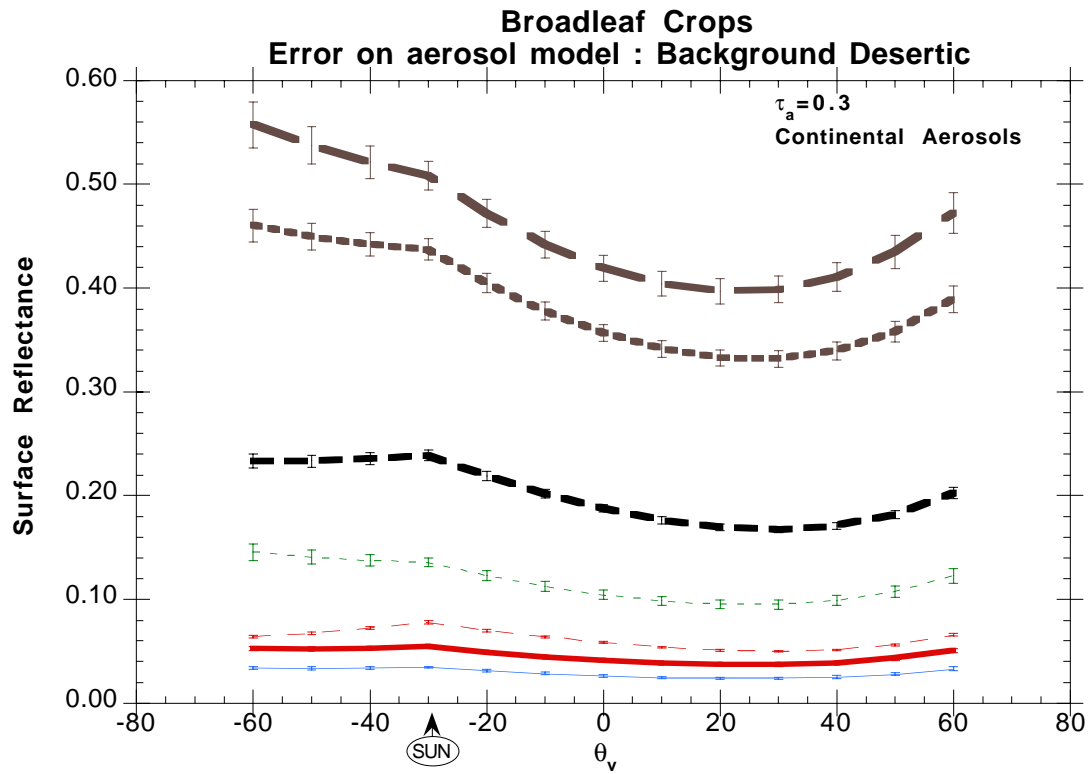
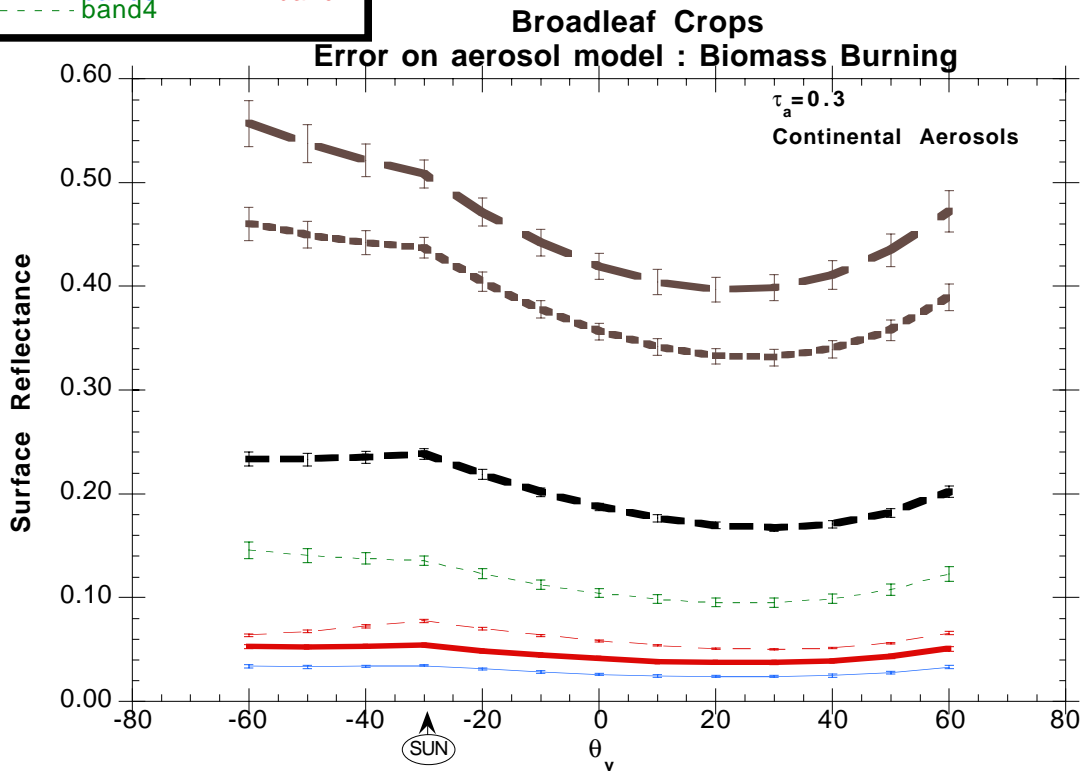
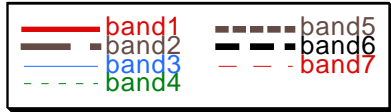


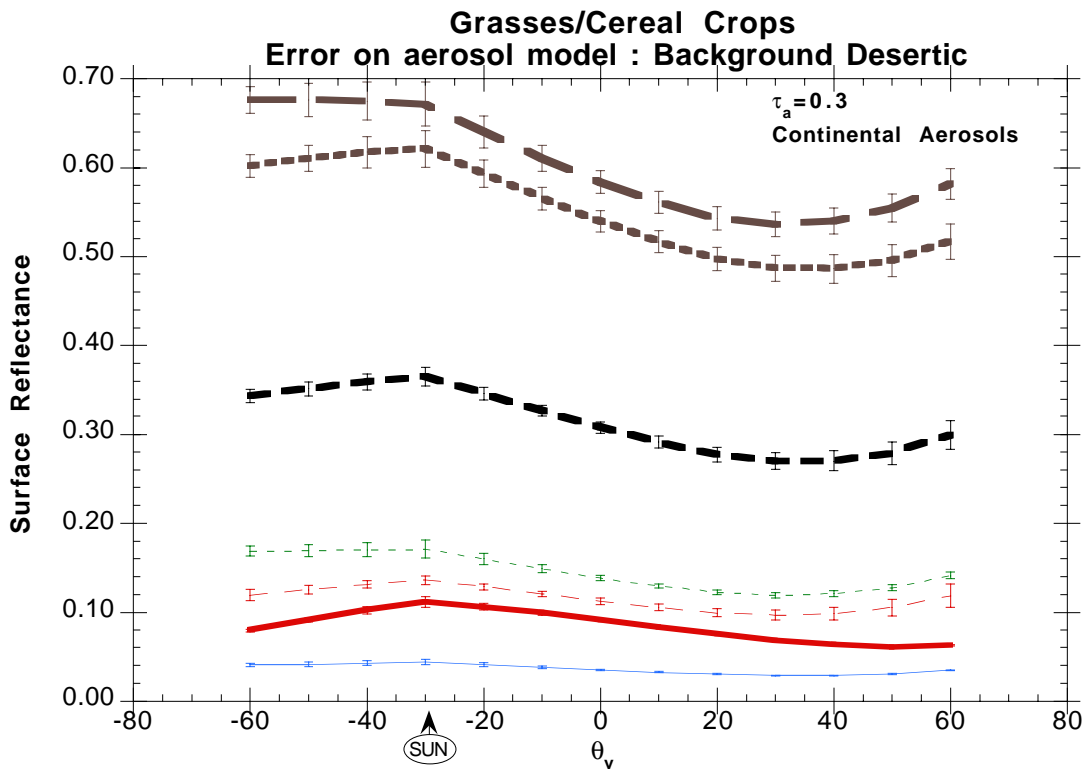
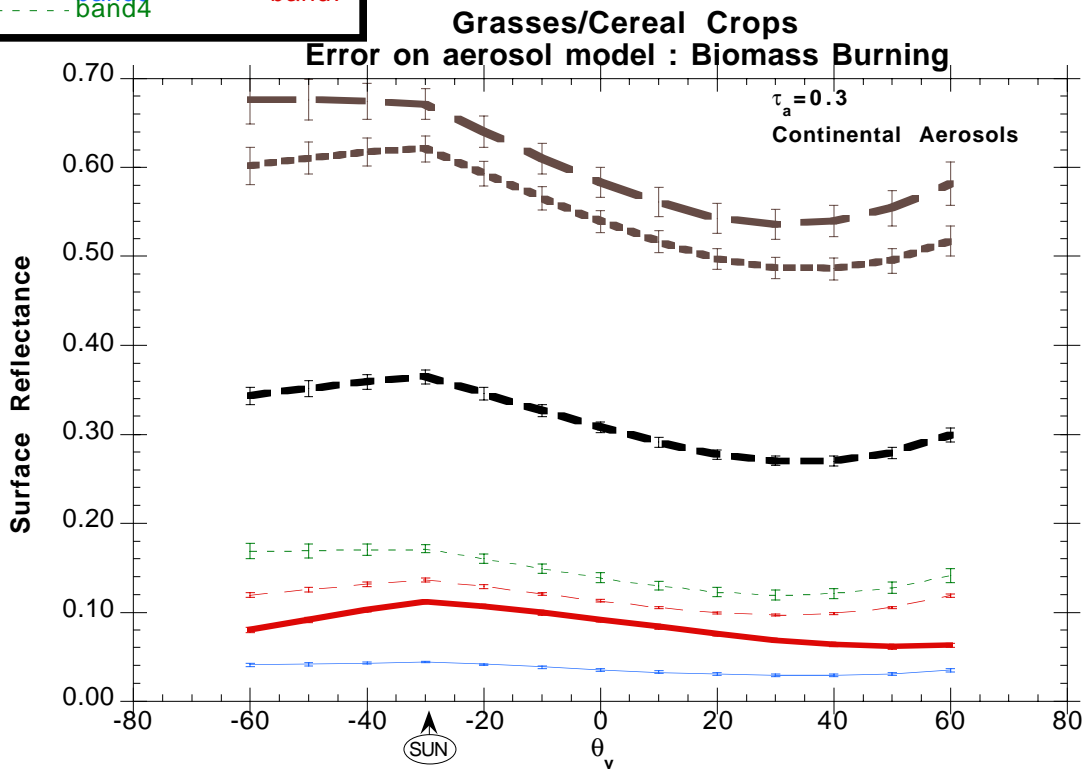


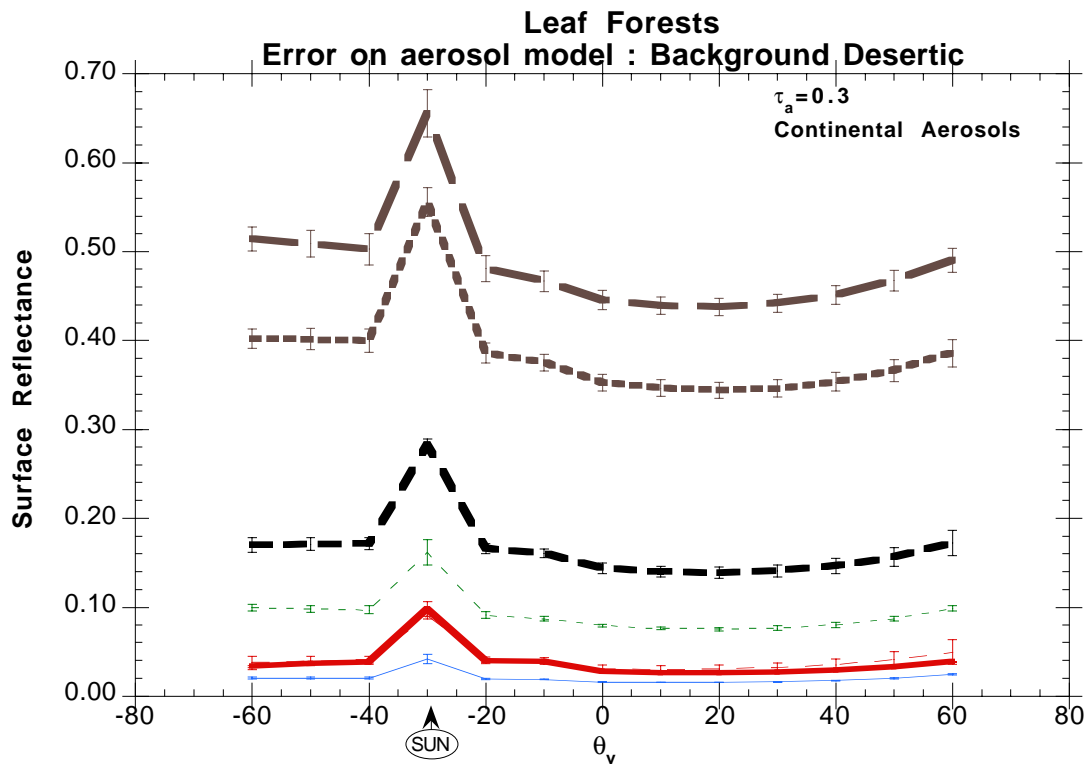
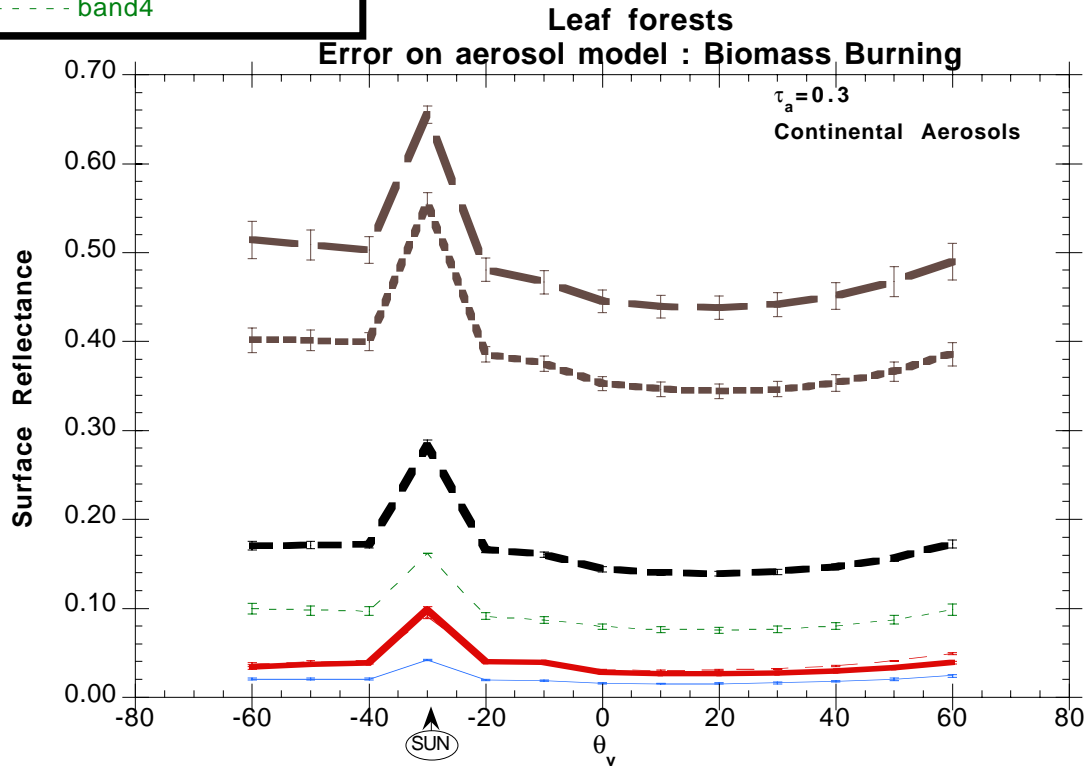
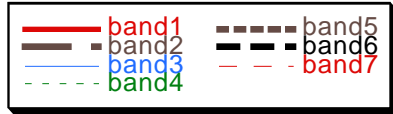


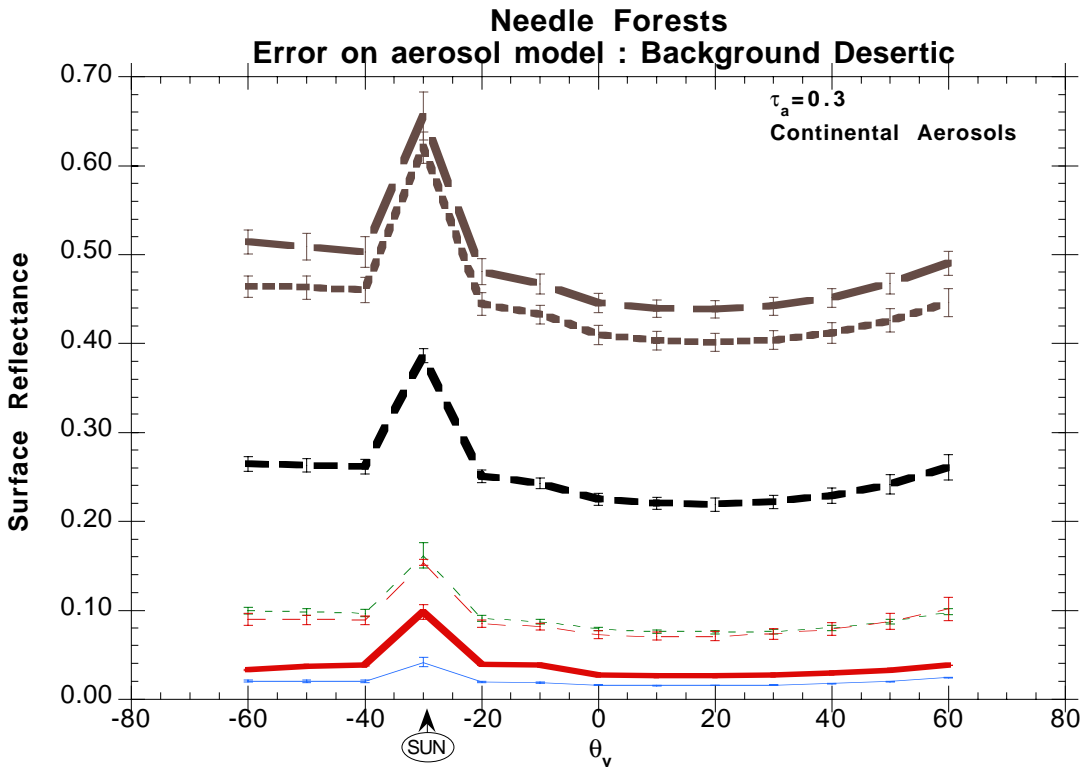
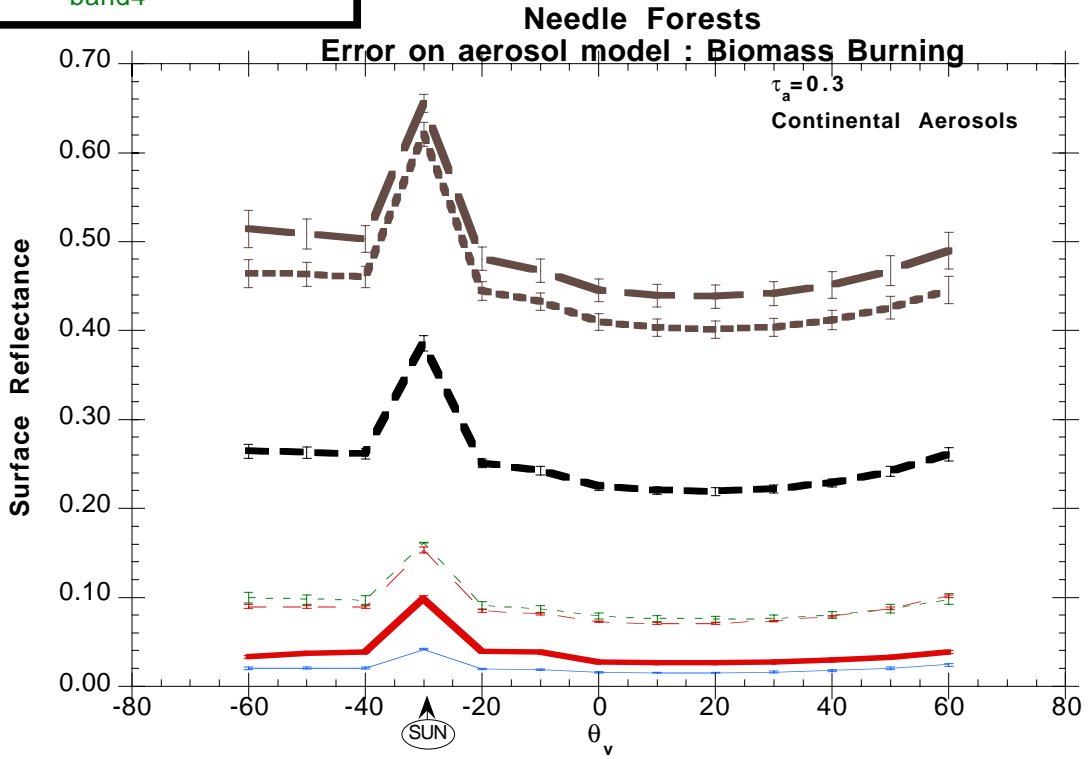
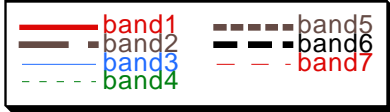
Appendix B3) Errors due to aerosol model choice (at optical depth of 0.3 at 550nm).

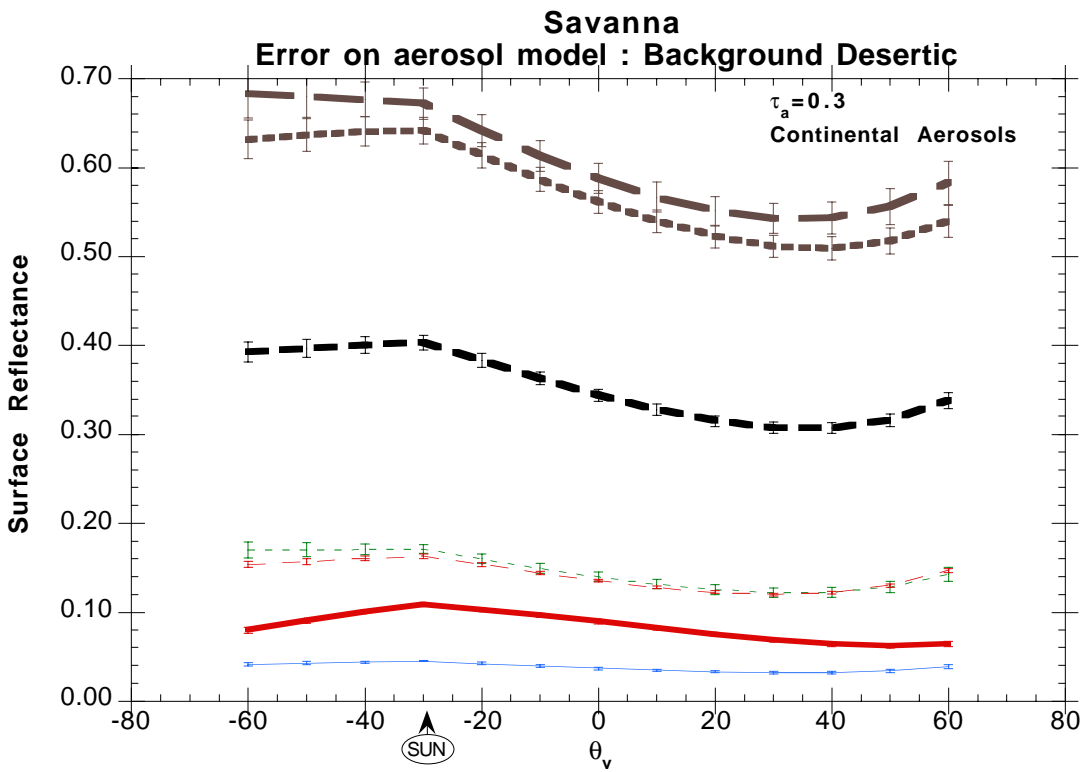
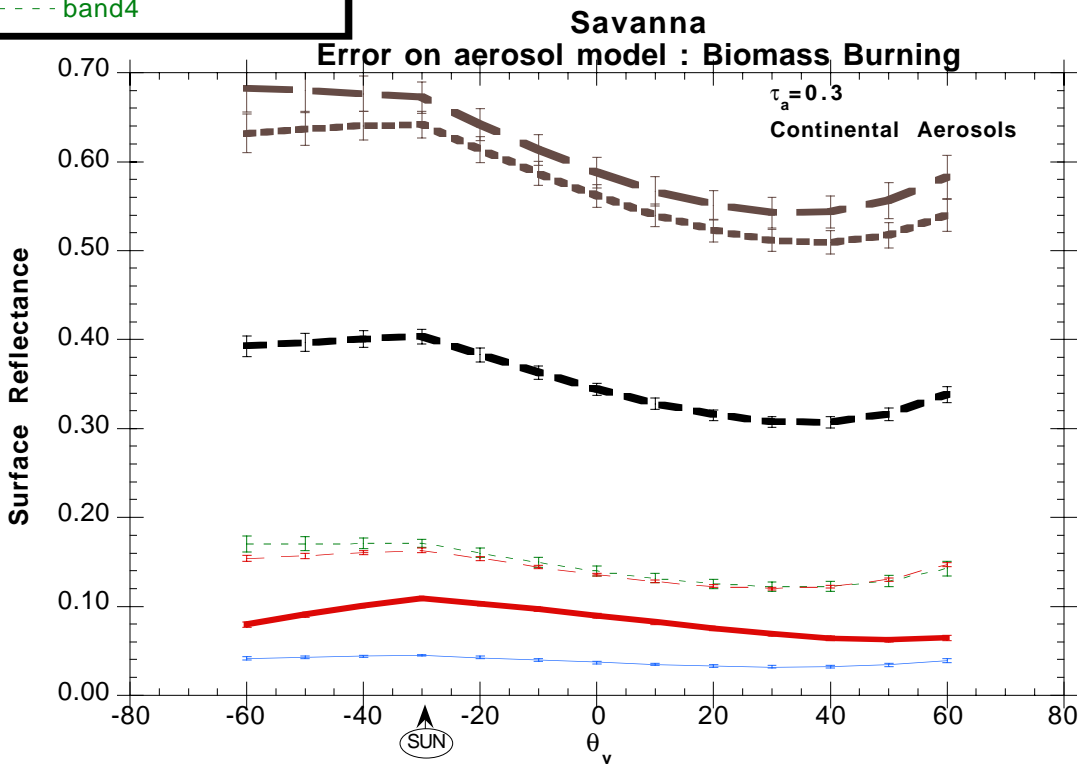
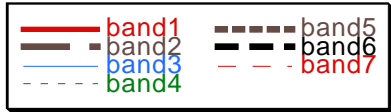
The data were corrected with a continental aerosol model. The actual aerosol model used to simulate top of the atmosphere reflectances was dust (6S background desertic model) or smoke (6S biomass burning model).

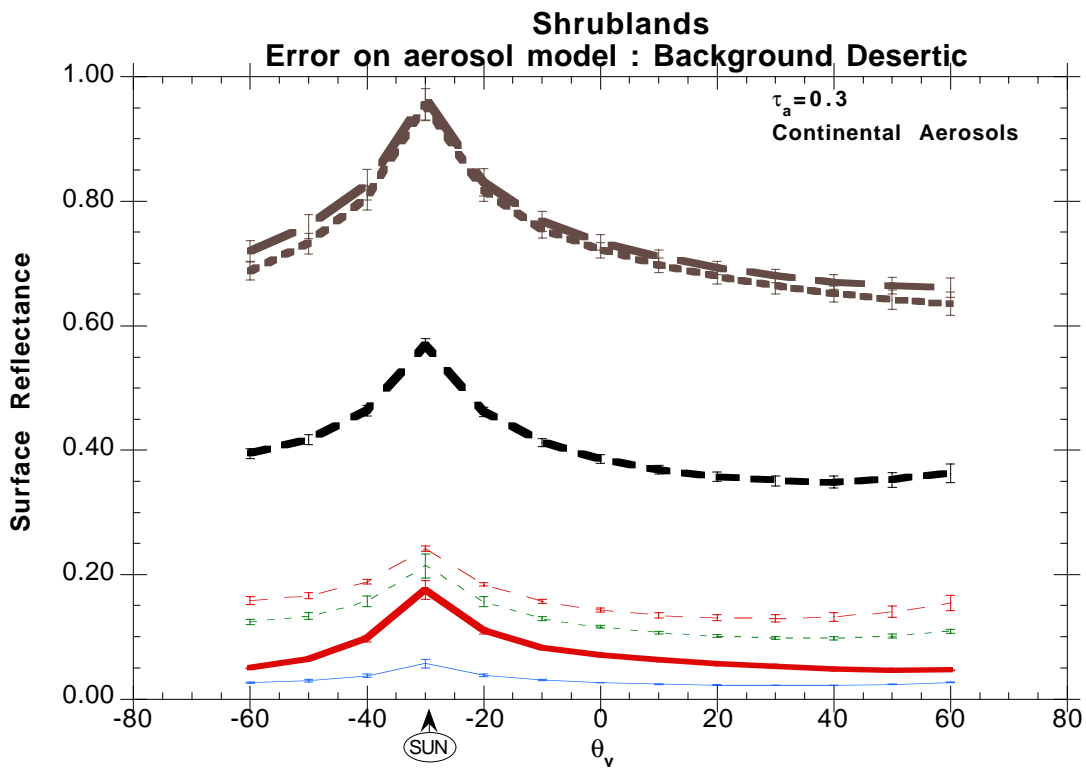
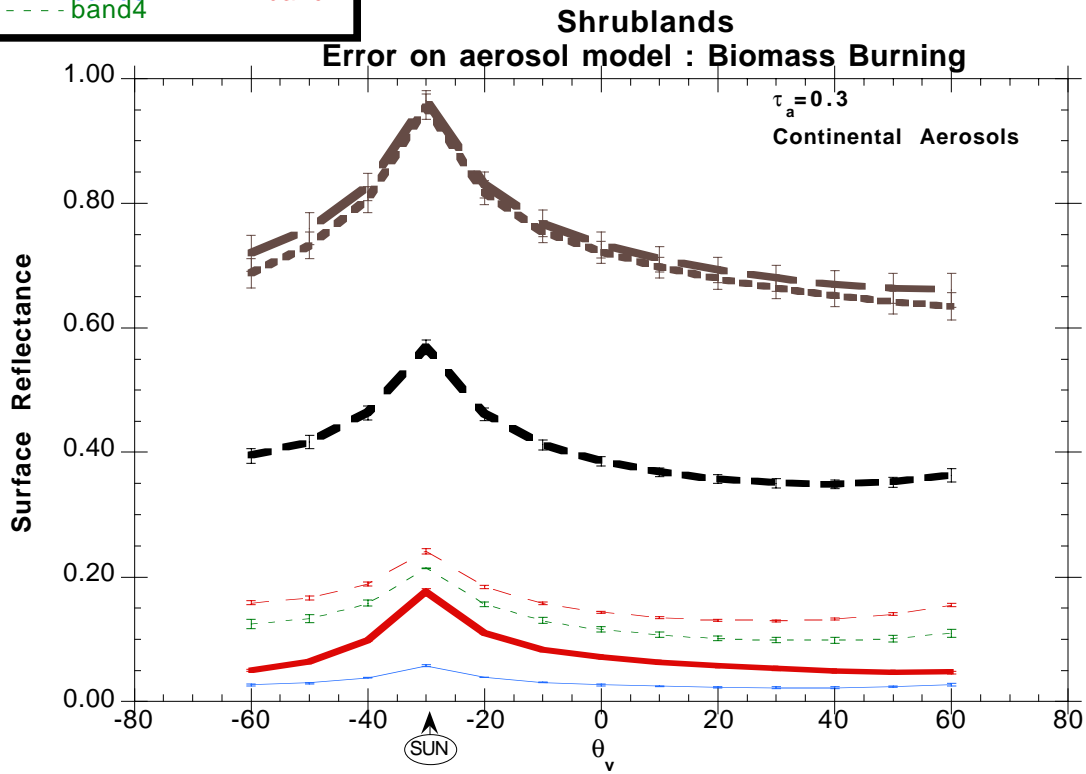
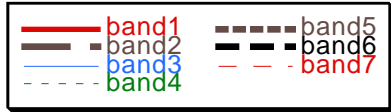










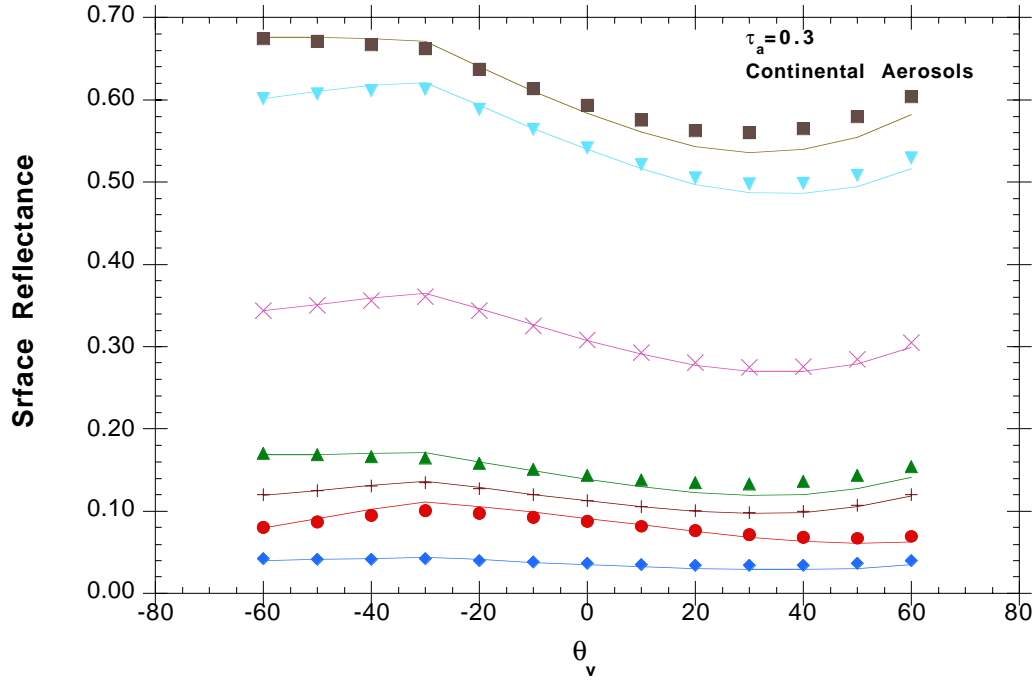


Appendix B4) Error due to BRDF atmosphere coupling (at optical of 0.3 at 550nm).

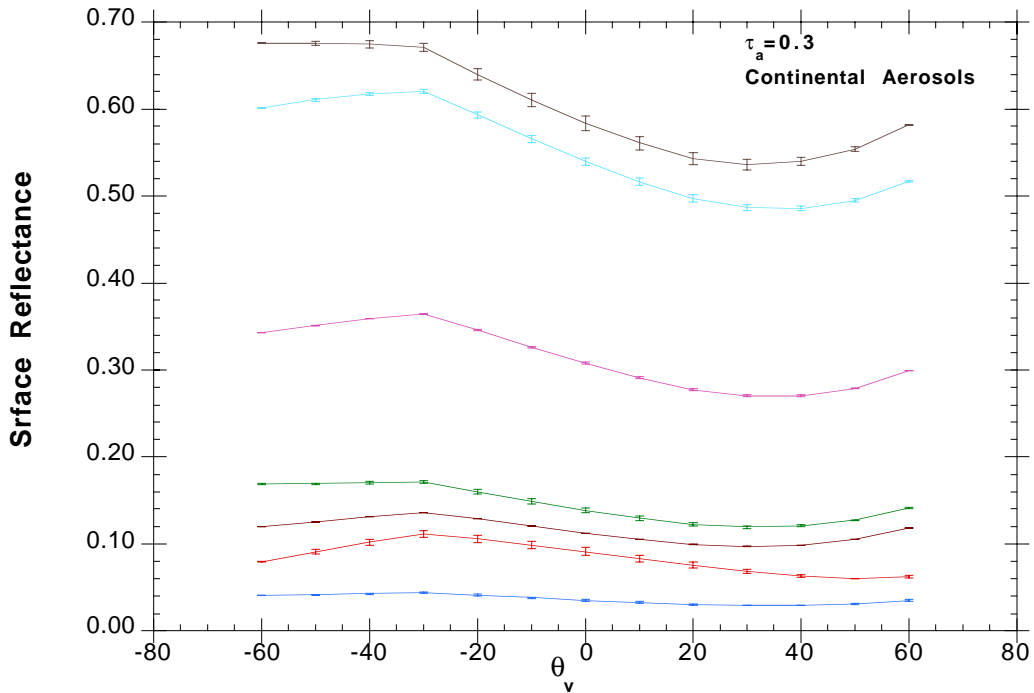
The error when using the lambertian assumption is presented (symbols) .The error bars are error estimate when using a generic BRDF and equations 15,16a-c for correction. Broadleaf and savanna BRDF are used for correcting grassland, leaf forest BRDF is used for correcting shrubland.

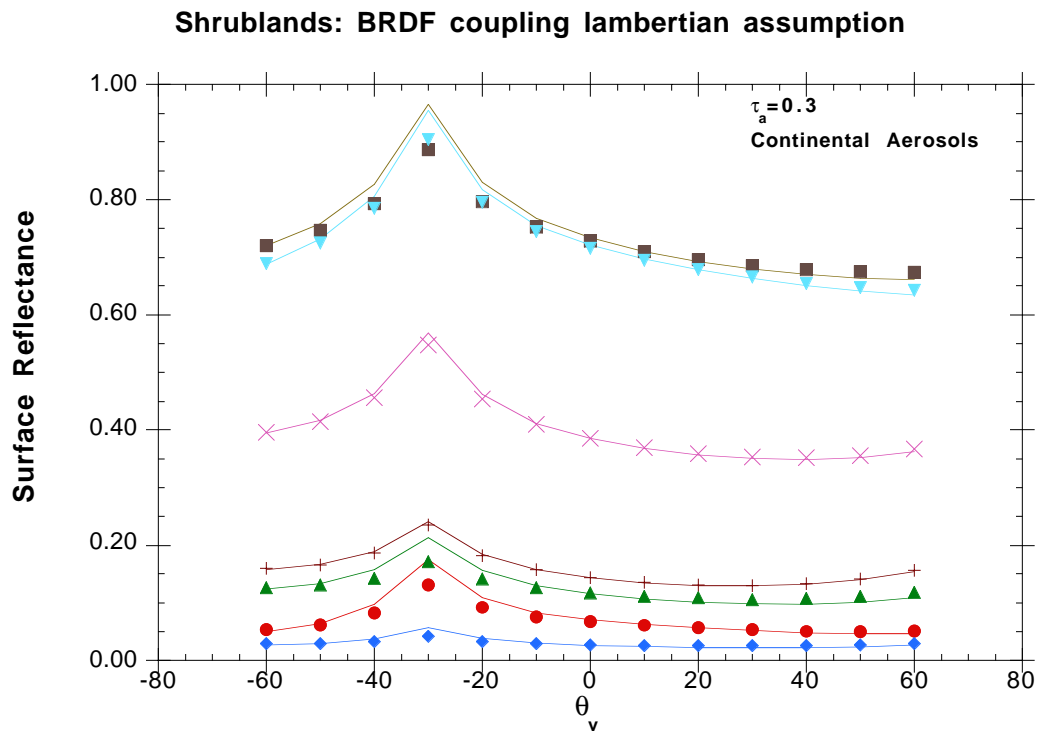
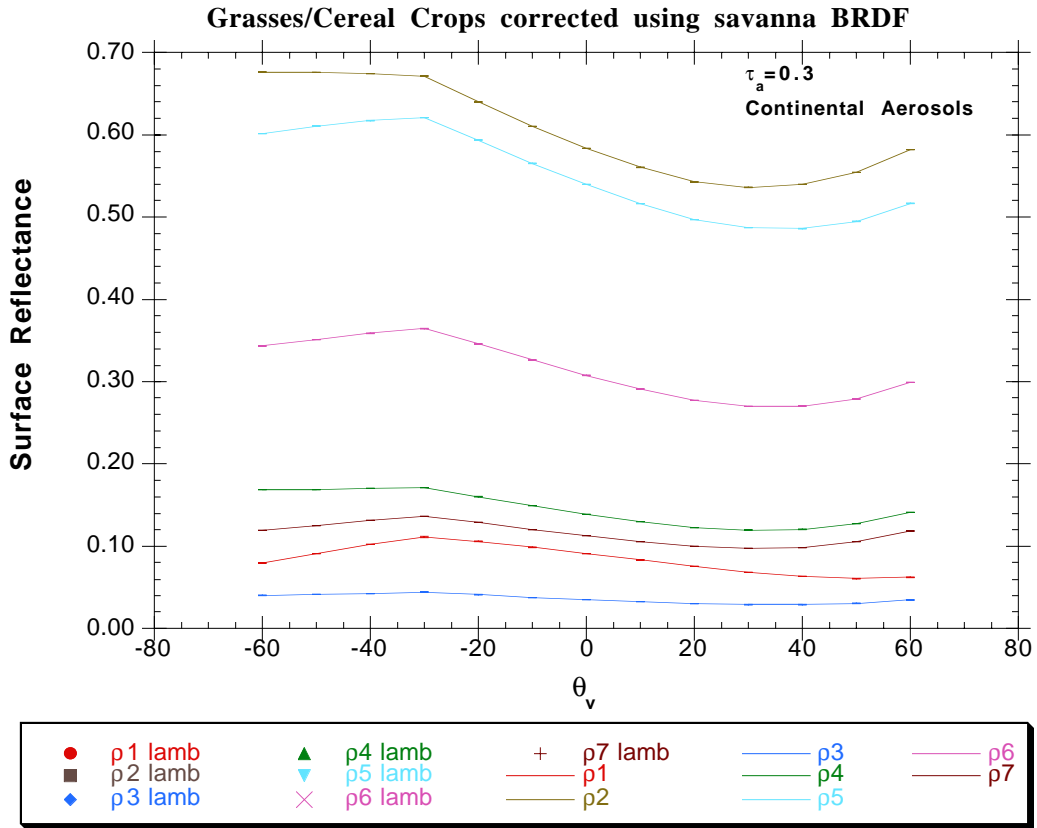


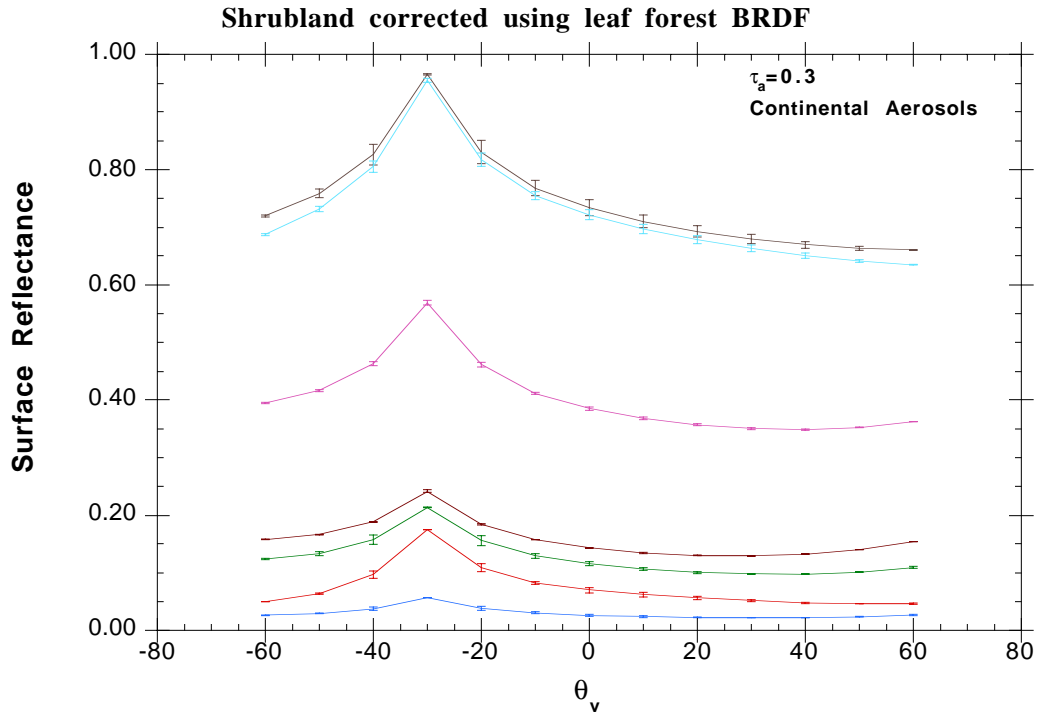
**Grasses/Cereal Crops : BRDF coupling
lambertian assumption**



Grasses/Cereal Crops Corrected using Broadleaf BRDF







Appendix C answers to the SWAMP 96 land product review.

Recommendation 3 *Consolidate atmospheric scattering (correction) models*

Several atmospheric scattering models are being used by various investigators within one instrument team and across-instrument teams. The main rationale given in using one rather than another approach is familiarity and implied confidence. However, it is possible that the atmospherically-corrected data based on one model may be different than from another model, leading to different results when corrected data is used. Also, cross-comparisons or joint use of similar or complementary products from various sensors may be thwarted. It is recommended that various atmospheric scattering investigators establish formal collaboration to compare and contrast different models to come to closure on this issue. It is our feeling that, at a minimum all the models use similar physical assumptions and have similar sensitivity to errors (it is realized that the technique used in solving appropriate equations may have to be different), such that corrections are consistent. If physically different models have to be used, a conversion table (if feasible) for one model against another will be desirable for the users.

-> The model we are using (6S) is available to the general community and has been compared to other scattering models. The EOS-AM1 atmospheric correction (Martonchik,Thome,Vermote:Chair) group plans to point out differences in the MISR/ASTER/MODIS approaches and compare the different models.

(a) technical/scientific soundness of the algorithm/approach described

(Rating: 6)

The algorithm is similar in spirit to those used by ASTER and MISR teams. The main questions are accuracy and uncertainty of the results (ATBD does not present a serious error analysis) and the size of the LUT table vs. fineness of the parameter grid (a finer grid will increase the size but ensure a more accurate retrieval). Note that the accuracy of the approach depends on the accuracy of the input parameters. Two of these parameters -- aerosol optical thickness and BRDF are themselves products of MODIS and/or MISR algorithms.

Since the MISR and ASTER teams are working on the same problem (although spatial resolutions are different), a collaboration with those team members will be beneficial. It is recognized that various atmospheric scattering models are being used by various investigators within one instrument team and across-instrument teams.

-> We try to improve on error analysis (appendix B of ATBD), error analysis shows that the LUT resolution is sufficient (error <0.001 reflectance unit). We recognize the value of working with other teams for the atmospheric correction and are going to embrace this recommendation by working out common issues in the EOS-AM1 atmospheric correction group.

(b) value of the data product to the Land science community (Rating: 6)

The data on spectral reflectances will obviously be useful, provided it is accurate. In the absence of error analysis, (see comments under technical/scientific soundness), it is difficult to properly assess the value of the product.

-> We are now addressing error analysis (see appendix B of the ATBD).

(c) soundness of the validation strategy (Rating: 5)

The atmospheric correction scheme will be validated using sun photometer data collected at a series of test sites with known land cover characteristics in conjunction with data from existing sensor systems (AVHRR, AVIRIS, TM, MAS), including SCAR-A data set intercomparison. The surface reflectance product will be validated using a combination of ground-based measurements, airborne measurements, comparison with other sensor data and image analysis.

The details of the validation approach are not given.

-> There is now more details for validation planning, both in the ATBD and in the MODLAND validation plan.

(e) near-term recommendations for improvements to the data product

- It is recommended that a formal collaboration be established between MODIS, ASTER and MISR teams to compare and contrast various algorithms. This should

lead to cross-fertilization of ideas with respect to the accuracy and efficiency of the algorithm(s) adopted.

-> *see (a),(b)*

(f) long-term recommendations for improvements or additions to the data product

- Atmospheric correction formal collaborations between MODIS, ASTER and MISR teams as recommended above would be expected to determine which of the model/algorithm (physical assumptions and mathematical approach) approaches are likely to give best surface reflectance and surface radiance.
- Likewise, the issues (described previously) regarding accuracy, speed, grid size, input parameters, and methodologies associated with the use of a look-up table (LUT) for model inversion could be investigated jointly.

-> *see (a),(b)*

==